2D Resistivity and Time-Domain EM in aquifer mapping: a case study, north of Lake Naivasha, Kenya

Thomas Tsiboah

March, 2002

2D Resistivity and Time-Domain EM in aquifer mapping: a case study, north of Lake Naivasha, Kenya

by

Thomas Tsiboah

Thesis submitted to the International Institute for Geo-information Science and Earth Observation in partial fulfilment of the requirements for the degree in Master of Science in *Earth System Analysis (ESA) - Applied Geophysics Specialization*.

Degree Assessment Board

Thesis advisor	Ir. R.J. Sporry
Thesis examiners	Prof.Dr. C. Reeves, **(Chairman)**, ITC Enschede
	Dr.Ir. Slob, **(External Examiner)**, TU Delft
	Dr. J. Roy, **(Member)**, ITC Enschede
	Drs. R. Becht, **(Member)**, ITC Enschede

INTERNATIONAL INSTITUTE FOR GEO-INFORMATION SCIENCE AND EARTH OBSERVATION

ENSCHEDE, THE NETHERLANDS

Disclaimer

This document describes work undertaken as part of a programme of study at the International Institute for Geo-information Science and Earth Observation (ITC). All views and opinions expressed therein remain the sole responsibility of the author, and do not necessarily represent those of the institute.

Abstract

Farmers in the north of Lake Naivasha in Kenya use mainly groundwater from the *lake beds* for irrigated agriculture. To model the groundwater system in this area, a systematic and dedicated effort have been made to collect two-dimensional (2D) Resistivity Imaging and Transient electromagnetic (TEM) data on three farms; Three Point, Manera and Homegrown. In all, thirteen (13) Resistivity Imaging Survey profiles of different lengths and 137 Time-Domain EM (TEM) soundings were carried out. The *formation resistivity* physical property, groundwater quality and lithological data were used to model of the aquifer. A representative aquifer model to meet the different needs of the farmers had a formation resistivity range of 12 - 335 Ohm.m. The aquifer exists generally between depths of 20 to 80m in the Three Point Farm. Towards Lake Naivasha in the Manera Farm, the aquifer splits up into two but remains hydraulically connected. The *top* aquifer occurs between depths of 20 - 40m and the *bottom* between 50 - 80m. The main aquifer materials include fine sands, medium coarse sands, gravels, pebbles and fractured volcanics. Laterally, the high quality and good yield portion of the aquifer occur within a radius of approximately 1km from where the Karati river turns from the NW direction to the SW (90 degree turn). The Karati river has been interpreted to be the main source of recharge into the aquifer. The very low resistivities at depths greater than 80m have been identified as a mixture of clayey materials and saline water. 2D and 3D models of the aquifer has been presented.

Keywords

2D Resistivity Imaging, TEM, inversion, Groundwater system, aquifer, 2D and 3D models, formation resistivity

Acknowledgements

> "Having come this far, means I have been carried on the shoulders of some giants" [*Shakespeare*]. To these, I am greatly indebted.

Firstly, this study was made possible through the Netherlands Government Fellowship and the International Institute for Geo-information and Earth Observation (ITC), for sponsoring my study and this research work respectively.

Secondly, I wish to express my profound gratitude to my supervisor - Ir. R. Sporry for his important guidance and helpful comments from the beginning of the project, fieldwork supervision till this finalized report. Every time's discussion with him made my thesis improve and I really learnt and improved a lot from him.

Thirdly, I wish to express my sincere heart felt gratitude to the rest of the Applied Geophysics staff Prof. C. Reeves, Dr. J. Roy, Dr. S. Barritt and Mr. Hugens for the knowledge imparted and the times shared together both in the classroom and the field.

Furthermore, I am thankful to the Farm Managers of Manera and Three Point Farms for their immense support and willingness to co-operate during the fieldwork. They willingly offered information on boreholes and some consultancy reports. I wish to also acknowledge the kind co-operation of the University of Freiberg, Germany, who made available their TEM-FAST instrument for this study. I am also grateful to Drs. Becht, R. Dost and R. Hennemann for their support during the fieldwork in Kenya.

My heartfelt thanks go to my colleagues in the Geophysics course and friends from Water and Soil Divisions for all the laughters and tears shared together. Many thanks also go to the Ghanaian Community in Enschede for making my stay here enjoyable. To Alfred (PhD) in particular, for sparing some time to read through some of my chapters. I am highly indebted also to my parents, for their moral and prayer support that kept me going. Finally, I wish to also acknowledge the prayer and spiritual support from the ITC Christian Fellowship. To God be all the Glory.

Contents

List of Tables

List of Figures

Chapter 1

Introduction

Lake Naivasha basin is far and wide the most settled and agricultural of the series of lakes in the Kenyan Rift Valley (KRV) mainly because of its freshness and altitude (1985m). Its major, perennial rivers come from the Aberdare Mountains in the north and it is also rich in a variety of underground aquifers. The socio-economic benefits of the Lake, include irrigated horticulture, wildlife conservation and tourism. Over the past decade, the immediate surroundings of the lake has become an important area for large scale dairy farming and export-oriented vegetable and fruit production. Flowers are grown in greenhouses on large estates particularly in the north and the southern fringes for export by air to Europe. Currently, the lake waters are also being used to cool the turbines of Africa's first geothermal power station at Olkaria.

Some farmers along the northern and southern fringes of the lake use the lake-waters directly for crop irrigation and other purposes. The use of lake water by these farms has increased in recent years. A recent Environmental Impact Assessment study carried out by an Environmental Services Consulting company from Australia in 1992 for the Olkaria Geothermal station indicated that about $59 \times 10^6 \mathrm{m}^3 \cdot yr^{-1}$ of water is taken from the lake for irrigation alone. This is far above the allowable quantity of $30 \times 10^6 \mathrm{m}^3 \cdot yr^{-1}$ [ESA, 1992]. As if that is not enough, there are reports of the lake being polluted with agro-chemical residues, a situation that may eventually lead to the lake becoming eutrophicated if not addressed, a view corroborated by Harper et al. (1993) and Lincer et al., (1981); cited in Aquasearch, (2001).

Concerns are growing for the lake that, if these issues are not properly addressed, the lake may not be able to sustain its various uses and its very existence may even be threatened. This has prompted some farmers, particularly in the northern plains, to tap and make use of the groundwater in the surrounding lake beds, where several

underground aquifers are reported to exist at different depths. Indeed the future of sustainable good quality fresh water in the Naivasha region would undoubtedly be a major socio-economic challenge, one that would certainly draw more and more attention from planners, decision makers, farmers and, of course, scientists and researchers.

This research work aims at using geophysics to map the groundwater system in the north of Lake Naivasha where there is high exploitation of the groundwater system for both domestic and irrigation purposes.

1.1 Background

The eastern arm of the Great East Africa Rift Valley has a series of relatively small lakes (tens rather than hundreds of square kilometers in their size) dotted in it. Many of them are saline but a few, with good inflows from the Rift edges, are fresh. In Kenya they range from the large and long Turkana Lake in the arid north to the highly saline Magadi Lake that supports a soda factory in the south (see Figure 1.1). A series in the middle of the country includes the economically important freshwater lakes (Naivasha and Baringo) and several saline lakes protected for their unique wildlife and scenery [EarthWatch, 2002].

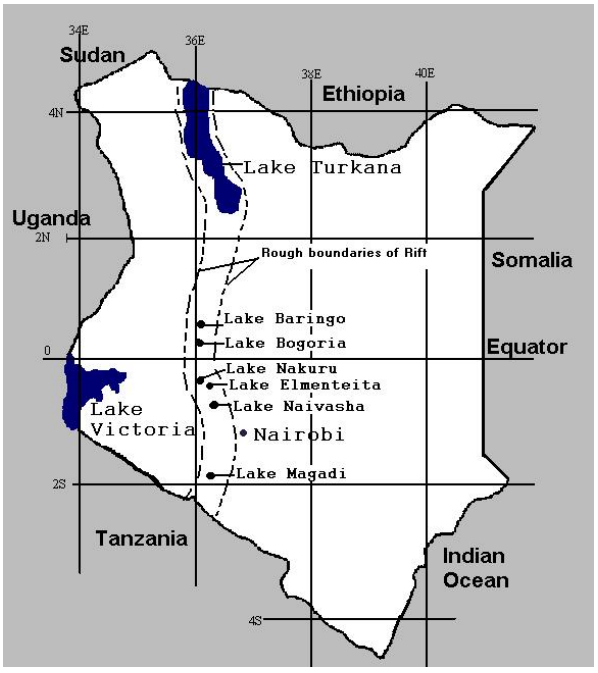

Figure 1.1: Lakes of the Kenyan Rift Valley.

Lake Naivasha is a relict lake that once belonged to a large freshwater body that comprised Lakes Naivasha, Elmenteita and Nakuru called the Lake Gamblian (see Figure 1.2). The large freshwater body is believed to have dried up due to changes in climatic conditions and volcanic activities. Lakes Nakuru and Elmenteita became saline but Lake Naivasha remained fresh though it has no known surface outlet. The mean electric conductivity is $330\mu Scm^{-1}$. The mystery of its freshness has been largely attributed to incoming water from rivers in the north and loss of water via subsurface seepage to the south and the north due to the extremely porous volcanic rocks that form the lake basin. An *"analytical signal image"* made from the airborne magnetic data on the area in this study, (see Figure 2.7) reveals two major faults systems beneath the lake and two others intercepting the Lake in a NW-SE direction that can also be channels of water lose from the lake if they are open faults.

Lake Naivasha receives water from two perennial rivers, the Malewa and Gilgil; and one ephemeral river, the Karati; that enters the lake from the north. Of these, Malewa River contributes more than 80% of the discharge into the lake and the rest by Gilgil and Karati Rivers [Vincent et al., 1979]. The lake has experienced several dry phases with alternating periods of high water level but the basin is thought to have completely dried up about 300 years ago. If this were so, then there could some evaporite layers in the *lake beds*.

Farmers surrounding the lake practice intensive horticulture using center-pivot overhead methods to irrigate the crops on the farms, and flowers in greenhouses. Some of these farms include Manera Estates, Three Point Farm also called Panda Flowers, Homegrown Farm and Kenya Agricultural Research Institute (KARI) and Marula estates. Manera Farm practises mixed agriculture, comprising dairy farming and irrigated horticulture. The main crops cultivated include, French beans, maize, cabbages and lucerne to mention a few whereas Three Point Farm is sorely into irrigated agriculture with main crops being 'Rose' flowers Cabbages, French beans and tomatoes.

1.2 Problem definition

The fact that groundwater supply from the farms in the north of Lake Naivasha was more than adequate due to the believe that several aquifers exist in the lake bed is being challenged by the recent increase in the exploitation of the resource. Recent reports show that there have been a drop in water levels in boreholes and groundwater quality has deteriorated over the time. There are reports of increase

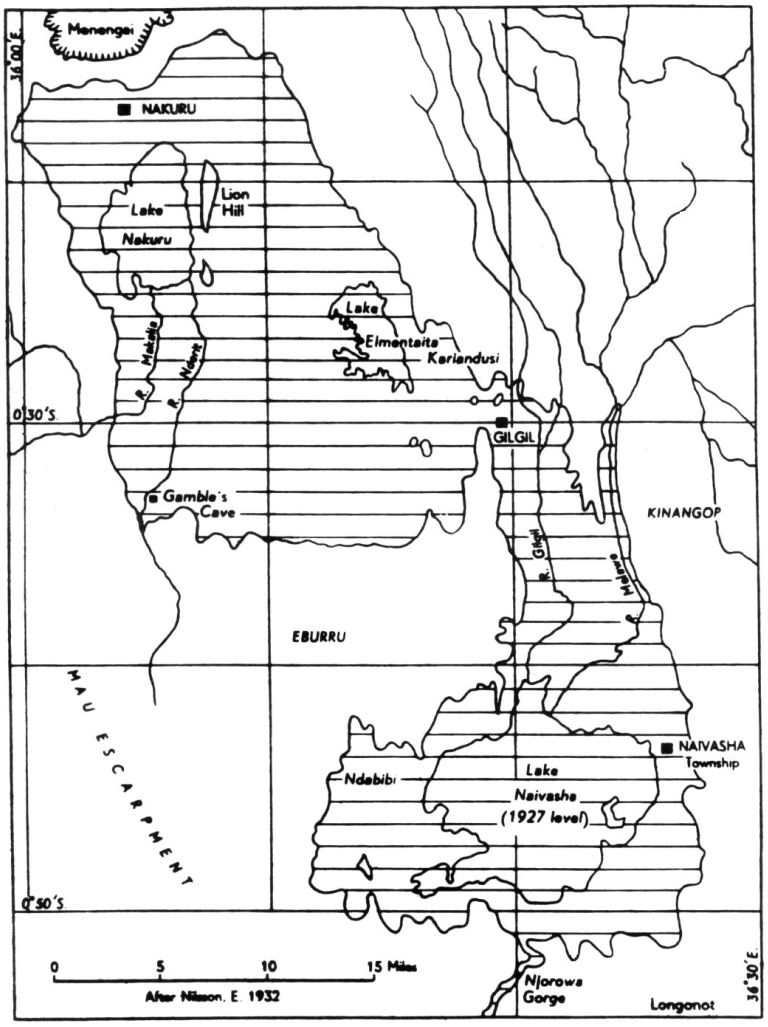

Figure 1.2: The maximum extent of Lake Gamblian.

in electrical conductivity (EC) from the northeast (rift wall) towards the lake ($420 - 1560\mu S \cdot cm^{-1}$) [Morgan, 1998]. Also, in a recent work by *GSK*, (1989), an inventory of the boreholes on these farms from 1960 to 1970 indicated that generally groundwater becomes mildly saline to brackish with proximity to Lake Naivasha. The electrical conductivity (EC) of shoreline boreholes ranged from $650 - 1120\mu S \cdot cm^{-1}$ at the time of drilling, while inland borehole ECs' ranged from $520 - 880\mu S \cdot cm^{-1}$. Generally, water quality has also declined over the years in the entire area, with ECs' nearly doubling in some cases [Aquasearch-Ltd., 2001].

There are also reports of the water becoming saline at larger depths, a view presented by the farm manager of the Three Point Farm in a personal communication

during fieldwork. The only deep borehole in the area, the 130m borehole on the Three Point Farm close to the Karati River was cited the evidence that led to the abandonment of the borehole. However, evidence from records of the borehole in question from the Ministry of Land Reclamation Regional and Water Development of Kenya archives indicated that the water had an Electrical Conductivity (EC) of $610\mu S \cdot cm^{-1}$ and the water was slightly colored, turbid and moderately mineralized due to high iron content ($> 1.5ppm$). Also in another isolated case on the Manera Farm near the Dairy, the EC of the water was unusually high ($5125\mu S \cdot cm^{-1}$) even at depths of 70m.

The geological condition in the Naivasha catchment area is complex and intricately related to the nature of the groundwater regime. A fact that could be attributed to the difficulty to fully model the aquifer with the conventional hydrogeological methods alone. The entire area is covered by volcano-sedimentary materials, intercalated with trachytic and obsidian lava flows. The exact distribution and depth of the lava has not mapped. Boreholes that encountered lava either within or beneath always gave low or no yield at all.

1.3 Research Motivation

Geophysical techniques have proved to be efficient tools in groundwater exploration and the steep technological growth of the last 15 years in geophysics, due mainly to advances in microprocessors and associated numerical modeling solutions, have greatly affected this field of geophysics. Not only has geophysics been used in the direct detection of the presence of water but also in the estimation of aquifer size and properties, groundwater quality and movement, mapping saline water intrusions and buried valleys even in areas of complex geology [UNESCO, 1998].

The cost of drilling large-scale farming water-supply boreholes almost demands that the risk of drilling a poorly yielding borehole should be lessened through the proper use of geophysics. Geophysics can be used to screen potential drilling locations, decreasing the risk of drilling in unproductive areas. Geophysics is cost effective since its proper application always increases the success of drilling.

Often groundwater models are used to simulate subsurface flow for a more quantitative hydrogeological analysis of the effect of proposed water-supply boreholes and for planning purposes in areas that depend heavily on ground water like in the area under study. These groundwater models are usually limited in accuracy by the hydrogeological data available. Geophysics can provide additional data to improve the accuracy of groundwater models.

The revealing complex nature of the geology and the groundwater system in the northern plains of Lake Naivasha makes a detailed and a systematic geophysical study, the appropriate alternative, as the conventional hydrological approach so far has proved its inability to exhaustively deal with the problem alone. In this research, both airborne and ground-based geophysical methods including the existing hydrogeological data will be used to study the groundwater system and to model the aquifer. The archives of airborne magnetic data in the area were collected for reprocessing and interpretation with the view to studying the regional features such as faults, lineaments and dyke intrusions. Also some existing DC resistivity sounding data from a previous M.Sc. theses work [Gressando, 1999] were selected for reprocessing and interpretation. The actual work involved a dedicated geophysical fieldwork to collect 2D Resistivity Imaging and Time-Domain EM data on the subsurface electrical resistivity properties.

1.4 Objectives

1.4.1 General Objectives

The main aim of this research is to map the groundwater system and its geophysical characteristics in part of the northern and northeastern plains of Lake Naivasha, Kenya.

1.4.2 Specific objectives

The specific research objectives set out include:

1. To establish the distribution of the electrical properties of the aquifer materials in the area,
2. To map the horizontal and vertical extension of the aquifer and its boundaries,
3. To map the saline-fresh water boundaries, if present and the degree and approximate depth of groundwater salinization,
4. To map hard rock intercalations and to map structural features like faults and shifted blocks.
5. To analyze the inversion performance of TEM compared to 2D Resistivity Imaging, and finally

6. To build a 3D aquifer model from the formation resistivity.

1.5 Methodology

This study involved four main stages, namely;

Review of available data

Fieldwork

Data processing, interpretation and Aquifer modeling

Reporting

1. **Review of available data:** This step involved the collection and review of all relevant available literature from existing files, reports, libraries, and the databases *"Mr.Data"* created by the WRES Division of ITC for a wide range information on Naivasha, such as:

   - topographical maps, aerial photographs and satellite images,
   - geographical and geological data,
   - reports of previous geophysical studies (magnetic, gravity, electrical resistivity) in the area,
   - borehole and well data files,
   - water quality data
   - data on the present water use and the future water demand irrigation by the farms.

   The findings of this survey were used to plan the fieldwork in a way that:

   - duplication of earlier investigations is avoided,
   - data are collected in the significant locations
   - the best results are obtained for the least cost

2. **Fieldwork:** The fieldwork involved the execution of 2D Resistivity Imaging survey and Time-Domain Electromagnetic (TEM) sounding on a number of survey lines that were selected based on the pre-fieldwork study.

3. **Data Processing, Interpretation and Aquifer Modelling:** This stage involved the processing of all the data collected both from the archive and from the fieldwork in Kenya. Geophysical anomaly maps, 2D **true** and **apparent** resistivity pseudo-sections and 3D models were made using the software packages Res2dinv, TEM-RES, Oasis Montaj and Groundwater Modelling System (GMS). Integration and overlay analysis of the processed field results were carried out the Geographical Information System (GIS) software package ILWIS.

4. **Reporting:** This stage included the reporting on the entire work (data collection, data analysis and interpretation) and establishment of recommendations for future developments.

Figure 1.3 shows the details of the methodology in a flowchart.

1.6 Previous Works

Geophysical surveys particularly resistivity, gravity and magnetics were carried out in the past on the geothermal areas in the Naivasha basin, (refer to Figure 2.3). Group Seven Inc. in 1972 undertook electrical resistivity depth sounding surveys in the geothermal prospects, Olkaria and Eburru, surrounding Lake Naivasha. The survey consisted mostly of direct current dipole-dipole mapping surveys, Schlumberger direct soundings and Time-Domain EM soundings. Barongo, (1982) also carried out electrical prospecting of the Eburru geothermal field directly to the northwest of Lake Naivasha for the Ministry of Energy, Kenya.

Groundwater investigations in the Naivasha area did not get much attention in the past as compared to geothermal prospecting. In 1976, VIAK EA LTD a consulting engineering and mapping services, carried out groundwater investigation in the Naivasha area under the Naivasha Water Supply project for the Kenyan Ministry of Water Development. On the subject of geophysics for groundwater exploration in the Naivasha area, little has been documented. The Ministry of Water Development in Kenya did carry out some resistivity soundings in the area to study the groundwater system in the past but the quality of these data leaves much to be desired. A consulting company, Groundwater Survey (Kenya) LTD (GSK), undertook five (5) resistivity soundings at the National Animal Husbandry Research Center (NAHRC) on the KARI farm in 1989, over a 3.3km long transect from the Nakuru-Naivasha road towards the lake. The results showed that resistivity values decrease with proximity to the lake [GSK-Ltd, 1989].

International Institute for Geo-information Science and Earth Observation (ITC), has been carrying out Hydrogeological and Environmental studies in the Naivasha basin, in the frame work of their Master of Science (M.Sc.) programs since 1997. Gressando, (1999) from the WREM division of ITC did his M.Sc thesis work on the topic "Application of geophysical techniques for groundwater investigation in the Lake Naivasha area, Kenya" . An "Assessment of the use of groundwater for irrigation in the southern part of Lake Naivasha, Kenya" was carried out by Oppong-Boateng, (2001) also from WREM as his M.Sc. thesis project. Pastor, (2001) from the Applied Geophysics Division of ITC for his M.Sc. worked on the topic "Geophysical Study of the Groundwater System south of Lake Naivasha, Kenya".

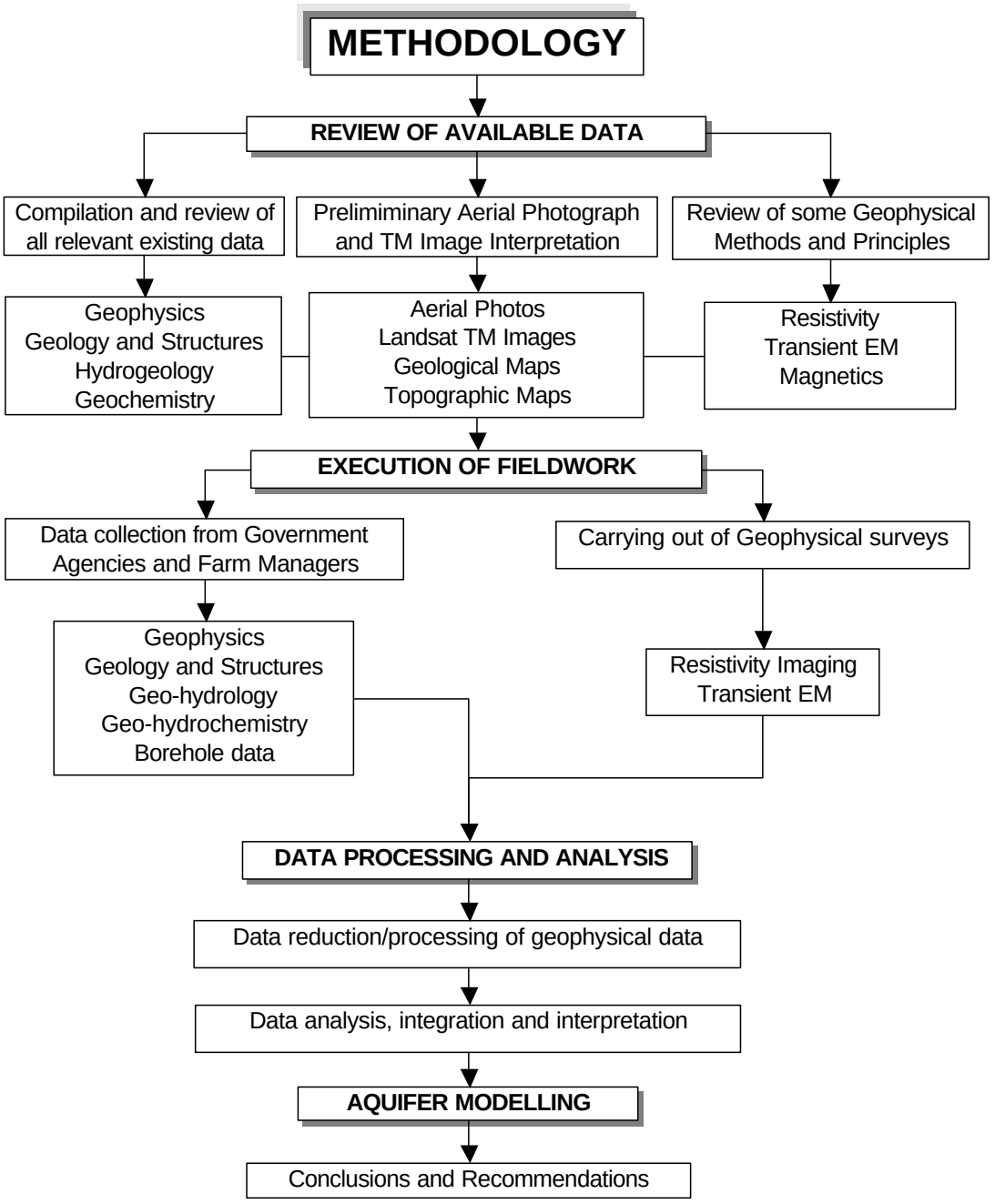

Figure 1.3: Flowchart of Methodology

Chapter 2

Literature Review

2.1 Study Area

2.1.1 Regional Setting

Kenya (Figure 2.1) is a republic of Africa located on the equator, on the continent's east coast. It has a total surface area of 582000 square kilometers. It is a country well known for its scenic beauty and varied wildlife. Although only about 20 percent of the land is suitable for cultivation, the majority of Kenyans are farmers who produce crops mainly for their own needs.

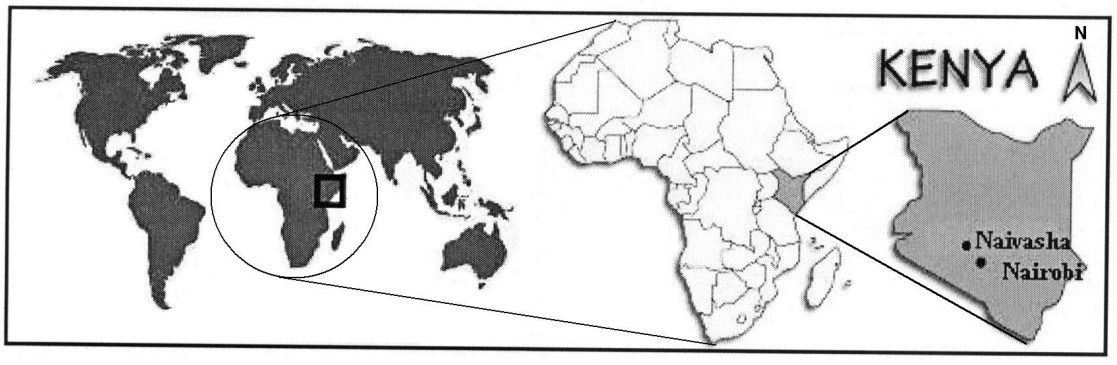

Figure 2.1: Geographical location of the East African country of Kenya

2.1.2 Local Setting

Lake Naivasha is located at Latitude $0^o5'$ S and Longitude $36^o20'$ E in the semi-arid Central Rift Valley region. It is at an altitude of 1,890m making it the highest of the Rift Valley lakes, and unique in many ways. Situated approximately 80 km south of the equator and 100km northwest of Nairobi, Naivasha can be approached by a good tarmac road which forms part of the planned Trans-Africa highway (see Figure 2.1).

The study area is located in the northern and the north eastern plains of Lake Naivasha. It lies between $0^o39'15''\mathrm{S}, 36^o26'40''\mathrm{E}$ and $0^o42'15''\mathrm{S}, 36^o21'54''\mathrm{E}$ with an area of about $40\mathrm{km}^2$. The farms in this area are Manera, Three Point, and Homegrown and KARI, however ground geophysics surveys were concentrated on the first three.

The Manera Farm ($11.36\mathrm{km}^2$) which lies immediately to the north-east of the lake is bounded in the south by the lake, and in the northeast and north by Three Point and Homegrown Farms respectively (see Figure 2.2). However, the area of the farm adjacent to Lake Naivasha is retained as a wildlife refuge, partly for conservation reasons and partly as a physical buffer to prevent the ingress of wildlife onto the farm, [Aquasearch-Ltd., 2001]. The main road and the railway linking Nakuru and Nairobi that passes through Naivasha divides the Manera farm into two main parts and hence the names; the Top Farm $6.1\mathrm{km}^2$ to the NE and the Bottom Farm $5.26\mathrm{km}^2$ to the SW. The Karati River passes through the entire stretch of the farm (see Figure 1 in the Appendix A). Three Point Farm ($2.9\mathrm{km}^2$) shares its western boundary with Manera and it is bounded on the east by the Rift wall. To the south, the Karati River acts as the boundary between the Manera and Three Point farms, (Figure 2.2).

2.2 Physiographic Setting

The Naivasha basin incorporates Lake Naivasha, the ***Ndabibi*** plains which lie to the west and the ***Ilkek*** plains which lie immediately to the north (see Figure 2.3). Lake Naivasha, the highest of the rift valley lakes dominates the Naivasha basin. It stands about 1885m above sea level with a mean depth of 4.9m. The size of the lake varies between $80 - 160km^2$ in response to climatic inputs [Ase et al., 1986]. The Naivasha basin is flanked on the east by Kinangop Plateau and on the west by the Mau Escarpment. The NNW trending South Kinangop Fault scarp characterized by very steep rock faces defines the western margin of the Kinangop Plateau. It is deeply incised by the Makungi, Kitiri and Engare Mugutyu tributaries of the Turasha river, which forms part of the Malewa river, the largest river flowing into Lake Naivasha.

The ***Ndabibi*** plains extend up to 9km west of Lake Naivasha and separates the Eburru and Olkaria Volcanic Complexes. The plains are about 1980m in elevation along their western edge and slope very gently eastwards towards the lake. The ***Ilkek*** plains extend up to 23km north of Lake Naivasha and it ranges from a maximum of 13km in the south near the Naivasha Town to a minimum of 4km in the extreme north near the Gilgil Town. The plains slope gently southwards from a maximum elevation of just below 2000m in the north. The study area is situated on the southern part of the plain which has a form of a delta fan up to 9km wide, associated with the Malewa river.

2.3 Climate

2.3.1 Rainfall

The Lake Naivasha basin is influenced by the Equatorial Monsoon climate hence there are two main rainy periods; April-May and October-November. Average rainfall of the lake area for the periods of 1931-1960 [Ase et al., 1986] and 1960-1985 were 608 mm/yr and 664 respectively [Morgan, 1998]. A ten year data series of rainfall for the Naivasha water supply rainfall station indicated a total mean rainfall of 759.59 mm/year for the period $1985 - 1996$. According to Clarke et al (1990), the rift valley floor receives relative low rainfall compared to the neighboring rift escarpments with rainfall ranging between 1250-1500 mm/yr .

2.3.2 Evapotranspiration

The Naivasha basin has low relative humidity, and an average daily temperature of 24^oC that combine to cause an annual potential evapotranspiration of $1500 - 1900$ mm/yr [Ase et al., 1986]. This is far in excess of the rainfall amount, resulting in a strong negative hydrogeological balance near the lake [Trottman, 1997]. Potential evapotranspiration would consequently be expected to be higher during dry seasons and lower during rainy periods.

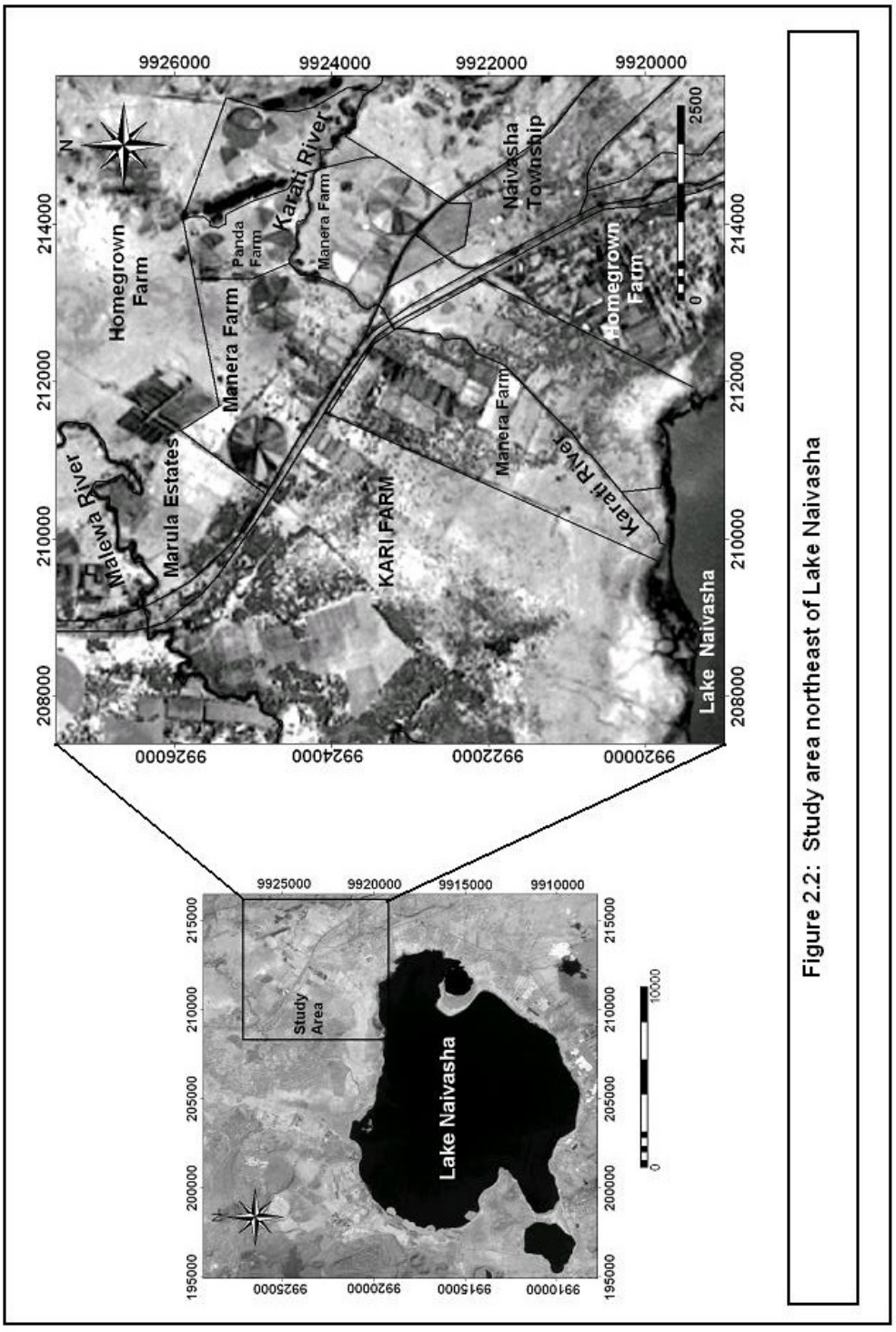

Figure 2.2: Study area NE of Lake Naivasha)

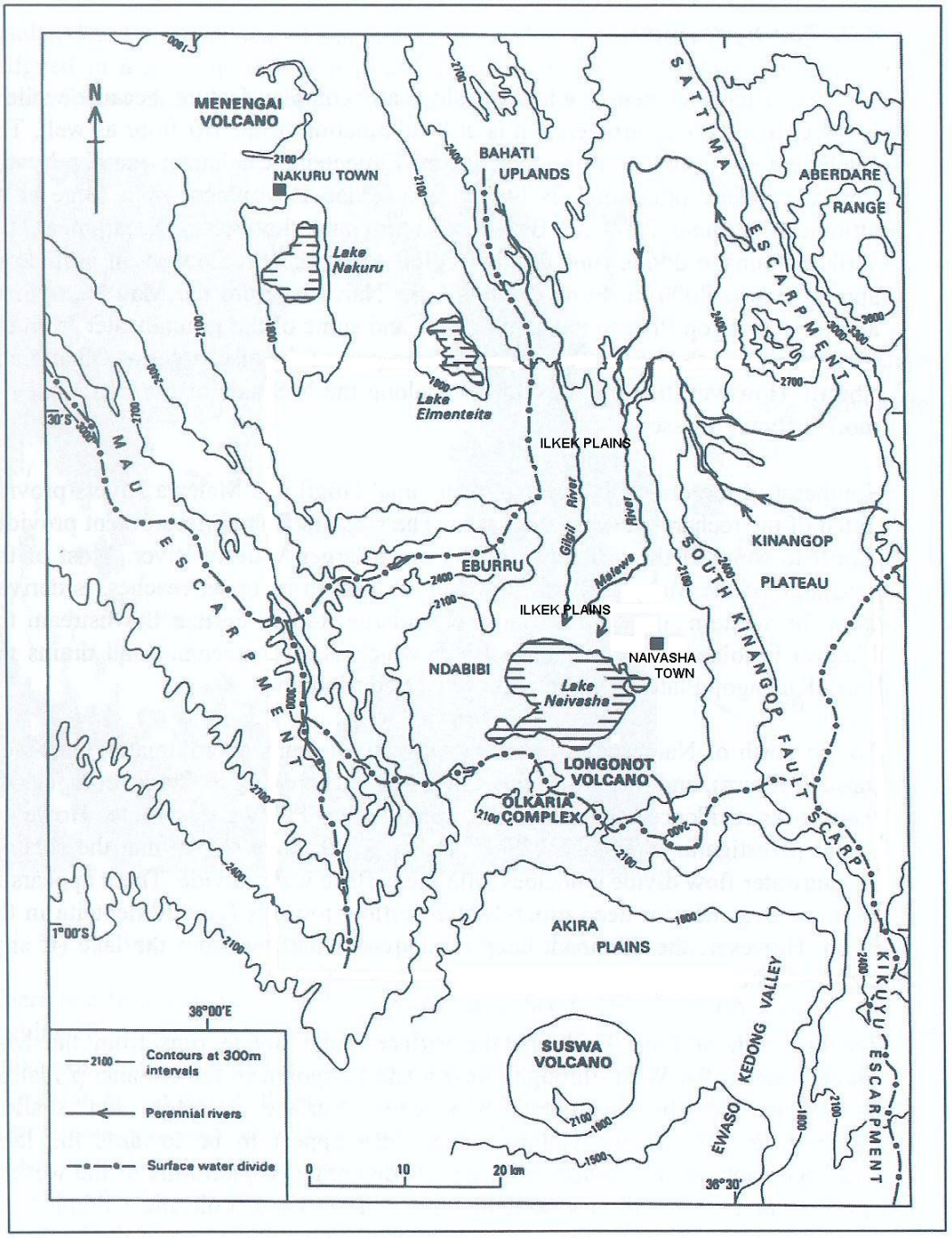

Figure 2.3: Physiographic setting of the study area on a regional scale

2.4 Geological Settings

The tectonic and volcanic regimes that led to the formation of the Kenya Rift as it is known today commenced in the early to mid-Miocene, i.e. approximately 25-30 Ma and only since 4 Ma has there been a graben. From about 1.7 Ma an inner narrow trough developed within which the well-preserved and active volcanoes are located. Characteristic magmatism changed from nephelinitic through phonolitic to trachytic and sometimes peralkaline salic, with basalt accompanying all stages but tending to change from alkali to transitional type [Clarke et al., 1990].

The geology of the Naivasha basin part of the rift valley floor is a succession of late Tertiary and Quaternary volcanics with inter-leafing lacustrine beds and alluvium of principally reworked volcanic debris (see Figure 2.4). There are also reports of diatomite beds. Precambrian Basement rocks are postulated to underlie this volcano-sedimentary succession at or below sea level, [Allen et al., 1989]. The volcanic rocks in the area consist of tephyrites, basalts, trachytes, phonolites, ashes, tuffs and felsic lavas (rhyolite, pumice, comendite and obsidian).

The part of the rift in the study area is defined by major Pliocene boundary faults of the Mau Escarpment in the west and the South Kinangop fault scarp in the east. The major part of this faulting took place in the Middle Pleistocene times, possibly along older fault lines. Minor faulting continued into Upper Pleistocene, probably even later [VIAK-EA, 1976]. The main rift faulting is aligned in a NNW-SSE direction, while the younger faults strike in the N-S direction. Slight unconformities are present in the “lake beds” on the floor of the rift valley.

The Pleistocene volcanic rocks, the oldest materials locally, occur mainly along the eastern margins of rift valley floor. They include the Eburru pumice which is composed of pentlandite and trachytic pumice and ash fall deposits; the Kedong valley tuff, comprising trachytes, ignimbrites and the associated pyroclastics; Kinangop tuffs; Limuru trachyte and Longonot alkaria pumice. Beneath or between lava flows, sediments may occur, comprising sands and clay and pyroclastics (scoriae, pumices, and tuffs) [Aquasearch-Ltd., 2001].

The rest of the study area are covered by Lake beds laid down during pluvial periods in the late Pleistocene and Holocene times. The lacustrine sediments (sand, silt and clay), are overlaid by recent alluvial sediments from the Malewa river north of the study area, see figure 2.4. The thickness of the sediments is variable; a recent borehole information from the farm of the KARI farm, east of the Manera Farm indicated that the thickness of the “Lake beds” exceeds 64m in some places.

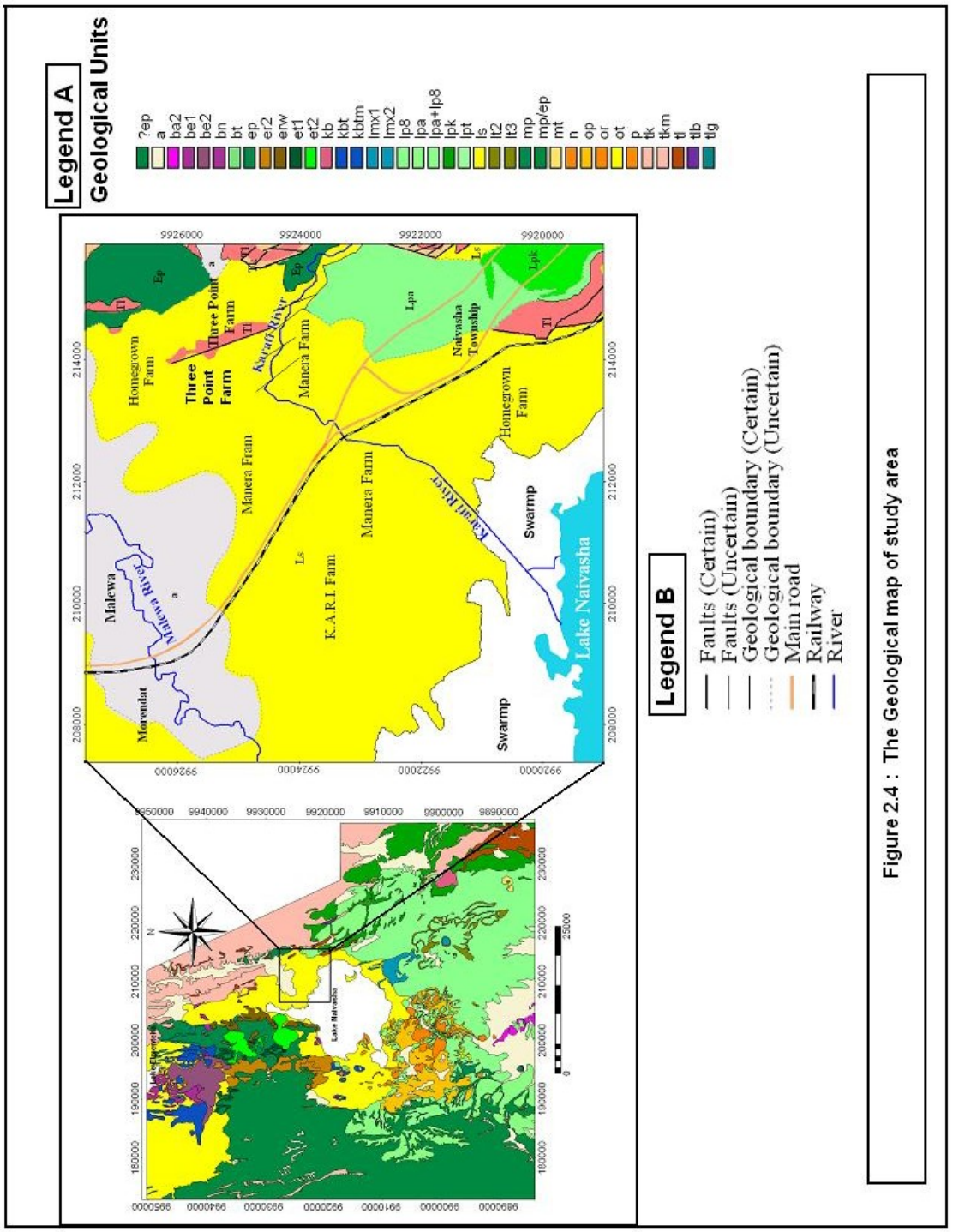

Figure 2.4: The geological map of the Naivasha basin and study area, *modified after WRES Database, ITC*.

Table 2.1: Description of Legend of the Geological map of the Naivasha basin

Unit	Description
?ep	Eburru pumice, pantellerite, trachytic pumice, ash fall deposits
a	Alluvial deposit
ba2	Alkaria basalt, basalt and hawaiite lava flows, pyroclastic cones
be1	Older elementeita basalt, hawaiite lava flows, pyroclastic cones
be2	Younger elmenteita basalt, basalt, hawaiite and mugearite / benmoreite lava flows and pyroclastic cones
bn	Ndabibi basalt, hawaiite lava flows, pyroclastic cones
bt	Surtseyan / strombolian ash cones
ep	Eburru pumice, pantellerite, trachytic pumice, ash fall deposits
er2	Eastern eburru pantellerite and trachyte pumice, ash deposit
erw	Waterloo ridge pantellerite, welded and unwelded pyroclastics
et1	Older eburru trachyte, lava flows and pyroclastic
et2	Younger eburru trachyte, lava flows and pyroclastic cones
kb	Kijabe hill basalt
kbt	Surtseyan tuff cones
kbtm	Surtseyan tuff cones with laterally equivalent fall tuffs
lmx1	Lower longonot mixed basalt / trachyte lava flows and pyroclastic cones
lmx2	Upper longonot mixed basalt / trachyte lava flows and pyroclastic cones
lp8	Longonot ash
lpa	Longonot alkaria pumice
lpa+ip8	Longonot ash and alkaria pumice
lpk	Kedong valley tuff, trachyte ingimbrites and associated fall deposit
lpt	Longonot volcanic, pre-caldera welded pyroclastics and lava flows
ls	Lacustrine sediments
lt2	Lower longonot trachyte, lava flows and pyroclastic cones
lt3	Upper longonot trachyte, lava flows and pyroclastic cones
Mp	Maiella pumice, trachyte, pantellerite pumice and ash fall deposits
Mp/ep	Maiella pumice/trachyte pumice
Mt	Magaret trachyte, unwelded and welded pyroclastics
N	Ndabibi comedite lava flows, domes and pyroclastics
Op	Olkaria comendite, pyroclastics (include pre-Ipk lacustrine sediments, reworked pyroclastics in ol Njorowa gorge
Or	Olkaria comendite, lava flows and domes (includeNjorowa pantellerite lava and welded pyroclastics
Ot	Olkaria trachyte, lava flows
P	Ndabibi pantellerite lava flows
Tk	Kinangop tuff (eastern rift margin)
Tkm	Mau tuff (western rift valley)
TI	Limuru trachyte
Tlb	Karati and ol mogogo basalt
Tlg	Gilgil trachyte

2.5 Hydrogeological setting

The Lake Naivasha catchment is hydro-geologically complex due to the rift floor geometry and tectonics [Clarke et al., 1990]. However, in the area just north of Lake Naivasha, the hydrogeological conditions can be described as excellent by Kenyan standards, says Aquasearch, (2001). Although there are reports of dry boreholes in some localities in the area, the general prognosis for drilling is good and high-capacity boreholes are not uncommon. Dry (or poor) boreholes in the farms are generally associated with the occurrence of shallow lavas and drilling technology. Figure 2.5 shows the boreholes on Manera and Three Point Farms; indicated are also boreholes that have been abandoned due to caving in or relatively high EC.

The Gamblian Lake beds form the main aquifer in the area. The lake beds are made of variable materials, including clay, fine sand, cemented sand, pebbles and gravels of trachyte and pumice, pyroclastics, as well as layers of pumice and tuff. The entire sedimentary-pyroclastic sequence is believed to be saturated, although occasional discontinuous clay bands act as aquiclude in some places.

Groundwater is encountered at depths of 3-35m below-ground-level (bgl) in the Lake Bed aquifer, which is usually semi-confined. The rest water level in the boreholes is always at a higher elevation than the aquifer ceiling, usually by 1 to 5m and this can even be more towards the east rift margin. Test yields in successful boreholes range from less than five to greater than $200\mathrm{m}^3/yr$, for draw downs ranging from 0.2 to nearly 50m. There is no correlation between depth at which water is struck and discharge. However, boreholes that encountered lavas beneath or within the Lake beds are either dry or gave very low yields. It is worth noting here also, that efforts have not been made to penetrate the lavas to find what exist beneath by the farmers.

Groundwater in the area is variable in quality both spatially and temporally, for reasons still unclear. Records (Groundwater Survey, (Kenya), 1989) show that water from Lake foreshore boreholes are poor in quality with an EC range of $1430 - 4550\mu S \cdot cm^{-}1$ and of the alkaline sodium-bicarbonate or sodium-chloride type in chemistry. Some boreholes in the inland lake beds have changed in quality after years of pumping, but the majority at the time of drilling were mildly to moderately alkaline and of sodium-bicarbonate type with ECs in the ranged of $300-1490\mu S\cdot cm^{-}1$ [Aquasearch-Ltd., 2001]. Poor water quality has always been associated with deep groundwater in areas far from Lake Naivasha, however this situation can also be observed at relatively shallower depths in areas not so far from the lake.

Recharge of the aquifer is believed to be a combination of several sources. The

groundwater level in the lake bed aquifer is governed by the lake level and water abstraction [VIAK-EA, 1976]. The rise in lake level since the 1950's and the corresponding increasing use of groundwater, is likely to have changed the gradient and the recharge of the aquifer in the north-east surroundings from the lake [Hernandez, 1999].

Another possible recharge source is via the fault zones in and along the rift walls and escarpments east of the study area. Darling et al., (1999) analyzed non-thermal groundwater samples 6-14km northeast of Manera Farm and found that these contained no Lake water at all, which according to Aquasearch consultants, (2001) is an indirect corroboration of the fault zone recharge hypothesis. Hernndez, (1999) in his M.Sc. thesis work indicated that an important proportion of the water from the rift valley walls flows through the fault system through which it infiltrates to deep zones and thus leaving the catchment.

The third possible recharge of the aquifer is via the permeable sections of the lake beds along rivers like the Karati, the Malewa and Gilgil.

2.6 Hydrology

A brief discussion of the hydrology of the study area is relevant due to the role surface water features can play in groundwater recharge. There are three main rivers in the Naivasha basin; Malewa and Gilgil are perennial and Karati is ephemeral (see Figure 2.3). The Malewa and Gilgil rivers collect runoff from the Aberdare mountains and their foothills to the NE of the lake, and discharge into the papyrus swamp forming part of the northern lake shore [Darling et al., 1990]. All, but the Gilgil river lie within the study area (see Figure 2.6).

The Karati river forms the southern boundary of Three Point Farm and also bisects the Manera Farm. In a good year the Karati river flows for more than six months [Ase et al., 1986]. It may be a significant source of recharge at the point where it crosses the Rift marginal zone and the faults that control its path. The Malewa river lies to the north west of the Manera Farm.

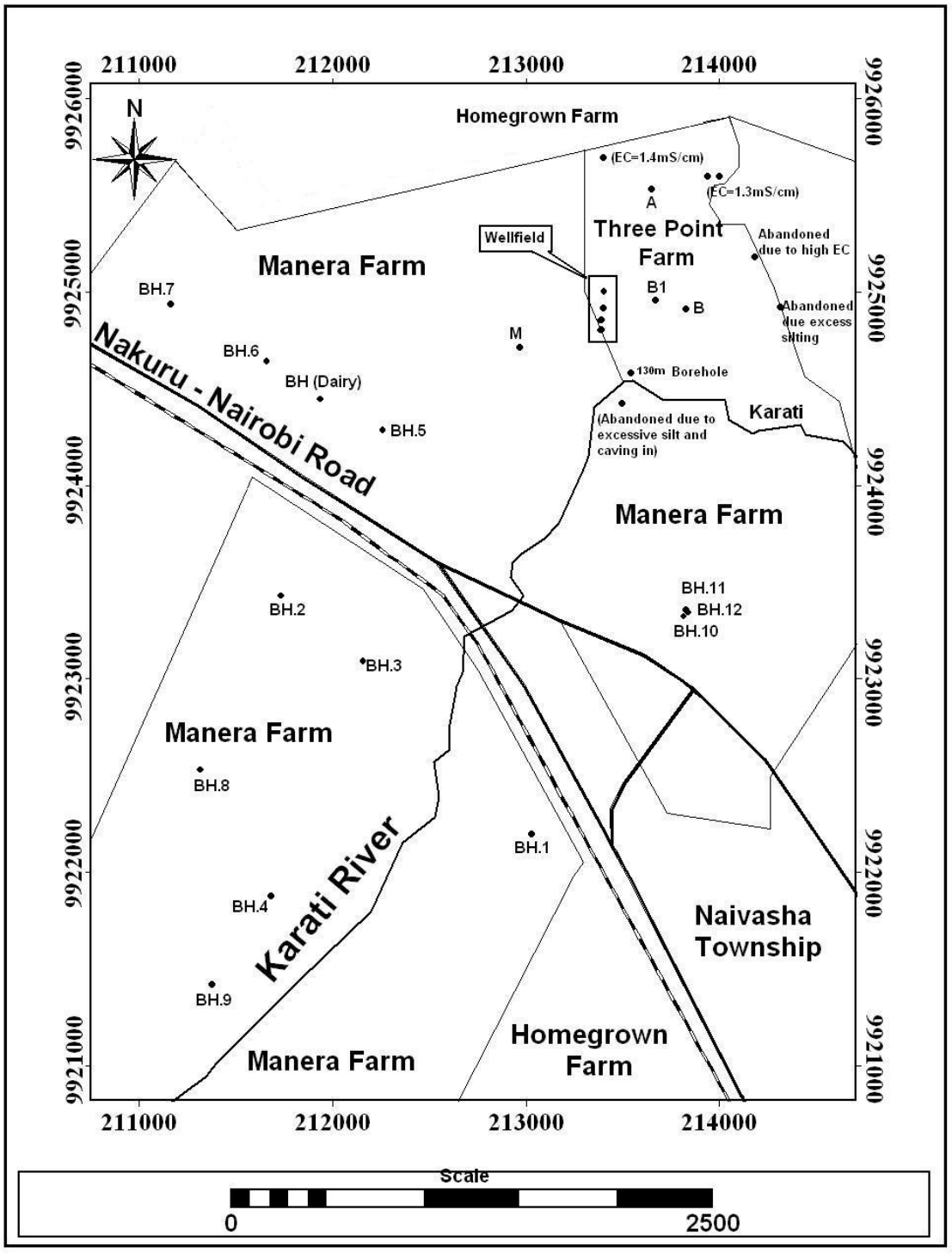

Figure 2.5: Borehole locations on the farms in the study area

2.7 Geophysics

There have been some geophysical studies in the past in the Naivasha area and its geothermal prospects. These include regional gravity, aeromagnetic and resistivity soundings. As part of the review of existing data, some resistivity soundings and airborne magnetic data on the study area were collected for re-processing and analysis to aid the interpretation of the groundwater situation.

2.7.1 Magnetic

Airborne Magnetic survey data can provide vital information about regional structural features such as faults, intrusions and basement rocks (that can be associated with an aquifer). The distribution of magnetic properties in rocks can also give rise to a complex magnetic anomaly pattern or signature which may be associated with a particular assemblage of rocks. This pattern may differ from the pattern over an adjacent rock type of different lithology in amplitude level, in number of anomalies and in shape of the anomalies. Criteria of this sort allow many hidden boundaries to be mapped out between often only limited areas of exposure suitable for conventional field mapping.

Magnetic data covering the study area, come from part of the African Database, Pastor, (2001). Refer to Barritt (1993), for the original source of African Magnetic Mapping Project (AMMP) results. The database is a compilation of regional magnetic anomalies of several African countries that have been re-processed (upward continued to 1000m) and merged together.

The magnetic field intensity of the study area is 34000 nT, at an inclination of approximately -5^o and a declination of -1^o. A colored magnetic anomaly map (Figure 2.6) and an analytical signal image (Figure 2.7) were produced from the data. The first presents the gross magnetic intensity differences caused by different rock types like the mafic rocks like the basalt outcrops and the felsic counterparts like the trachytes, rhyolites and pyroclastics. The second image presents an enhancement of the linear features like faults, joints and lineaments. Three fault generations are represented in the Analytical signal image. The NW-SE regional faults have been intercepted by later NE-SW and E-W responsible for the horst and graben structures visible on the eastern margin of the rift floor. An important revelations from the Analytical signal image were the E-W running faults across the lake and the NW-SE faults intercepting the Lake in the north and the south directions. These fault directions rightly coincide with the Lake's outflow directions mapped by Clarke et

al. (1990), thus enforcing the conclusions on the water loss paths from the lake, (see Figure 2.7).

2.7.2 Resistivity Soundings

Measurement of the electrical resistivity of the earth has been a tool for groundwater exploration for many years. The conventional direct current (DC) surveys are designed to discriminate between anomalies reflecting subsurface electrical resistivity contrasts associated with lithologic and hydrologic characteristics. The interpretation of the resistivity sounding data is usually made assuming a stratified earth and can only provide the apparent resistivity parameters of a horizontally layered model with limited resolution [Keller and Frischknecht, 1966]. Spatial variations of earth materials or topographic effects, however, invalidate such assumptions.

Some DC Schlumberger soundings were carried out in the north of Lake Naivasha in the past by organizations like the Kenyan Ministry of Water Development, Ministry of Energy, Kenya and Groundwater Survey (Kenya) Ltd, a consulting company. Some of the data collected by the Ministry of Water Development, Kenya were obtained from their archives (file No. C6048), WRES Database, ITC. The location of the soundings were not indicate precisely except for some relative locations, and more so, the quality of most of data was low and therefore cannot be used for any serious study. The causes of irregularities in DC resistivity data could be due to several factors such as; faults or abrupt lateral changes in properties, faulty equipment and current leakage and buried metallic pipes. Therefore exact location and azimuth of a DC Sounding survey especially in farms where there a lot buried irrigation pipelines are paramount importance.

In a recent work, Gressando (1999), undertook 25 Schlumberger vertical electrical soundings (VES) in the east and northeastern parts of Lake Naivasha, as part of his M.Sc. thesis work. The locations and azimuths of some data were available and therefore some were selected and re-processed with the RESIST program developed and written by Vander Velpen (1988) in ITC . The results obtained from 1-D inversion of vertical electrical sounding (VES) data were used in compiling a 2-D geoelectrical model that subsequently served as the starting model for TEM inversion algorithms. The results of the 1-D inversion indicated that the various lithological layers; the clays, silts and saturated sand do not have sufficient different apparent resistivity contrasts to guarantee detection (See Figure 2.8). The “apparent resistivity” values near the lakes were much lower compared to sounding data from inland.

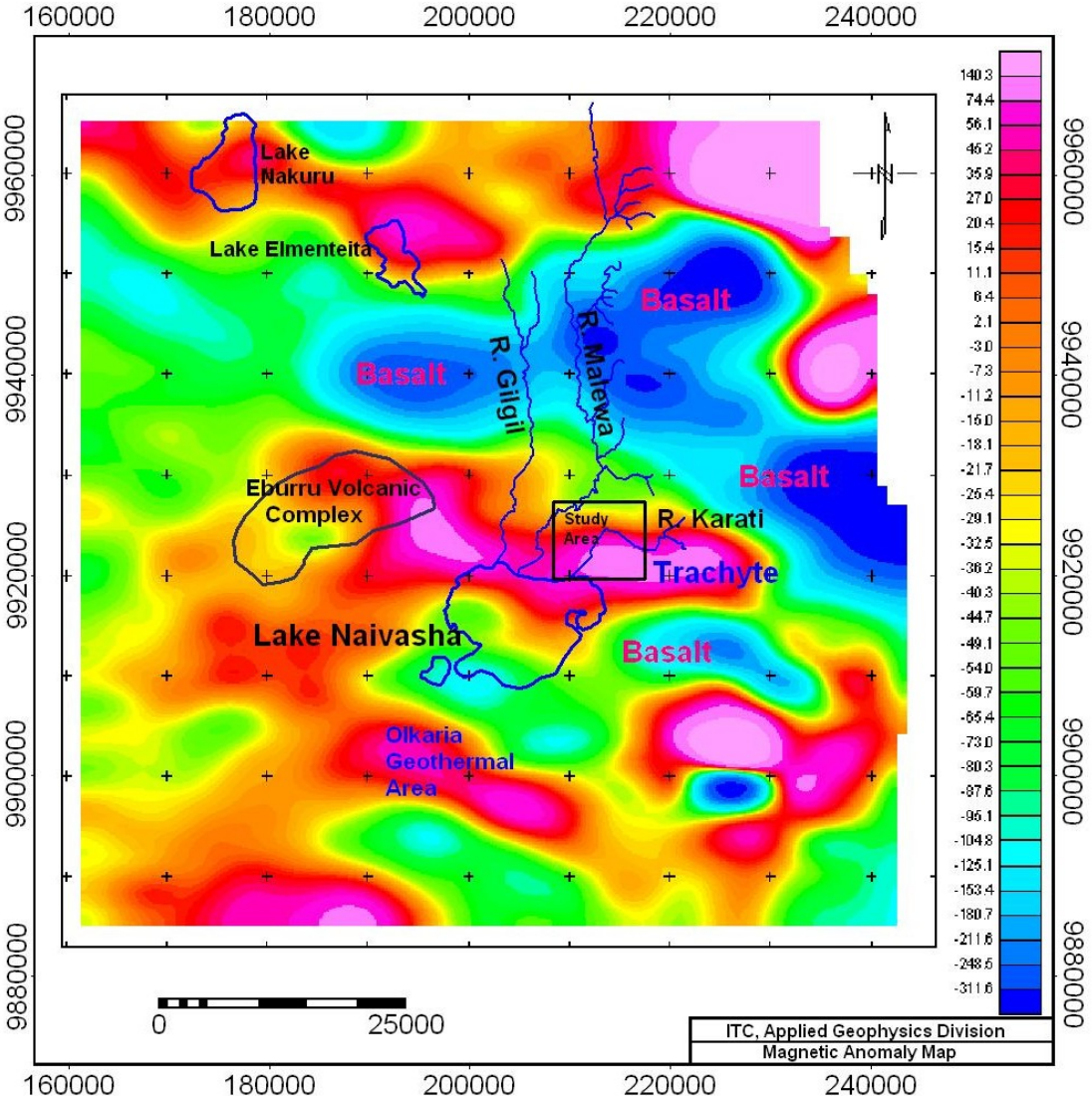

Figure 2.6: Magnetic Anomaly Map of the Naivasha basin

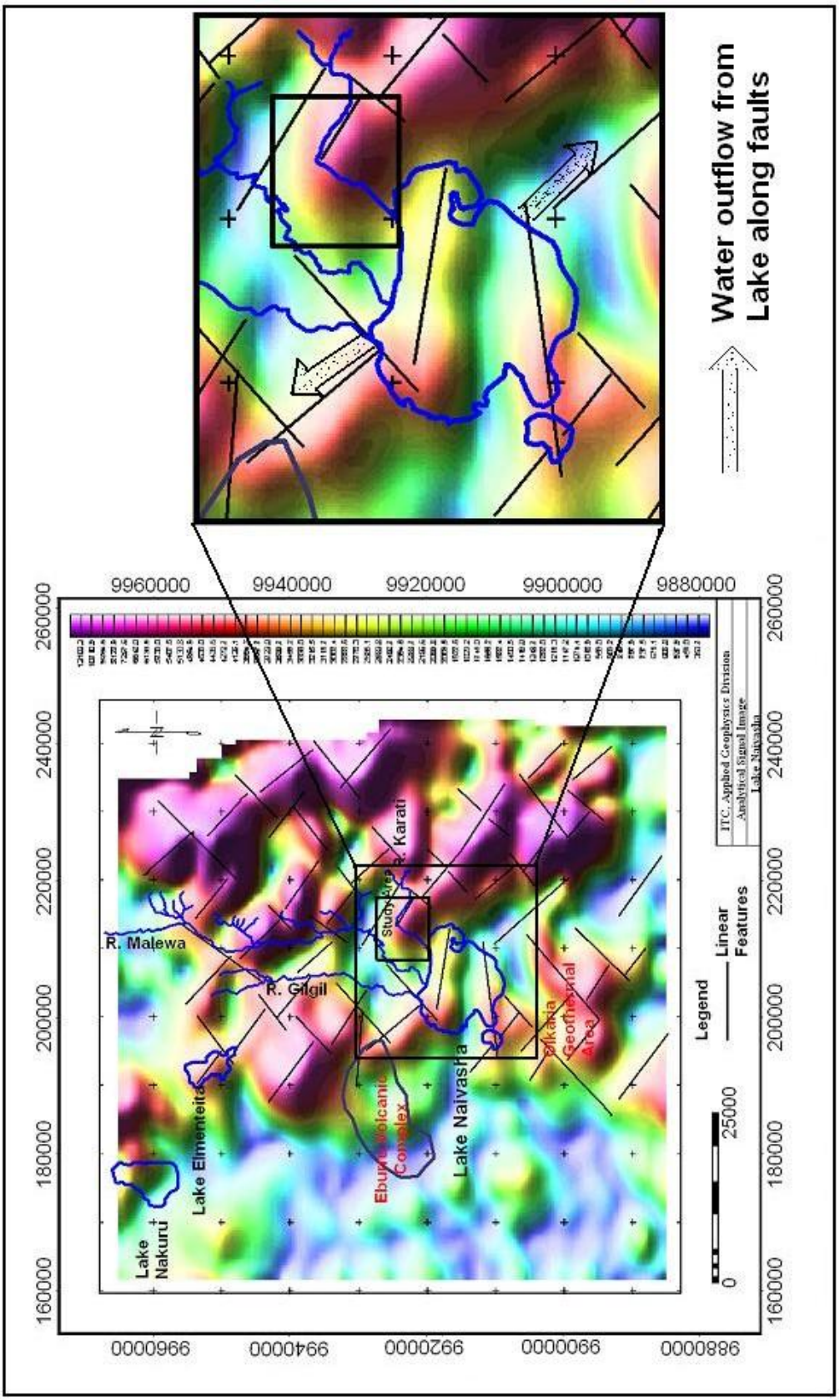

Figure 2.7: Analytic Signal Image

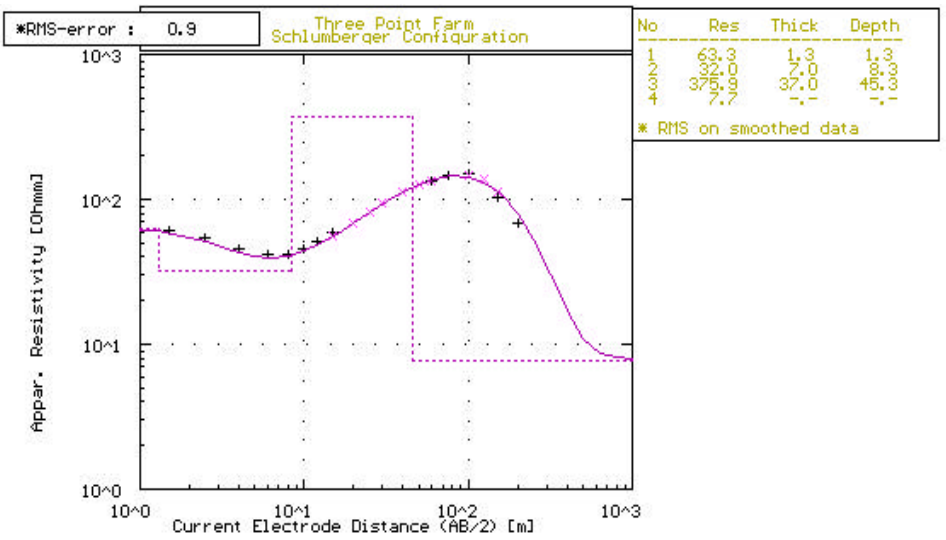

a. VES18 – 200m from the Karati River on the Three Point Farm

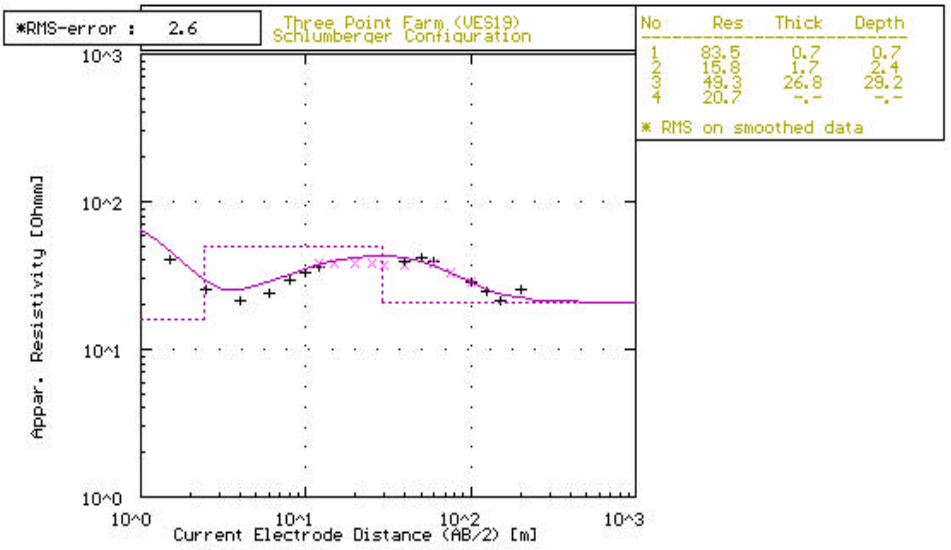

b. VES19 – Eastern part of the trachyte ridge on the Three Point Farm

Figure 2.8: DC Schlumberger soundings *source:* Gressando, (1999)

Chapter 3

Geophysical Survey

3.1 Introduction

A variety of geophysical techniques have been successfully used for groundwater studies, including electrical methods [Zohdy, et al., 1974; Fitterman and Stewart, 1986; Taylor, et al., 1992], seismic refraction [Bonini and Hickok, 1969], gravity [Carmichael and Henry, 1977] and MRS [Roy and Lubczynski, 2000].

Of these, the electrical method (particularly DC Resistivity) is the most commonly utilized because of its user friendliness, low cost as well as availability of interpretational aids [Fitterman and Stewart, 1986]. In the past, such measurements were carried out using arrays of grounded electrodes (Wenner, Schlumberger, dipole-dipole, etc) to inject current into the ground and to measure the resulting potential difference. Though this was often successful, the conventional DC method has always been laborious and time consuming. Addressing these issues and other shortcomings in the interpretation of the DC resistivity data, led to the recent development of the Electrical imaging or electrical tomography technique. It allows for the collection of more data in the same time as in the *"traditional"* profiling and sounding techniques and also useful in areas of both "simple" and "complex" geology. The electrical resistivity imaging method [Griffiths and Baker, 1993] differs from the DC survey in using a multi-electrode array system and in recording the maximum number of independent measurements on the array [Michel et al., 1999].

The use of electromagnetic techniques for groundwater exploration, while not as widespread as the "traditional" DC resistivity and the modern "resistivity imaging", has increased considerably in recent years, especially the Time-Domain (Transient) technique. The physical property measured by the EM method is conductivity (the

inverse of resistivity), a fact that often makes small variations in terrain conductivity to de detected.

3.2 Data acquisition

Detailed 2D Resistivity Imaging and Time-Domain EM surveys were carried out in the *Ilkek* plains, north of Lake Naivasha where Manera Farm (Delamere), Three Point Farm (Panda) and Homegrown Harms are located, from the 14th of September to the 4th of October, 2001. Selected locations, based on the pre-field work study were surveyed with both methods. The TEM soundings were made first, followed by the 2D Resistivity Imaging due to logistical reasons.

Resistivity Imaging and Transient EM were used together in order to compliment one another and also to enhance the interpretation of the subsurface information in terms of conductivity for the aquifer mapping. The output of the 2D resistivity imaging inversion results and layer thicknesses from borehole information could be used to generate the initial model parameters of the 1-D inversion of Transient EM sounding data. The maximum depth investigation in the case of the 2D resistivity imaging was limited to 72m because of the maximum allowable electrode spacing (15m) whereas the Transient EM had a much larger depth investigation (> 100m) with a loop dimension of 75m by 75m.

The use of grounded electrodes in the case of the Resistivity Imaging means it can encounter problems in areas of high surface resistivity, where obtaining sufficient current flow can be difficult. Under such conditions the non-contacting Time-Domain EM can provide terrain resistivity data. The transient EM method allows measurement to be made rapidly and therefore, larger areas could be surveyed in greater detail for comparable time. In general electromagnetic systems are most suited for detecting conductivity targets such as salt-water-saturated sediments and are ineffective in searching for resistive materials [McNeill, 1989; Fitterman, 1988].

3.2.1 2D Resisting Imaging

2D Resistivity imaging involves the deployment of an array of co-linear, equidistant electrodes on the surface of the ground for data collection. The survey technique involves measuring a series of constant electrode separations with the electrode separation being increased with each successive measurement. The sequence of measurements to make, the type of array to use and other survey parameters (such as the

current to use) is normally entered into a text file which can be read by the computer program in the equipment. After reading the control file, the computer program then automatically selects the appropriate electrodes for each measurement [Loke, 2000]. The measured apparent resistivities are then presented in a contoured pseudosection, which reflects qualitatively the spatial variation in resistivity in the vertical cross-section [Griffiths and Turnbull, 1985]. The unit electrode spacing determines the length of the profile, depth of investigation and resolution.

The contoured data can be modeled using a two-dimensional (2D) finite or finite difference algorithm [Dey and Morrison, 1979]. Alternatively the data can be inverted automatically with the commercially available computer program, RES2DINV to provide an image of true resistivity [Griffiths and Baker, 1993].

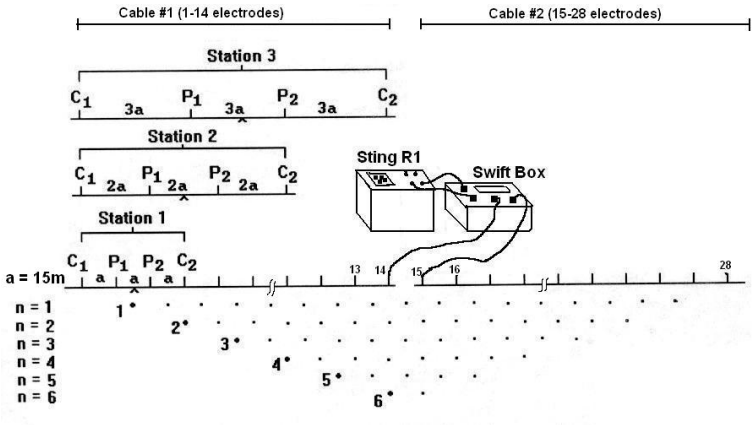

Figure 3.1: Sequence of measurements to build up a pseudo-section using a computer program controlled multi-electrode survey setup

Instrumentation

The 2D Resistivity data were recorded using the STING R1 (Memory Earth Resistivity Meter) by Advanced Geosciences Inc (AGI). The complete system consists of the Sting instrument console, the Swift interface box (the electronic switching unit), Sting to Swift communication cable, Sting to Swift ABMN cable, Swift-cables with addresses 1-14 (cable no.1) and 15-28 (cable no.2) totalling 28 smart electrodes and stainless steel electrode stakes. The Sting R1 can be used in four basic modes, namely the Manual, Automatic, User and PC modes. More information on these can be obtained from the Sting R1 Instruction Manual [RES2DINV, 2000].

In this survey, the User mode was used. This allows the user to program any

automatic array *command file* in a computer and download the command file into the Sting. The Sting/Swift can then be used in the field to record data, without having to carry the fragile computer to the field.

Measurement procedure

Three command files were created to record "Wenner-Schlumberger" *"roll-along"* data at a 15m electrode separation (Figure 3.1) within the user mode option of the Sting. The three command files were designed to measure different parts of the profile line. The first spread begins with cable1 followed by cable2 with electrodes 1-14 and 15-28 respectively. Measurement commences at electrodes 1, 2, 3, and 4 using its corresponding command file. The spacing is then doubled with active electrodes becoming 1, 3, 5, and 7. At each measurement, spacing is increased by one unit until the maximum spacing is reached (n = 10 in the case of 28 electrode arrays) see Figure 3.1, after which the sequence is repeated starting with electrodes 2, 3, 4, and 5. After collecting data for the whole spread, the electrodes 1 to 14 are picked up and moved to the front of the line, the cable shifted forward and reconnected. The electrode order now becomes 15-28 and 1-14. Measurements were carried out with the designed corresponding command file in which overlapping measurements are avoided. In the third spread the electrodes 15 to 28 and the cables are moved forward such that the electrode sequence becomes similar to the first. However, its corresponding command file omits taking double (overlapping) measurements. This process is repeated until the traverse is completed.

Giving the maximum allowable electrode spacing of 15m by the equipment, and an array of 28 electrodes, some constraints were consequently placed on the length of profiles and the depth of investigation. Wenner-Schlumberger spread with an array of 28 electrodes, and the maximum inter-electrode spacing, (a), of 15m, gives the maximum possible measurement separation of 150m with $n = 10$ (*dipole number*). Half of the maximum possible measurement separation is the guide for the depth of investigation (75m). The Horizontal distance for one spread is 405m. The true depth after inversion of the data can be approximated to one-sixth ($\frac{1}{6}$) of the horizontal distance of one spread, 67.5m.

In the field, the data collection always starts with placing the stainless steel electrode stakes into the ground at intervals of 15m along selected lines. The swift cables are then laid out on the ground and a rubber band is used to tie the *"smart" electrode* to its electrode stake, making sure that there is a electrical contact between them. The switching on and off of the *"smart" electrodes* are controlled automatically

by the electronics in the swift box. The electrode stakes were mostly watered with ordinary water and sometimes saltwater in parts north of the farms that have been left un-ploughed for a long time.

The cables of electrodes 14 and 15 are then connected to the Swift box. The Sting and the Swift are also connected as shown in Figure 3.2. The details of the traverse from which data is to be collected are entered into the Sting and made ready for data collection. A contact resistance test is run to check for poorly connected electrodes or abnormally high contact resistance reading. The actual measurement was carried out after the contact resistance test output gave good results, otherwise, the causative electrode(s) were checked and properly connected or watered some more. It took between 30 to 45 minutes to complete one spread, so during the data collection period a new survey section was prepared for the next spread. The start and end locations of survey lines were mapped with a Global Positioning System (GPS). The Resistivity Imaging lines were carried out more or less along the Time-Domain EM sounding profiles.

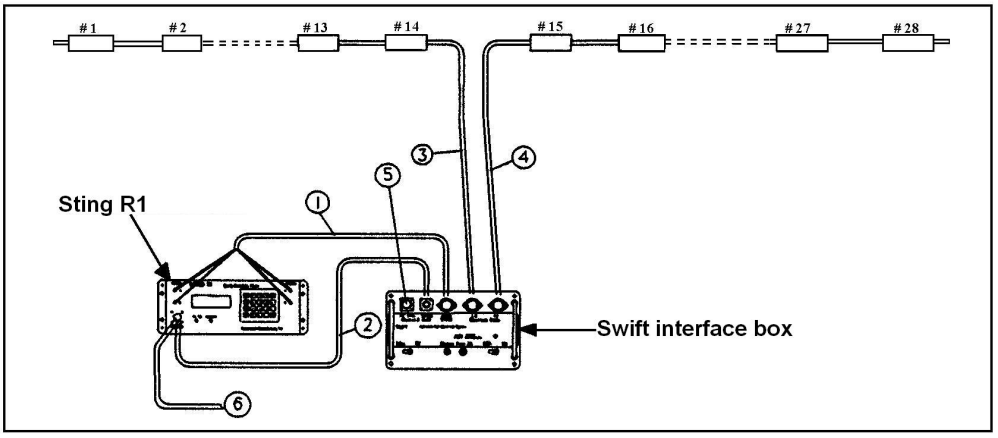

Figure 3.2: Sting-Swift connection. 1=ABMN cable, 2=Sting-Swift communication cable, 3=Swift cable with numbers (1-14), 4=Swift cable with numbers (15-28), 5=receptacle for PC connection, 6=optional connection to 12V DC battery.

After a successful collection of data from a particular spread, the measured apparent resistivity data was downloaded to a Laptop. Negative data are automatically removed during this process. The cable and electrodes to be moved forward in the case of *roll-along* surveys are then picked taken to its new location. In all, fourteen (14) profile lines were surveyed, including one "instrument test" profiles, see Figure 3.11. Majority of the survey time was used in the packing, carrying and laying out

Figure 3.3: The author setting up the AGI sting and swift devices to collect 2D resistivity image measurements

of cables, 'hammering-in' of the metallic stakes, tying of the electrodes to the stakes and watering of the electrodes. The main factors that determined daily progress included, the battery's power supply, the weather condition (rain and thunderstorms) and terrain accessibility (obstructions). The longest and the shortest traverses made in a day by a crew of 4 depending on the factors outline earlier were approximately 1km and 600m respectively.

The survey area, especially *"Three Point Farm"* had a lot of buried water "plastic" pipes lines and electricity cables in the ground. The approximate locations of these sources of cultural noise in the Three Point Farm are sketched in Figure 3.12. The approximate depths of burial of these pipes and electricity cables are between 1 to 2m. Therefore with 15m electrode spacing in the 2D resistivity imaging, any material within the shallow layer of 0 - 4m have little or no effect on the data collected as the setup collects data from depths beyond 4m. Line2 was one particular traverse that was carried out in an area several of the buried features existed. The results is shown in Figure 3.4.

All, except survey *"Line10"* were carried along the same traverse line made with TEM soundings. The first three(3) Profiles were carried out on the Three Point Farm. Profile Line1 was made because TEM soundings were carried out along that place to investigate the effect of the metallic overhead irrigation structure of pivot A and the nearby high tension electric power lines (see Figure 3.12). Line 2 starts from the area close to the "Well-field" and runs across pivot B towards the Karati river in an

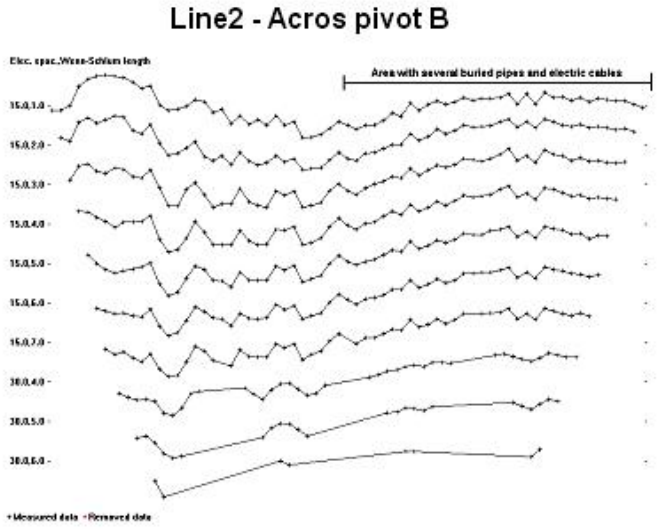

Figure 3.4: Effect of buried pipes and electric cables on Line2

approximately N-S direction to map the aquifer material of boreholes B and B1. Line 3 begins the foot of the Trachytic Ridge and runs also, across Pivot B in an approximately E-W direction to study the subsurface effect of the ridge. Profile Line 7N was the only one carried out in the Homegrown Farm, where the lithology is believed to be partly of alluvial nature due to the nearby Malewa river. The remaining traverses were made in the Manera Farm. Profiles Line 8N and Line 10 were carried out in the area of center pivots 10, 11 and 12 (*cf* Figure 1 in the Appendix) where trachytes are encountered in boreholes at an approximate depth of 40m. Line10 was carried to map *hard rock* that was reported to have been struck at depths 30m in a borehole that was being drilled on the Manera Farm at the time of the fieldwork. The rest of the profiles were spread out to cover the remaining parts of Manera Farm where Borehole numbers 2, 5, 6, 7 and 8 are located (*cf* Figure 1 in the Appendix).

3.2.2 Time-Domain (Transient) EM

The use of Time-Domain electromagnetic (TEM) technique for groundwater exploration, though not as wide spread as other electrical geophysical techniques (DC resistivity and Resistivity imaging) has increased considerably in recent years . Examples of its applicability to groundwater exploration include among others; characterizing local ground water system in arid alluvial environment [Taylor et al., 1992], detection of salt or brackish water interfaces in fresh water aquifers and determina-

Table 3.1: 2D Resistivity Imaging Survey profiles

Profile	Begin	co-ordinates	End	co-ordinates	Length(m)	Farm
Line1	213889.50	9925676.68	213497.71	9925403.39	405	Three Point
Line2	213638.38	9925221.53	214199.46	9924317.31	1005	Three Point
Line3	214318.50	9925042.95	213483.71	9924564.08	1005	Three Point
Line4E	213328.45	9923995.34	212938.16	9924741.10	405	Three Point
Line4W	212696.93	9924776.09	212006.61	9924940.10	600	Manera
Line5	213112.69	9924160.76	212704.64	9923613.44	600	Manera
Line5N	212694.22	9924350.81	212480.29	9923987.57	405	Manera
Line6	212491.30	9924494.64	212131.19	9923995.34	600	Manera
Line7N	212834.45	9926293.91	213186.89	9925793.08	600	Homegrown
Line7S	213202.65	9925665.16	213202.65	9925060.87	600	Manera
Line8N	213576.81	9924402.98	214401.51	9923908.35	1005	Manera
Line9	212027.60	9923743.28	211383.01	9922815.82	810	Manera
Line10	214224.75	9923790.09	213745.83	9923146.97	600	Manera
Line11	213400.82	9924841.94	212744.81	9924565.73	600	Manera
				Total	8,430m	

tion of hydro - stratigraphy [Fitterman and Stewart, 1986].

Transient EM soundings are carried out with a receiver and transmitter loops. The loops are usually either circular, square or rectangular. A steady current is run through the transmitter loop for sufficiently long time to allow turn-on-transients in the ground to dissipate. The current is then sharply terminated in a controlled fashion. In accordance with Faraday's Law, an electromotive force (emf) is induced in the ground. This emf causes horizontal loops of eddy currents to flow in the ground, expanding in radius and diffusing to greater depths with the passage of time (Figure 3.10). By measuring the decaying secondary magnetic fields from these eddy currents (or more accurately the time derivative of the decaying magnetic field, dB/dt), information is derived from successively greater depths. The values of dB/dt are converted to an apparent resistivity as a function of time, from which a layered earth interpretation can be made using techniques analogous to those for the conventional DC resistivity soundings. The signal recorded by the receiver is called a transient. Several hundred transients are typically recorded and averaged to reduce the effect of background EM and instrumental noise [Fitterman, 1986]. The transient decays quickly with time and therefore it is necessary for the receiver to have a wide dynamic range. A principal advantage of this technique is the high degree of lateral resolution, together with relatively good rejection of localized resistivity inhomogeneities, [McNeill, 1989].

It is important to indicate that since transient-field measurements are made after

the primary field has been turned off, the transmitter loop can also double as the receiver. Figure 3.5 shows this and other common layouts. Factors affecting the choice of configuration type include the amount of space available to lay out the loop and the labor-intensity of each configuration

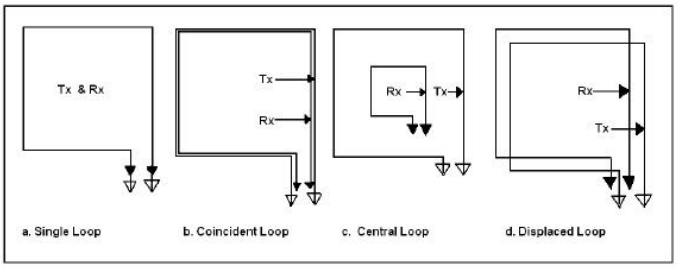

Figure 3.5: Commonly used transmitter (Tx)-receiver (Rx) loop configurations

Instrumentation

Measurement of the TEM soundings were carried out with the Russian TEM-FAST 32 ProSystem, kindly made available by the University of Freiberg, Germany. It is a device designed for easy and fast electromagnetic sounding with high efficient operation under all kinds environments and conditions [AEMR, 1996]. TEM-FAST ProSystem operates with any compatible (Notebook or Laptop) computer using a standard interface RS 232 (*cf* Figure 3.6). The computer controls the operations of the instrument and visualization of measurements. The instrument itself is small ($290mm \times 207mm \times 60mm$), light (2.1 kg) [AEMR, 1999] and easy to carry over long distances and difficult terrain (*cf* Figure 3.6).

TEM-FAST ProSystem generates in the transmitting unit unipolar current pulses and the receiver measures the amplitude of the current pulses' induced in the receiver loop in different moments of time (delay times). Power supply to the equipment can be from its internal battery ($12 - 13.5$ V) or an external battery ($12 - 13.5$ V). TEM-FAST 32 has 32 geometrically spaced time gates to measure the transient within a time range of $4 - 1000\mu s$. It has a fixed transmitter current of 1 Amp and the loop sizes can vary from $5cm \times 5cm$ to $100m \times 100m$. The instrument sensitivity is $\approx 1\mu V$.

To improve the signal/noise ratio, the process of measurements is done in two stages in TEM-FAST:

* analog stacking of the E.M.F. pulses and
* digitizing of analog signal and numerical stacking.

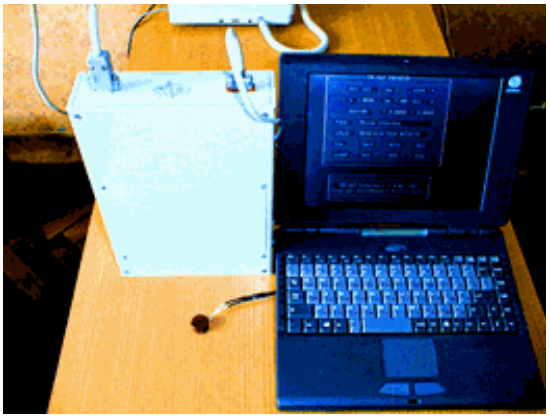

Figure 3.6: The TEM-FAST 32 equipment

The option of numerical (digital) stackings, also called the "stack parameter" is determined by the user. It ranges between 1 and 15. One stack contains 6 sets of analog stackings with n current pulses (a function of the sensitivity value), refer to Table 3.2. TEM-FAST has five sensitivity parameters options (from 1 to 5) that determines the main pulse characteristics, i.e. the period of current pulse's repetition (ms), the number of integrated pulses and the number of active channels. Details on these specifications can be obtained from the TEM-FAST Manual and Table 3.2.

Table 3.2: Details of the Sensitivity parameters of TEM-FAST

Table a

Number of Sensitivity range (Sen)	Base period of current pulse's repition, ms	No. of Integrated pulses	No. of active channels
1	5	64	1 -- 32
2	2.5	128	1 -- 28
3	1.25	256	1 -- 24
4	0.625	512	1 -- 20
5	0.3125	1024	1 -- 16

Table b

	Sensistivity (micro-Volt)				
No. channel	Sen = 5	Sen = 4	Sen = 3	Sen = 2	Sen = 1
1 -- 4	8*k	16*k	32*k	64*k	128*k
5 -- 8	4*k	8*k	16*k	32*k	64*k
9 -- 12	2	4	8	16	32
13 -- 16	1	2	4	8	16
17 -- 20	not active	1	2	4	8
21 -- 24	not active	not active	1	2	4
25 -- 28	not active	not active	not active	1	2
28 -- 32	not active	not active	not active	not active	1

The k co-efficient can be switched in the equipment plate and it takes the values of k=1 or k=7.05

It must be indicated here that the depth of such investigation of transient EM depends mainly on factors such as the strength of the transmitter pulse which also depends on the amount of current, the loop size and resistance, and also on the local

physical properties of the earth. A high current gives a stronger transmitter pulse which in turn gives a stronger received signal. The output current level is set by the transmitter's electronics in combination with the length of the loop size. In this instrument, the controlling factor of the wire length is the electric resistance of the wire (5 - 8 Ohm). This therefore allows a maximum loop length of 300m.

TEM data collection

A single square loop configuration of dimensions 75x75m (the maximum allowable) was used in the TEM soundings. Exploratory surveys demonstrated that a depth of 100m or even more could be achieved with the transmitter current of 1 Amp, as the target aquifer in the area is reported to be between 30 to 80m depths or even less near the lake. However, it was later recognized that in more conductive areas (clays or saline water) the depth of investigation was reduced to less than 80m with same instrument and loop configuration due to attenuation. Test soundings were carried out with different sensitivity parameters between 1 - 5 and different stack values also between 1 - 5 at two different locations near the Three Point Farm offices to check the effect of the cultural features like the electric power line and metallic structures nearby. The results of these test soundings gave similar response with the different sensitivity and stack parameters. Figure 3.7 shows $\rho_a(t)$ curves of the test measurements at the two different locations. The influence of self-transient is visible up to $t = 8\mu s$, while noise is seen at later stages, especially in those close to the electric poles and wires. A stack of 5 and sensitivity parameter of 1 were chosen because theoretically they offer the greatest possibility of collecting more readings and more active channels $(1 - 32)$. With $Stack = 5$ and $Sen = 1$ the system produces and analyzes $5 \cdot 6 \cdot 64 = 1,920$ pulses while at the same time in the analog regime there is averaging of 64 pulses and 30 digital codes for each active channel by the TEM-FAST ProSystem, (refer to Table 3.2).

To be able to construct an image of the subsurface, the survey was conducted along profiles with sounding location spacing of 75m. Some survey lines were made to intercept each other in areas where much detailing was required, especially in sites where good yields are reported. The layout of the Time-Domain EM loops adopted for a speedy survey is as shown in Figure 3.9. The location of all the TEM soundings in principle is represented by the loop center, which meant that in this work, the survey lines are offset laterally by 37.5m from the Resistivity Imaging lines. However, in this study, the location of the loop centers by mere visual inspection in the field was considered not to be very accurate and therefore loop corner (usually where

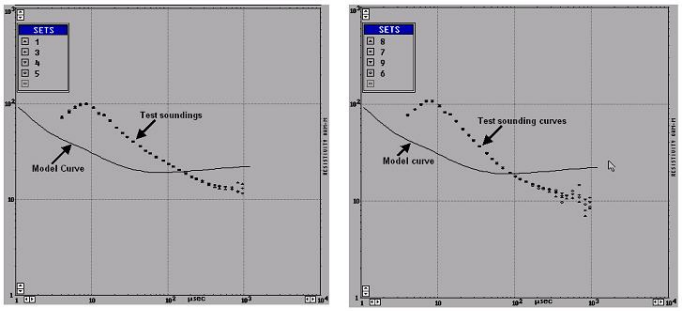

a. TEM test soundings about 50m away from the Office of Three Point Farm.

b. TEM test soundings near an overhead electric wire about 200m from the Office of Three Point Farm

Figure 3.7: Test TEM sounding output at locations near the office of the Three Point Farm

the TEM-FAST equipment was located was adopted) see Figure 3.9. The TEM-FAST equipment, as the name suggests, indeed works fast, it took between 10-15 minutes per sounding. A four-person crew was able to take 20 to 25 soundings per day. The location co-ordinates of the loop corners were recorded with a Global Positioning System (GPS). In all 12 profiles with a total of 137 soundings were carried out over the entire study area, see Figure 3.11. The reasons for the selected survey lines have discussed in section 3.2.1.

Some of the TEM soundings were seriously affected by the presence of the buried water pipes and the electricity cables. Also soundings close to the Trachytic Ridge on Three Point Farm had much noisier *late time* results. Examples of 2 soundings that were seriously affected and 2 nearby soundings that were not affected by the buried materials on Line 2 are shown in Figure 3.8.

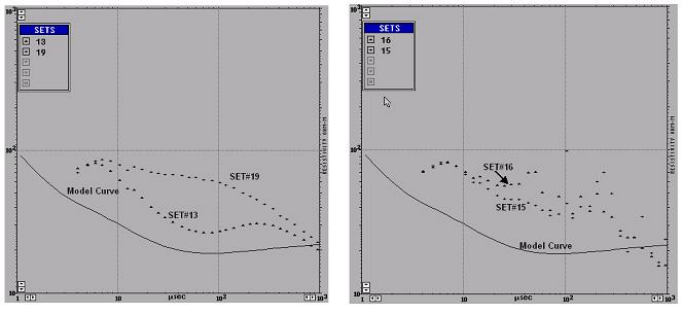

a. Two good soundings, one before and one after the buried pipes and electric cables on traverse Line2.

b. Two soundings affected by buried pipes and electric cables on traverse Line2.

Figure 3.8: Examples TEM soundings affected by buried materials and soundings that were not affected

Table 3.3: Details TEM Soundings

Traverse	No. of Soundings	Soundings Details	Profile Length (m)	Remarks
Line1	4	TEMS4 - TEMS7	300	Three Point Farm
Line2	12	TEMS8 - TEMS19	900	Three Point Farm
Line3	12	TEMS20 - TEMS31	900	Three Point Farm
Line4	20	TEMS32 - TEMS51	1500	Manera Farm
Line5	10	TEMS52 - TEMS61	750	Manera Farm
Line6	10	TEMS62 - TEMS71	750	Manera Farm
Line7N	9	TEMS73 - TEMS81	675	Homegrown Farm
Line7S	11	TEMS82 - TEMS92	825	Manera Farm
Line8N	12	TEMS93 - TEMS104	900	Manera Farm
Line8S	5	TEMS105 - TEMS109	375	Manera Farm
Line9	16	TEMS122 - TEMS137	1200	Manera Farm
Line10	22	TEMS110 - TEMS121	1650	Manera Farm

Note: TEMS1, TEMS2, TEMS3 and TEMS72 were isolated soundings.

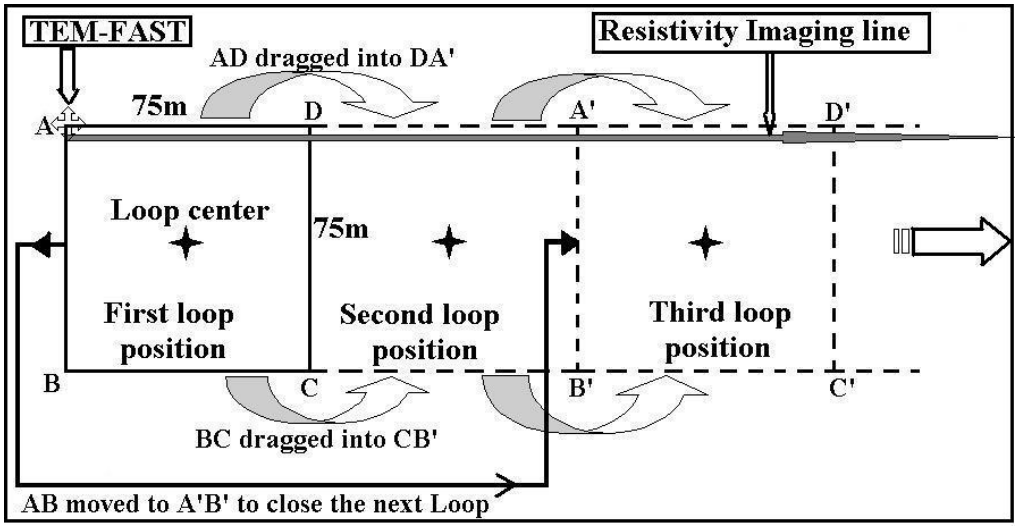

Figure 3.9: Survey Layout of TEM Soundings 2D Resistivity imaging profiles.

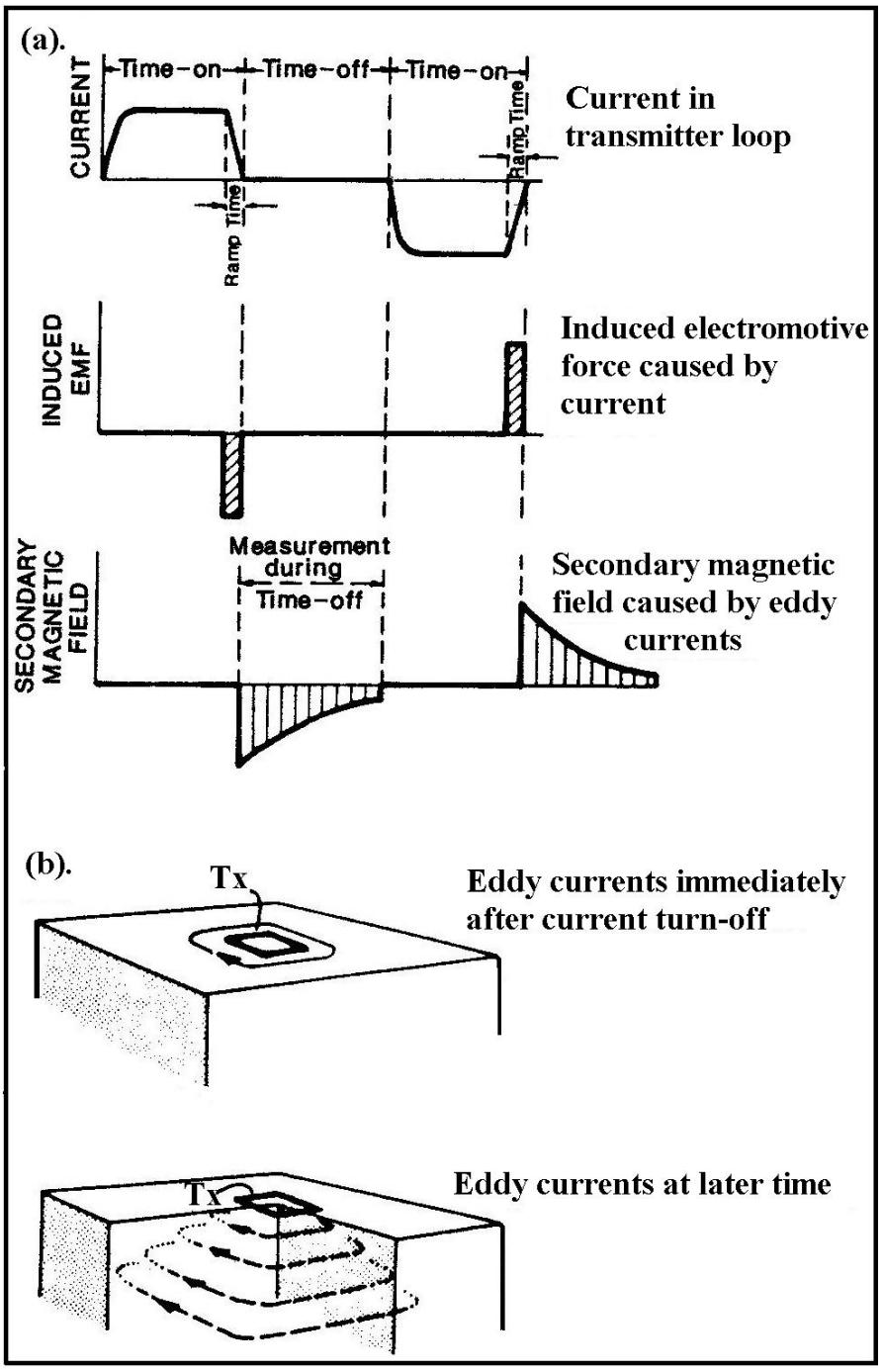

Figure 3.10: Time domain EM waveforms (a) and homogeneous half - space current flow (b)

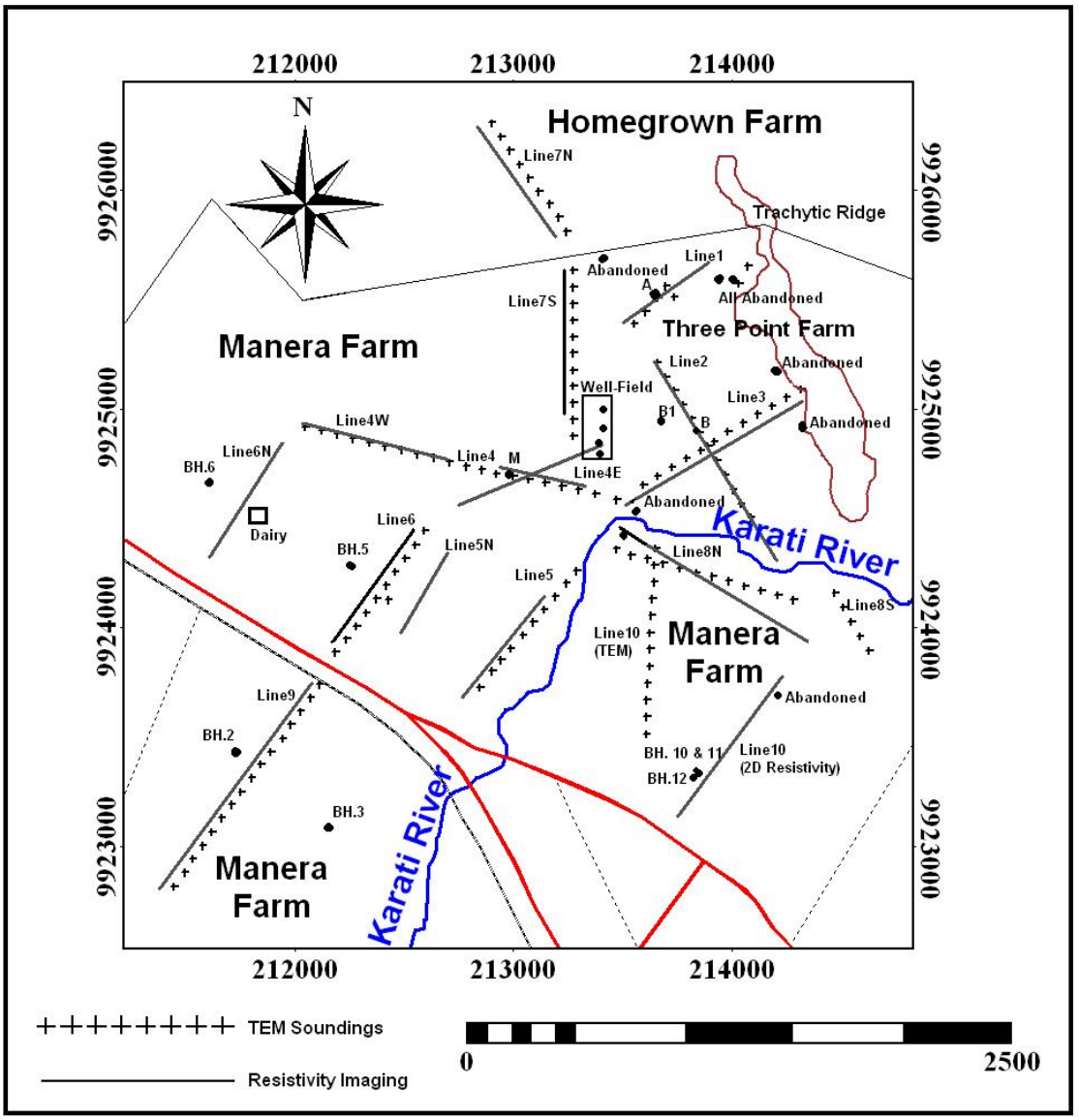

Figure 3.11: Time Domain EM Sounding Positions and Resistivity Imaging profiles locations.

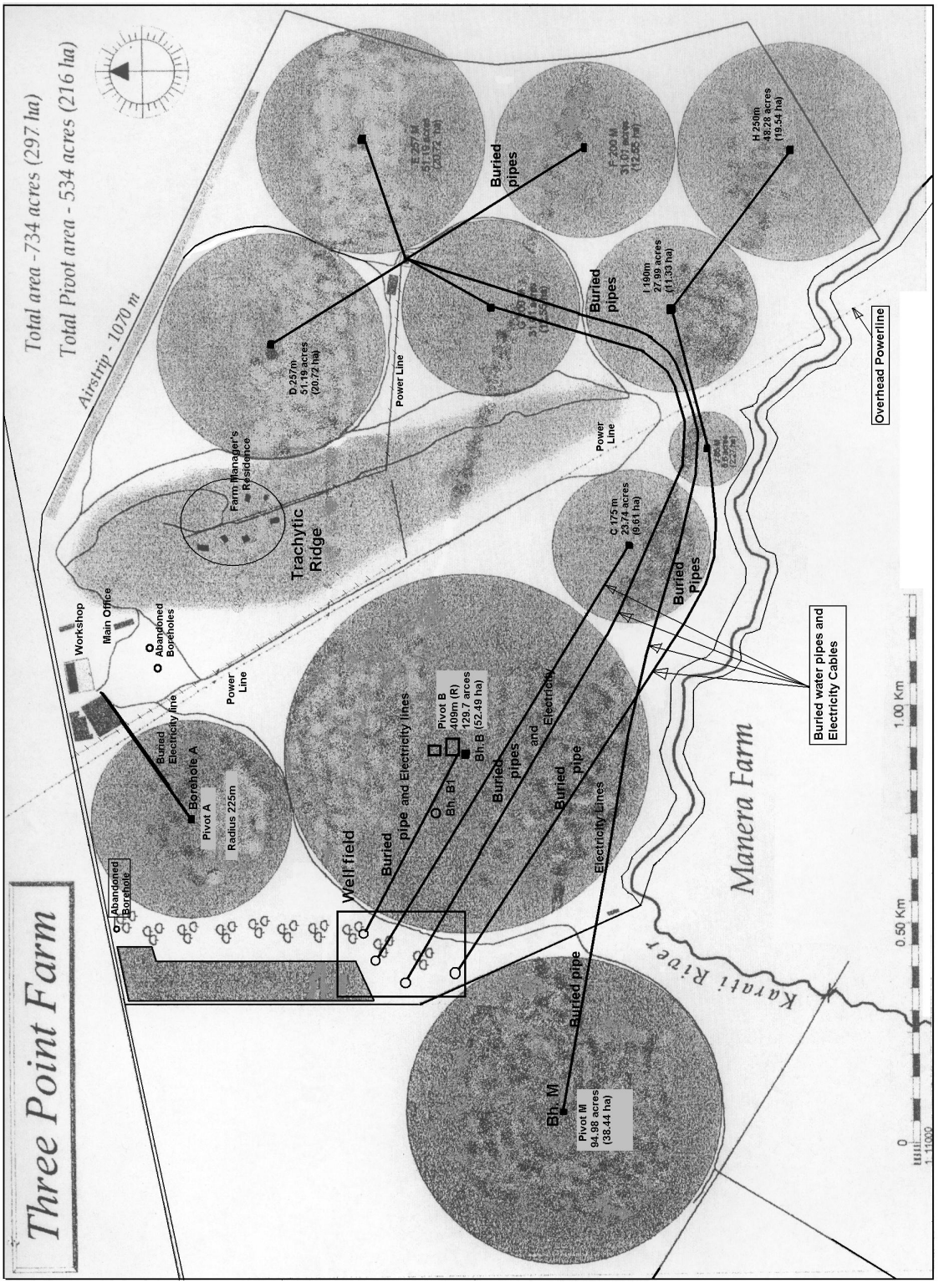

Figure 3.12: Approximate location of buried pipes and electricity cables in Three Point Farm

Chapter 4

Data Processing and Analysis

4.1 2D Resistivity Imaging

4.1.1 Introduction

RES2DINV software package was employed in the processing of the Resistivity Imaging Data. **RES2DINV** is a computer program designed by Loke, (1997) to invert the *"apparent resistivity"* data obtained from electrical imaging surveys into a two-dimensional (2D) *"true resistivity"* model of the subsurface in an automatic and robust manner with minimal input from the user. Therefore the program basically determines a resistivity model that approximates the measured data within the limits of data errors and which is in agreement with all *a priori* information.

The program first subdivides the subsurface into a number of rectangular blocks, the arrangement of which is loosely tied to the distribution of the measured data points in the pseudosection but it can also be manipulated. It then determines the resistivity of the rectangular blocks that will produce an apparent resistivity pseudosection that agrees with the actual measurements. It is worth stating that for the same data set, there would be a range of equivalent models whose calculated apparent resistivity values would agree with the measured values to the same degree. Thus the program takes off by not only trying to minimize the difference between the measured and the calculated apparent resistivity values, but the inversion method also attempts to reduce other quantities that will produce certain undesired characteristics in the resulting model [Loke, 2000, Loke and Barker, 1996].

The **RES2DINV** program uses a forward modelling subroutine (smoothness - constrained method) to calculate apparent resistivity values and a non-linear least-

squares optimization technique [deGroot-Hedlin and Constable, 1990] for the inversion routine. As indicated earlier, the optimization method tries to reduce the difference between the calculated and the measured apparent resistivity values by adjusting the resistivity of the model blocks [RES2DINV, 2000]. The difference between the measured and calculated apparent resistivity values is given by the root-mean-squared (RMS) error.

4.1.2 Data procession procedure

The ***AGI* Sting** data were downloaded to a computer where bad data, particularly negative values are deleted in the process by the program. These raw Sting data files are converted with the 2D-CONV.EXE software into the appropriate format *(·DAT)* readable by the inversion software RES2DINV.EXE. The individual ($\cdot DAT$) input files for all the resistivity imaging survey lines were generated and made ready for inversion into 2D "true resistivity" image in the program.

The routine practise is to open a file of a particular traverse results, and view the apparent resistivity data values in a form of profiles for each data level and to *eliminate or remove* any inherent bad datum points. The main reason for this step is to manually remove bad data points (i.e. obviously too large or too small compared to the neighboring data points). Though, careful procedures were adopted in the field, during the data collection, nevertheless, bad data could come from sources such as, the failure of the relays at one of the electrodes, poor electrode-ground contact due to dry soil, or shorting across the cables due to the very wet ground conditions. If such data points occur, then they must be removed, else they can influence the final output model.

After editing the input data, inversion of the data set was then carried with least-squares inversion routine. The depths of layers were adjusted to coincide with known depths from boreholes if available. In this way the influence of equivalence on the inversion results is reduced. A model was accepted at the iteration beyond which the RMS error does not change significantly. This usually occurred between the 5th and 8th iteration. The final output file displayed after inversion was the measured and the calculated apparent resistivity pseudo-sections and the true resistivity model section as shown in Figure 4.2.

The Digital Elevation Model (DEM) of the study area was created from the topographic map of the area (WRES, ITC Database). The elevation values on the survey lines were obtained from the DEM and fitted to all the 2D Resistivity Imag-

ing model produced in the RES2DINV by entering the location of the electrodes and the elevation values into the $\cdot DAT$ in the acceptable format by the program [RES2DINV, 2000].

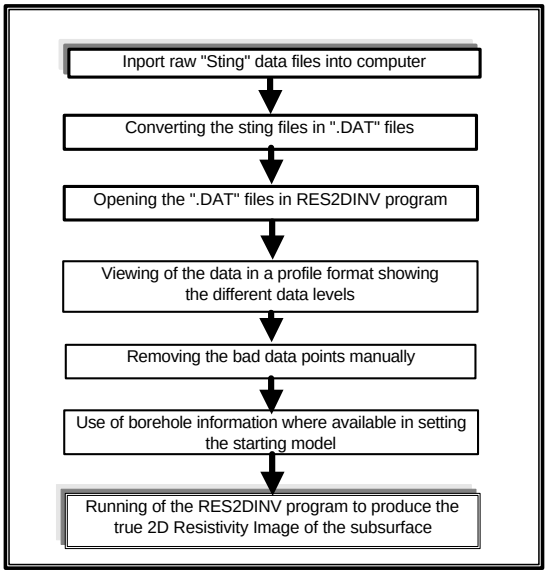

Figure 4.1: 2D Resistivity Imaging data processing flow chart

4.2 Time-Domain (Transient) EM

The "TEM-FAST 32" data were processed with the **TEM-RESearcher (TEM-RES)** package developed by the *Applied Electro - Magnetic Research* in the Netherlands and delivered with the equipment. The TEM-RES program offers several data processing possibilities. Among them is the possibility of inversion of the field data in an eight-layered horizontally uniform earth model, with opportunity to constrain any of the resistivity (ρ) and depth (h) parameters with all *a priori* information. Details on the TEM-RES program can be found in the TEM-RESearcher manual [AEMR, 1996].

The following are the processing steps of the TDEM field data in the TEM-RES program.

- The program offers the opportunity to visualize five TEM sounding data in one graph. These data are displayed with the program's theoretical curve in a graph with time in μs on the horizontal axis and the apparent resistivity on the (ρ_a) in Ohm.m on the vertical scale. All values of the measured process *E(t)* which are less than 0, are ignored automatically and cleared from the screen.

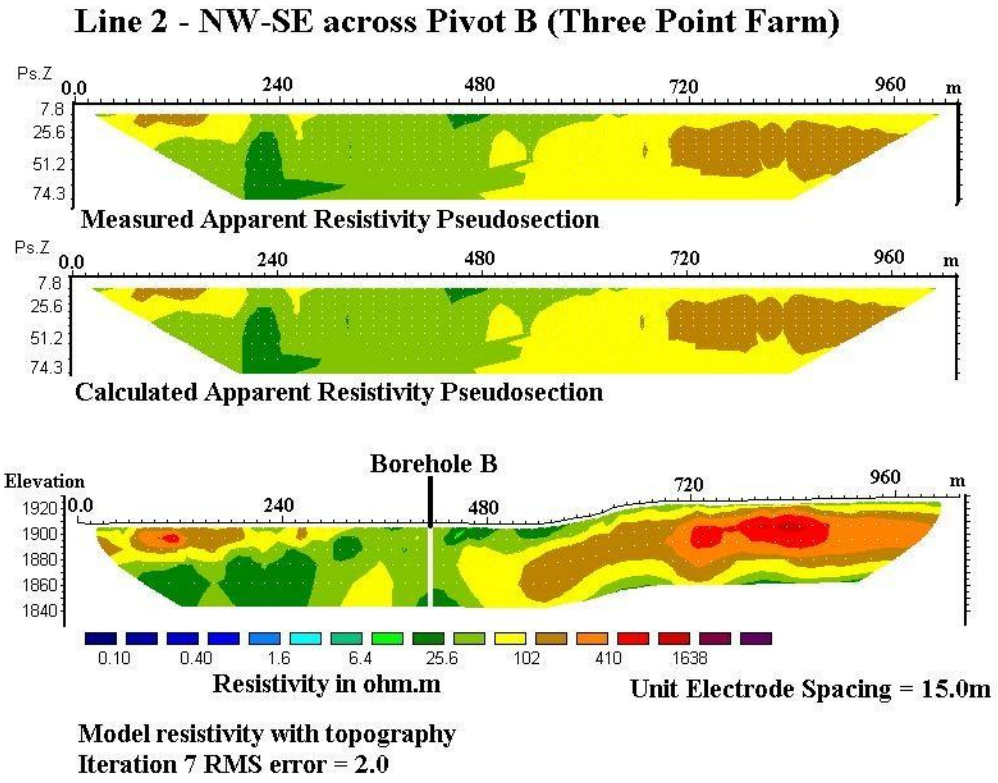

Figure 4.2: Observed and calculated apparent resistivity pseudo-sections of Line2 together with the topography incorporated model section

- A sounding data is selected at a time and smoothed to obtain a continuous averaged representative curve. However, before smoothing points with very large errors were removed manually. The smoothing process ignores automatically values of *E(t)* < 0 and points having large errors. The smoothing technique used by the program is the exponential spectra approach, represented as;

$$min \sum_{i=1}^{N} \left\{ w_i (E_i - E_i^*)^2 \right\}, \tag{4.1}$$

where E_i is the field value which is the amplitude of the transient process for a delayed time t_i and w_i is the weight factor which also depends on errors in initial data (E_i), also

$$E_i^* = \sum_{j=1}^{M} A_j exp(-s_j t_i), \tag{4.2}$$

an approximation function, which is the sum of exponential components $M < N$(s_j - given parameters) with constraints on exponents' amplitude A_j imposed.

These constraints do change the result of smoothing by allowing for the calculation of the derivatives of any order with restrictions on their monotony $(-1)^n d^n E(t)/dt^n > 0$ for any t and n [AEMR, 1996].

- After smoothing the field data, initial or base model parameters are established by consulting all *a priori* information. These included obtaining layer thicknesses and resistivity values from boreholes where available and the 2D Resistivity Imaging outputs respectively. After selecting an acceptable base model for a particular set of measurements, the parameters were then saved in the program. An 8-layered model section and in some cases 5-layered model were used in the inversion because of the very thin nature of the subsurface materials and also because it provided a better fitting than the other options.

- The next step was the transformation of the field data E(t) into a gradient pseudo-section $\rho(h)$ by the program. Four different algorithms of inversion options are available, the *Simple, Soft, Optimum and Strong*. The transformation equations involved in the inversion algorithms as presented in the TEM-FAST user manual, (1999) are as shown below.

  Simple

  $$\rho^*(t) = \rho_*(t); h(t) = \sqrt{(t\rho_*(t)/\mu_o)} \tag{4.3}$$

  where $\rho_*(t)$ is the apparent resistivity in normalization on all stages of process, $\rho^*(t)$ is the transformed apparent resistivity, h(t) is the apparent depth and μ_o is the magnetic permeability of vacuum $(4\pi \cdot 10^{-7}$H/m).

  Soft

  $$\rho^*(t) = K^+(t)\rho_*(t); h(t) = \sqrt{(t\rho_*(t)/\mu_o)} \tag{4.4}$$

  $K^+(t) = 1$ if $\partial\rho_*(t)/\partial t \leq 0$ and differs from 1 if $\partial\rho_*(t)/\partial t > 0$. The form of the function $K^+(t)$ is rather complicated and fitted empirically on the basis of the analysis of experimental and model data. This transformation emphasizes high resistivity layers in the section.

  Optimum

  $$\rho^*(t) = K^{\pm}(t)\rho_*(t); h(t) = \sqrt{(t\rho_*(t)/\mu_o)} \tag{4.5}$$

  Function $K^{\pm}(t)$ differs from 1 if $\partial\rho_*(t)/\partial t$ differs from 0. This transformation works well practically for majority of geo-electrical sections.

  Strong

  $$\rho^*(t) = K^{\pm}(t)\rho_*(t); h(t) = \sqrt{(t\rho^*(t)/\mu_o)} \tag{4.6}$$

This transformation works well when there is poor contrasts in sections.

A combination of the first three transformation algorithms Simple, Soft and Optimum in that order gave very good fits for most of the data except for a few where the "Strong" transformation algorithm was applied especially in soundings characterized by small resistivity contrasts. The result of the inversion of the data was saved into a txt-file (where the exact location and altitude values were entered) for later construction of an *apparent depth* geo-electric section along profiles. Sounding positions were connected to form profiles from the output of the txt-file and a pseudo-section of apparent resistivity $\rho(h)$ along the profile constructed by the program (see Figure 4.4).

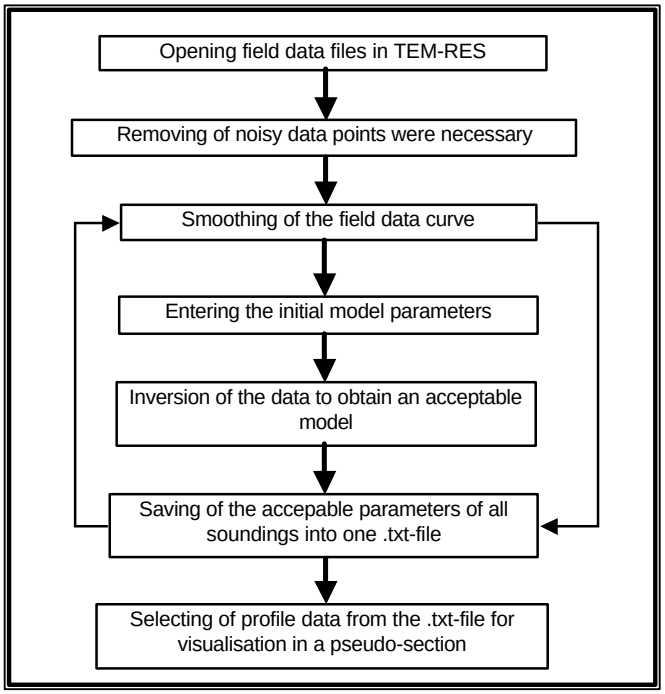

Figure 4.3: TEM data processing flow chart

The output of the $\rho(h)$ transformation data was imported in "Oasis Montaj" program where bi-directional gridding of the apparent resistivity data was carried out and presented in a 2D colored image. This presentation of the output was similar to the 2D Resistivity Imaging output from the RES2DINV output. The inversion results and Borehole data were also manually contoured for a true resistivity and true depth output for Lines 2 and 3 (see Figures 4.5 and 4.6).

4.3 Resistivity Imaging versus the TEM Inversion results

The inversion results of the 2D Resistivity Imaging data with the **RES2DINV** program and the TEM data with **TEM-RES** gave similar patterns of distribution of the subsurface resistivity. 2D Resistivity imaging output represented the *"true resistivity"* and *"true depth"* parameters of the subsurface materials whiles the TEM results represented the *"apparent resistivity"* and *"apparent depth"* parameters. However, the TEM results can be said to approximate fairly well with the real situations and the 2D resistivity imaging results, particularly in terms of its layer thicknesses. This was possibly due to the use of both borehole information and the resistivity imaging results as the base model for the TEM inversion. However one clear distinction between the two inversion results is in their ranges of resistivity values. The resistivity imaging results gave values in the range of 0.1 to 2130 Ohm.m while the TEM resistivity values were in the range of 0.1 to 125 Ohm.m. This indicates that though, transient soundings can be used to detect resistive zones which may be associated with fresh water; it cannot assess the actual resistivity of these zones. The 2D resistivity imaging provided a solution to this limitation and also gave enough resistivity contrasts within the clay, silty clays and the fine sand materials that were difficult to clearly discriminate in the TEM results.

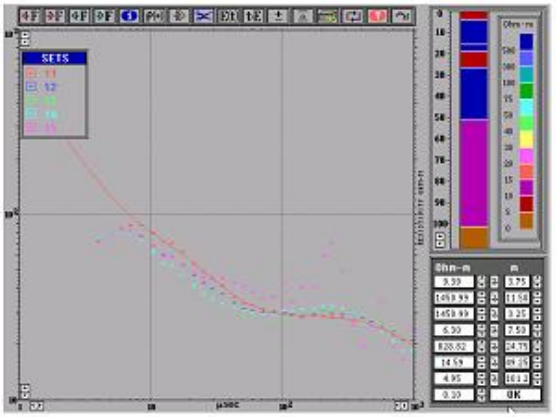

a. 5 soundings and the model curve

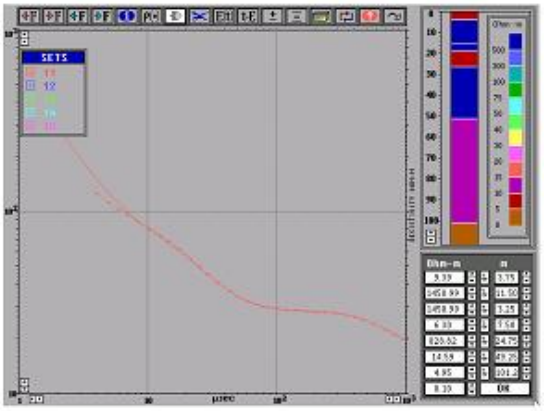

b. 1 sounding smoothed and initial model entered

c. Optimum inversion algorithm output

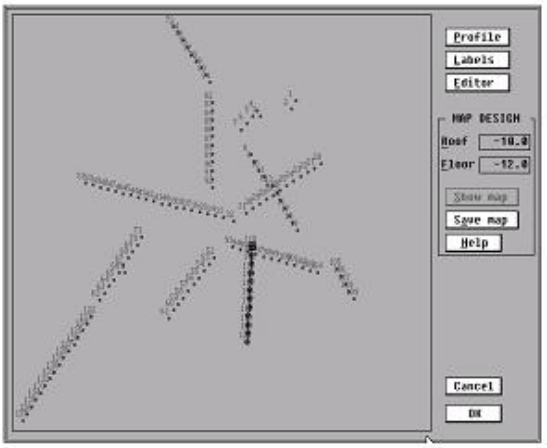

d. Database of all saved results

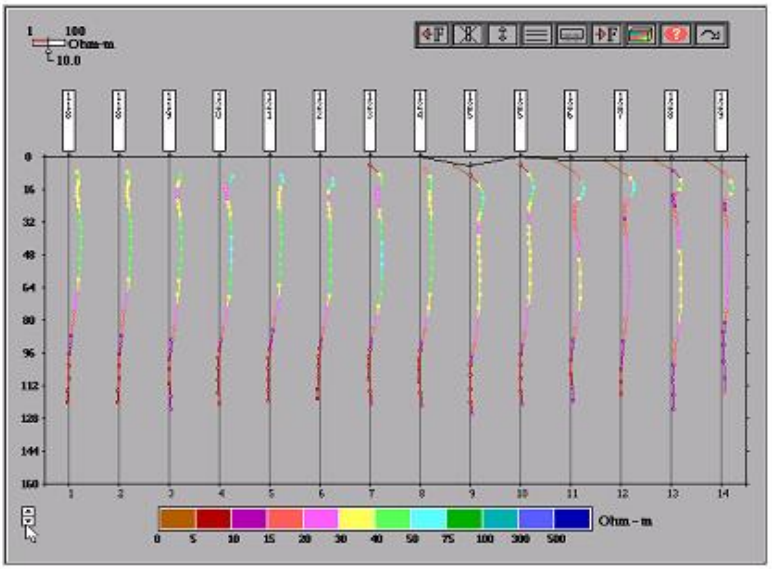

e. Resistivity pseudo-section of a profile selected from (d.) above in a double representation of apparent resistivity.

Figure 4.4: Stages in the TEM data processing with TEM-RES

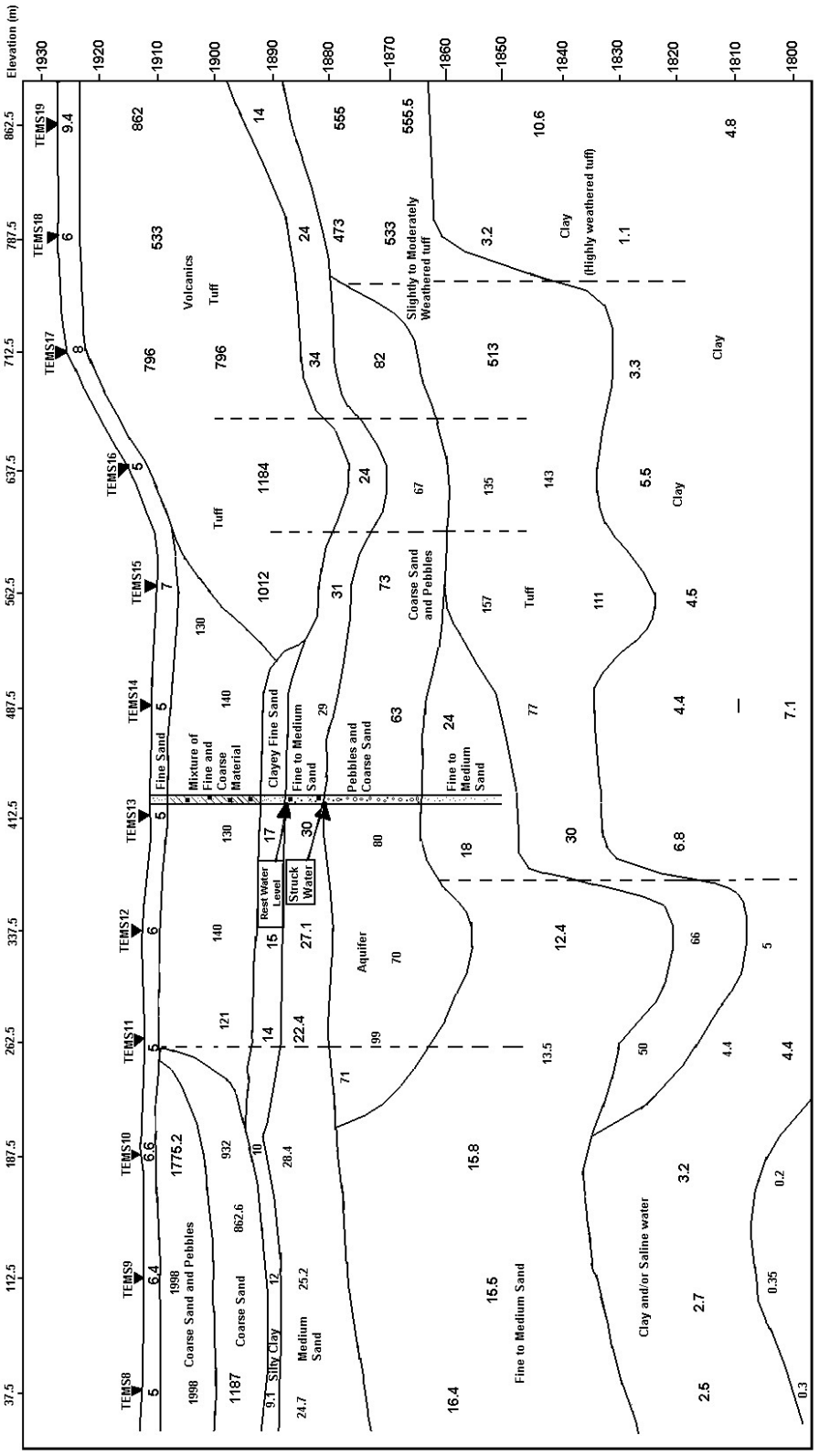

Figure 4.5: Resistivity sections of TEM Line 2

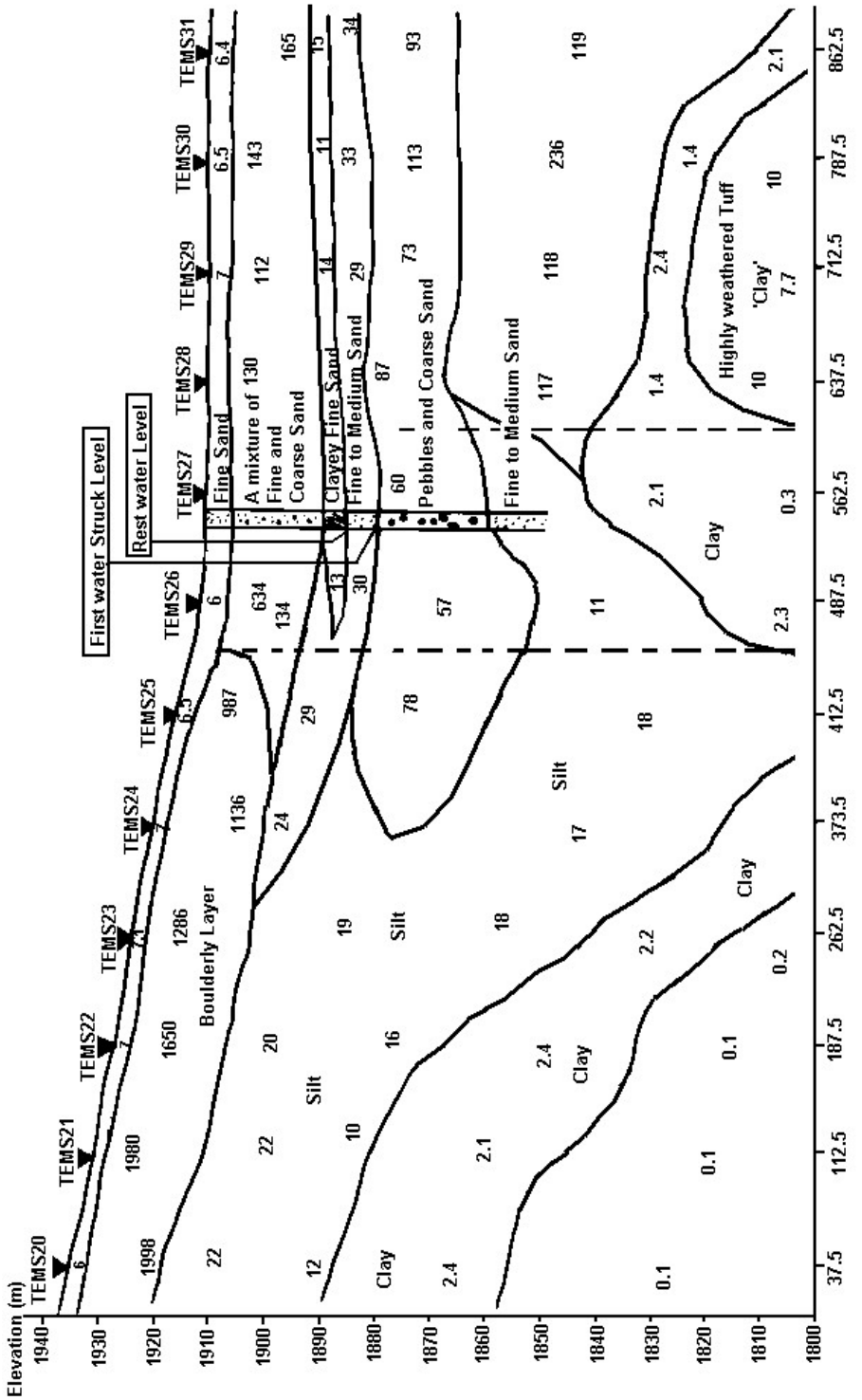

Figure 4.6: Resistivity sections of TEM Line 3

Chapter 5

Results and Geological interpretation

5.1 Introduction

Resistivity is a fundamental electrical property of rocks, that is closely related to rock lithology of which the main controlling factors are bulk rock porosity, pore structure, amount and salinity of water, temperature and the presence of clays. To convert the resistivity picture into a geological one requires some knowledge of the typical resistivity values for the different types of subsurface materials and geology of the surveyed area.

5.2 Analysis of results

Though most of the geological data from existing boreholes were incomplete, the information obtained from the available lithological logs and sources showed that the subsurface materials are basically clay, clayey silt, fine to medium sand, coarse sand, pebbles, boulders, tuff and lava. There was an equivocal description of *"grey stone", "medium hard" and "hard"* in BH.8 (see Figure 2.5 in Chapter 2) at 33 m below ground level (1862m). This may possibly be interpreted as weathered lava, though lavas are not reported in any of its nearby boreholes [Aquasearch-Ltd., 2001].

Groundwater quality analysis information on boreholes from the farms indicate a variable water chemistry. It is basically of the ($NaHCO_3$), ($CaHCO_3$) and ($NaCl$) types. The mean electrical conductivity (EC) of the waters is approximately $750\mu S/cm$ and therefore its mean resistivity (ρ), the reciprocal of ***EC*** is 13.3 Ohm.m.

The formation factor (F) have been calculated for five (5) boreholes along which 2D Resistivity imaging surveys were carried out and the groundwater EC are also known and therefore its resistivity ρ_w, from records. Empirical studies have demonstrated that a correlation exists between F and the particle size of sedimentary materials [Sporry, 2001]. Electrical formation factor (F) is given by the relation;

$$F = \frac{\rho_f}{\rho_w} \tag{5.1}$$

where ρ_f is the resistivity of formation and ρ_w is the resistivity of pore water. This relation is a derivation from Archie's Law [Keller and Frischknecht, 1966]. The general relationship between F and grain-sizes established in NW-Europe [Sporry, 2001] has been adopted as a *rough guide*, because it fitted well with borehole evidence and the calculated F values, (see table 5.2 and Figure 5.3).

F	Grain size
1	clays
1.5 -- 2	sandy slays
2 -- 2.5	silty and clayey Sands
3	fine sands
4 -- 5	medium coarse sands
6 -- 7	coarse sands
> 8	very coarse sands and pebbles

Figure 5.1: Relationship between *F* values and grain sizes from various studies in NW-Europe

Borehole	Location	EC (mS/cm)	r_w (Ohm.m)	r_f (Ohm.m)	F	Grain size
B	Three Point Farm	600	16.7	70	4.2	Medium coarse sand
BH. 5	Manera Farm	760	13.2	27.5	2.1	Silty and clayey sands
BH. 6	Manera Farm	920	10.9	22	2	Silty and clayey sands
BH. 7	Manera Farm	1025	9.8	20	2	Silty and clayey sands
BH. 10	Manera Farm	600	16.7	60	3.6	Fine to medium sands

Figure 5.2: *F* values for five boreholes: BH.5, BH.6, BH.7 and BH.10 (Manera Farm) and Bh.B (Pivot B), Three Point Farm

The determination of F values was extended to cover the entire area. Table 5.1 gives the percent of the data collected with the Resistivity Imaging and the TEM. The resistivity values from each method were combined and formation factor calculated by dividing by the average resistivity of groundwater in the area (i.e. 13.3 Ohm.m).

This also gives a rough estimate of the percentage by volume of the grain-sizes in the study area. The total surface area for the two surveys is the same but the maximum depth of investigation was much deeper in the TEM (100m) compared to the 2D Resistivity imaging (65m), hence the total volume under consideration in TEM is 35% more than the 2D Resistivity imaging. Based on the F values, a rough guide to subsurface materials and their expected formation resistivity ranges have been provided in Table 5.2. Details of the materials have discussed for the individual profiles in the next section.

Table 5.1: Percent of data corresponding to formation materials

Borehole	Location	EC (mS/cm)	r_w (Ohm.m)	r_f (Ohm.m)	F	Grain size
B	Three Point Farm	600	16.7	70	4.2	Medium coarse sand
BH. 5	Manera Farm	760	13.2	27.5	2.1	Silty and clayey sands
BH. 6	Manera Farm	920	10.9	22	2	Silty and clayey sands
BH. 7	Manera Farm	1025	9.8	20	2	Silty and clayey sands
BH. 10	Manera Farm	600	16.7	60	3.6	Fine to medium sands

Table 5.2: Resistivity Ranges for Materials in the Study area

Material type	Formation resistivity Range (Ohm.m)
Boulder and fractured lava	335 -- 2150
very coarse sand, gravels and pebbles	110 -- 335
coarse sand	80 -- 110
medium coarse sand	55 -- 80
fine to medium sand	35 -- 55
silt and clayey sand	27 -- 35
silty and sandy clays	20 -- 27
clays	< 20

5.3 Discussions of Results

5.3.1 Geological interpretation

As has been discussed earlier, both the 2D Resistivity and the TEM data gave similar subsurface distribution patterns of resistivity, and hence the individual sections are discussed here together. However, some lines that were carried out for purposes of instrument test (2D Resistivity imaging Line 11) and background noise measurement (Line 1 in both methods) are not discussed. The discussion incorporates information from boreholes and previous works in the area by two consulting companies, VIAK EA Ltd., (1976) and Aquasearch Ltd., (2001).

Line 2 runs across the *Pivot B* of Three Point Farm in an approximately N-S direction, starting some 400m east of the well-field area of the same farm and terminating close to the Karati river (see Figures 3.11 and 3.12 in Chapter 3). The geological interpretation of the models of the resistivity section of the 2D resistivity imaging and the pseudo-section of the TEM of Line2 indicate the presence of a shallow material of *medium to coarse sand* of thickness between 15 to 20m spanning over some 300m in the north where the profile begins (*cf.* Figures 5.4 and 5.5). *Boulders and fractured lava* of thickness of about 40m occur from about midway of the profile, immediately after the location of Borehole B and towards the end of the profile near the Karati river, (see Figure 3.11). The presence of the volcanic layer can also be seen in the VES carried closed to the Karati River (see Figure 2.8) [Gressando, 1999]. The rest of the area is covered by a mixture of *fine and medium coarse sand* with some *silt and sandy clay* materials up to depths of 80m. Between the depths of 80-85m is a layer of *very fine sand and clayey silt* material and below this layer exists a very conductive material which could be *clay and/or saline water*.

Survey Line3 runs almost perpendicular to Line2. It starts from the foot of the trachyte ridge on the Three Point farm and runs approximately E-W across *Pivot B* (see Figures 5.4 and 5.5). The results indicate the presence of a *bouldery Trachytic layer* at near surface depths (0 - 30m) from the foot of the trachyte ridge to some 300m away where a sub-vertical fault seems to have thrown the material further down. The materials beneath the bouldery layer are *silt and silty clay* in nature. Two near by boreholes one on each side of the profile (refer to Figure 3.11 in Chapter 3) were abandoned due to excessive silt [Aquasearch, 2001]. The depth of investigation by the TEM sounding in this area was much reduced due to the high conductive nature of the material below the silty layer. This could be clay or saline water. The rest of the section is made up of fine to medium sand with lenses of medium to coarse sand and pebbles as explained above on traverse *Line2*.

Survey profiles *Line4E and Line4W* in the case of the 2D Resistivity imaging and *Line4* for the TEM (refer to Figure 3.11 in Chapter 3) run across borehole M on Manera Farm where good quality water and high yields are reported. A gap of some 200m exist between *Line4E and Line4W* in the 2D Resistivity Imaging survey. The model sections of the two survey methods indicate the presence of a *fine sand and silt* layer from near surface to 25m depth. Below this material, is a layer of *fine to medium sand*, up to depths of approximately 80m. A layer of *silty clay* material that moves into *clay and/or saline water* at larger depths. Line4W is the continuation of Line4E but to the west. This portion of the survey is covered almost entirely by

fine sand and silt with lumps of clay and lenses of medium coarse sand. The *medium coarse sand* appears as a continuous thin layer of between 5-8m thick just below the soil layer. The results of these surveys have been presented in the Appendix C, Figure 2.

Traverse Line5, runs NE-SW almost parallel and near to the Karati river (refer to Figure 3.11 in Chapter 3). It has a thin surface layer of *medium coarse sand* between shallow depths of 0 - 10m. This layer is underlain by a *fine sand and silty* layer with *lumps and lenses* of *clay*. This occurs between the depths of 10 - 30m. Beneath this layer is a *medium to coarse sand* with a *"pinch and swell nature"* between depths of 30 to 80m and even deeper towards the end of the traverse, (see Figures 6.2 and 6.3 in the next Chapter).

Line6 runs near Borehole No.5 (BH.5) on the Manera Farm in the SW-NE direction south of the Dairy House while Line6N runs across BH.6 in a NE-SW direction north of the Dairy (refer to Figure 3.11 in Chapter 3). Line6 has a *medium to coarse sandy* surface layer up to depths between 15m to 20m. This is underlain throughout by *silt and clayey sand*. *Silty clay and clay* materials occur in appreciable amounts at larger depths. The litho-log of BH.5 recorded as *"alluvial deposits of volcanic origin"* throughout and up to depths of 91.4m with no caving (refer to Figure 5.3). This implies that the material labelled *"alluvial deposits of volcanic origin"* is *silty and clayey sand* in nature.

Line6N is largely covered by very low resistive material (< 10.5 Ohm.m) and therefore with a formation factor F of approximately 1. This is in the range of *clays*. However no such large amounts of clay has been reported in any of the nearby boreholes but rather tuff (refer to Figure 5.3). Therefore this could be interpreted as *decomposed or weathered tuff*. There are also some *fine sand and silt* and with small lenses of *medium sand* present. The Litho-log of BH.6 also recorded as *"Alluvial deposits of volcanic origin* throughout (0-91.4m), (see Figures 6.2 and 6.3 presented in the next Chapter).

On survey profiles Line7S and 7N (refer to Figure 3.11 in Chapter 3) only the TEM soundings gave subsurface information as the resistivity imaging along these profiles yielded poor data due to high background resistance to the injection of current even with watered grounds around electrodes. Line7N was the only traverse made in the Homegrown Farm, immediately to the north of Manera and Three Point Farms. *Line7S* the continuation of *Line7N* southwards, runs on the Manera Farm parallel to the the NE boundary of the farm with the Three Point Farm. The apparent resistivity pseudo-sections show immediately below the thin soil cover, a continuous high

resistive layer (45 - 65 Ohm.m) of *medium coarse sand* with an average thickness of 8m. Below this layer in the Line7N, is a mixture of *clay and silt* which grades into clay or saline water at larger depths (resistivity less than 10 Ohm.m). Beneath the thin resistive *sand* layer in the section of Line7S is a a thin continuous layer of *clay* with intermittent breaks (pinch and swell in nature) see Figure 5.7. The *clay* is underlain by *fine to medium sand* of the thickness of about 40m to the south but thins out towards the north where large volumes of clayey materials exist (see Figure 5.7). Larger depths have resistivity values less than 10 Ohm.m suggesting the presence of *clay and/or saline water*.

Resistivity Imaging Lines 8N and 10; and TEM survey profiles 8N, 8S and 10 were carried in the southern part of the *"top farm"* of Manera Farm, where center pivots 10, 11 and 12 are located (refer to Figure 1 in the Appendix). The results of these surveys show a relatively high resistive subsurface materials up to depths of about 60m. This has been interpreted as *medium coarse sand, pebbles, gravels, boulders and trachytic lava* (see Figure 5 in Appendix). *Fine sand and silty clay* materials exist beneath this layer at greater depths. Evidence from three abandoned boreholes indicated that *hard rocks (trachytes)* were encountered at an approximate depth of 40m.

Profile Line9 in the two survey methods were carried out in front of the offices of Manera Farm (Delamere Office) along borehole numbers 2 and 8. The sections show a high resistive top layer of about 12m thick but not continuous. This could possibly be coarse sand, though it is labeled as *sandstone* in near by borehole No.8 litho-log (see Figure 5.3). Beneath this layer layer is a complex mixture of *coarse sand, silt and clay*. However, towards the south where BH.8 is located, a continuous appreciable amount of clay exists at greater depths (refer to Figure 4).

5.3.2 Structural interpretation

Prominent structural features were not much in the mainly sedimentary environment of the study area. However, vertical and sub-vertical faults occur in areas close to the rift wall that marks the eastern margin of the study area. These were clearly seen in the resistivity and apparent resistivity models sections of traverse lines 2 and 3 in the Three Point Farm (see Figures 5.4 and 5.5) and 8N and 10 (see Figure 5 in Appendix). The presence of these minor faults have resulted in minor block shifting leading to a horst and graben topography. The Analytical signal image (refer to Figure 2.7) and the satellite images also showed that the NW running portion of the

Karati river is fault controlled. Areas to the north (Three Point Farm) and south (Manera Farm) on this portion of the river is underlain by a mixture of fractured volcanics and lake sediments, however, faulted but unfractured volcanic material occurs immediately north (within a distance 100 - 200m) of the river on the Three Point Farm (see Figure 5.4).

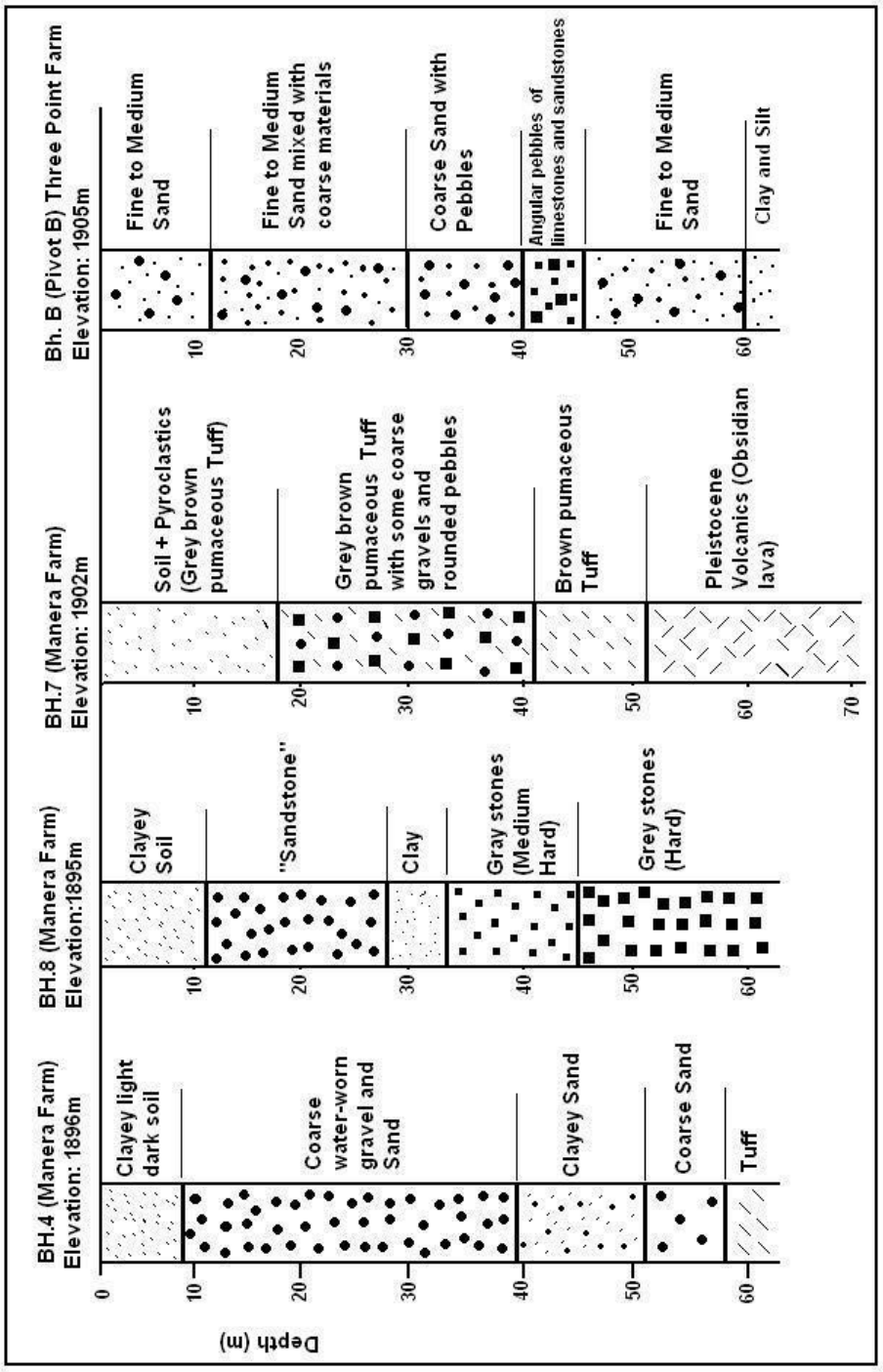

Figure 5.3: Lithological logs for four boreholes: BH.4, BH.8, BH.7 (Manera Farm) and Bh.B (Pivot B), Three Point Farm

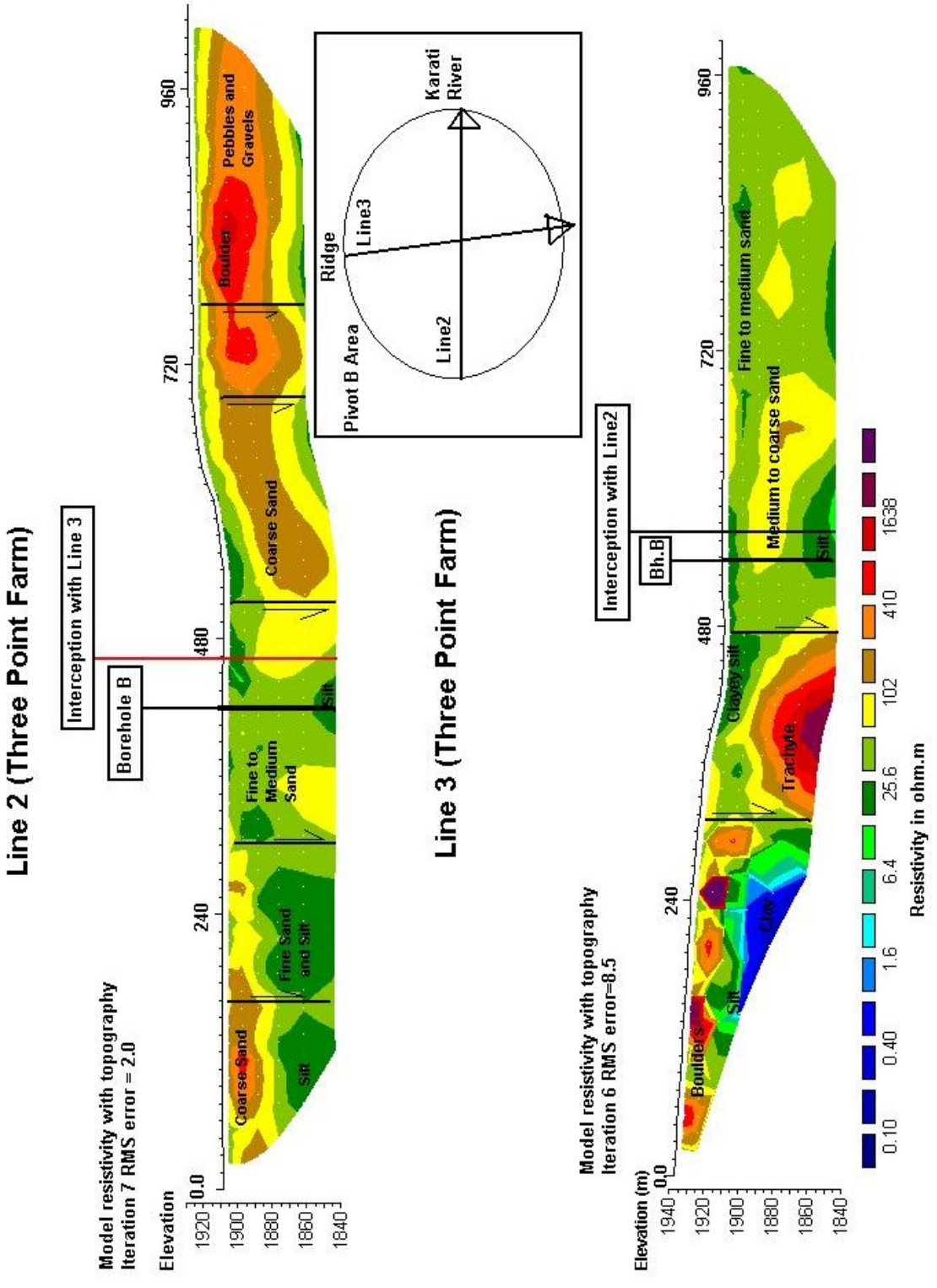

Figure 5.4: Geological Interpretation of 2D Resistivity Imaging Lines 2 and 3

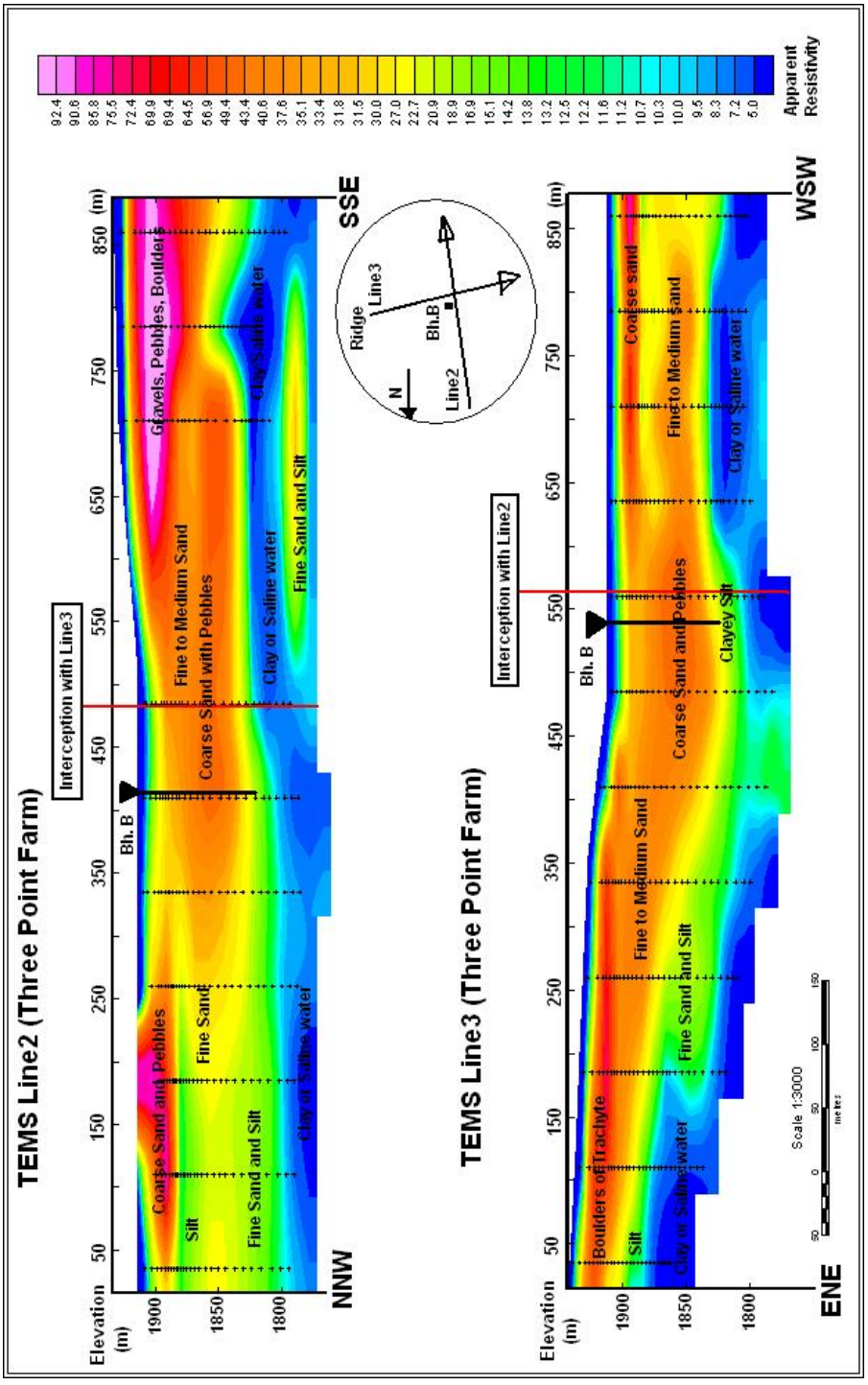

Figure 5.5: Geological interpretation of TEM profiles 2 and 3

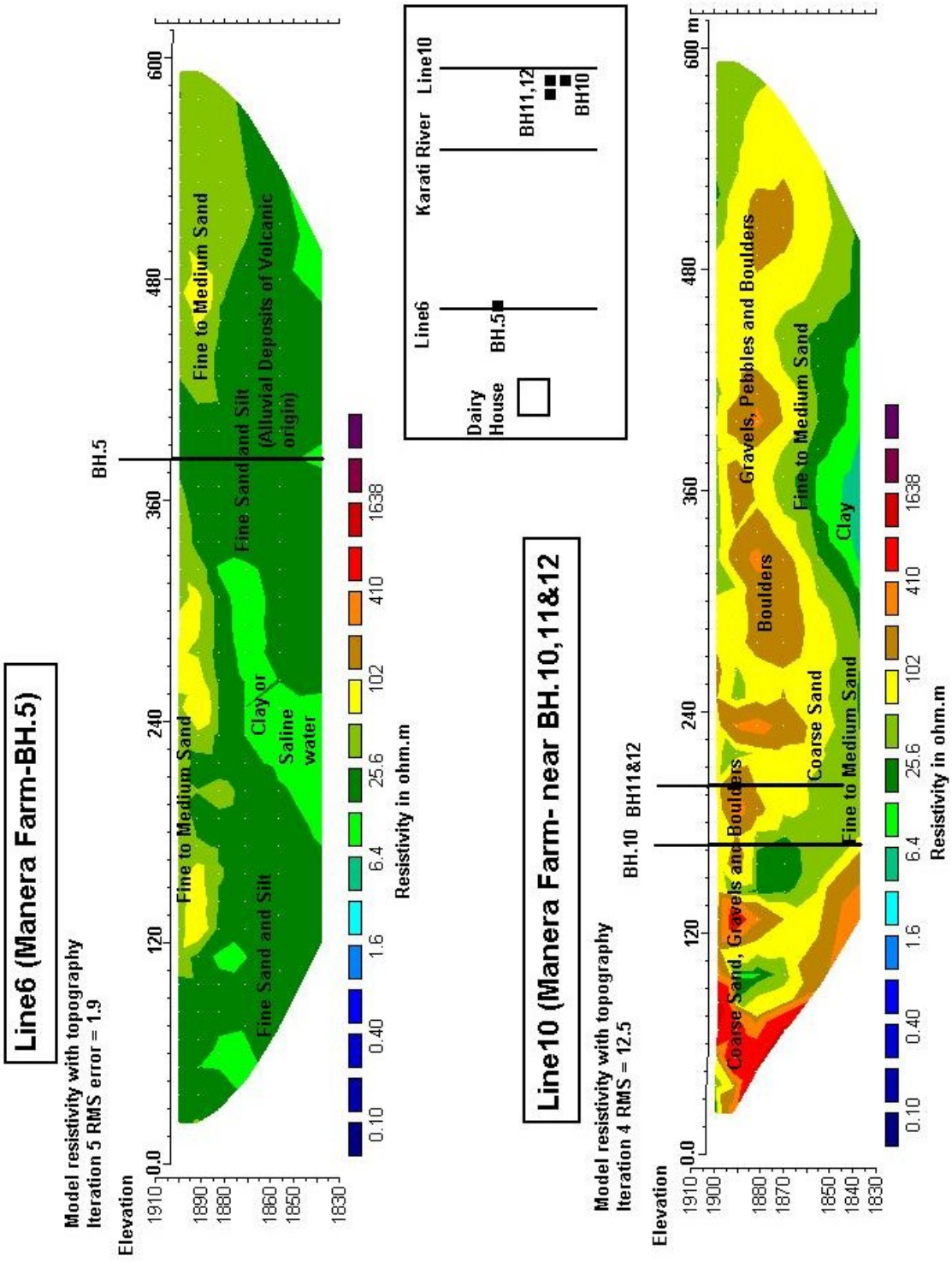

Figure 5.6: Geological interpretation of resistivity Imaging Lines 6 and 10

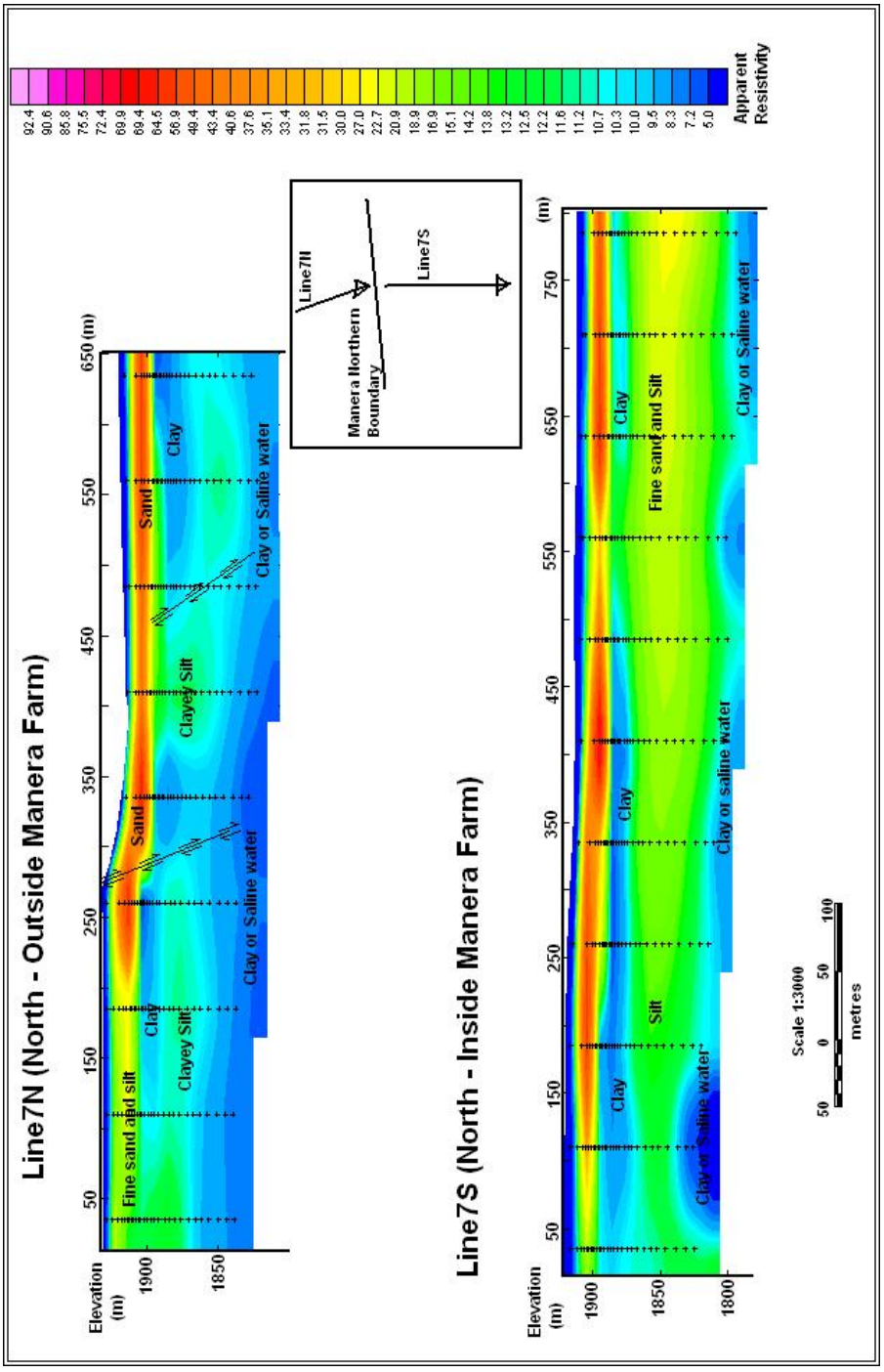

Figure 5.7: Geological interpretation of TEM profiles Lines 7N and 7S

Chapter 6

Aquifer Modeling

6.1 introduction

Aquifers are commonly regarded as both reservoirs for groundwater storage and as pipelines for groundwater transport [Ward and Robinson, 1990], although as Nace, (1969) observed, due to the often slow nature of the flow, the pipeline analogy is rather less apt. Groundwater can either be fresh or saline depending upon the amount of total dissolved solids. *Aquifer models* can be used to simulate the subsurface parameters of the groundwater system for a more quantitative hydrogeological analysis of the effect of proposed water-supply boreholes and for planning purposes. Groundwater models can also employed to determine the extent of the groundwater resource in areas which are threatened due to contamination or saltwater intrusion resulting from over-pumping.

The main properties or parameters of concern in any aquifer modeling include; the extent, depth, porosity, permeability and water (fresh or saline). These properties determine the available groundwater quantities under prevailing discharge and recharge conditions. These parameters can be related to the physical properties of the formation e.g. resistivity. Therefore, electrical geophysical techniques (resistivity imaging and TEM in this case) can be used to model a potential aquifer.

6.2 Boundary conditions

The lithological and structural setting of the subsurface has been elaborated in Chapter 5.3.1. The main subsurface materials in the study area up to an approximate depth of 100m include clays, clayey silts, fine to coarse sands, gravels, pebbles, boul-

ders of trachytic lava. The hydrogeological setting borehole water chemistry have been presented in Chapter 2.5 and Appendix A.

To estimation the limits (boundary conditions) of the formation resistivity associated with an aquifer suitable for large scale dairy and horticulture farming *production* boreholes, the following assumptions were made:

- A productive sedimentary aquifer should in general have a porosity of at least 20% ; see Figure 6.1. Formations with porosity less than this are likely to have poor (less suitable) hydraulic conductivity and storativity characteristics [Taylor et al., 1992]. An exception to this however, is the case of fractured volcanics that may have a low matrix porosity, but still have a high hydraulic conductivity due to the interconnected fractures. Similarly, porosities greater than 20% do not necessarily ensure that good hydraulic characteristics exist, particularly if clay exist. The formation factors F calculated for five boreholes in Chapter 5.2 indicated that the aquifer materials in some of the boreholes had some clays and silt. Clays and silts have porosities greater than 40% and therefore, have the ability to contain large amounts of water, but are not capable of transmitting water and therefore not potential aquifer materials. But the presence of such materials in desired aquifers cannot be ignored. Coarser materials (silty sand, sand, gravels, pebbles and fracture lava) on the other hand, can collect, store and transmit significant amounts of groundwater and therefore are good aquifer materials. From these arguments therefore, the maximum porosity for the aquifer likely to occur in the study area would be 42%.

- In a semi-arid environment of the Naivasha basin where the average annual rainfall is 635mm and evapo-transpiration is high, the quality of groundwater would certainly deteriorate with the accumulation of salts. According to Clarke et al., (1990), the mean monthly potential evaporation at the Naivasha basin exceeds mean monthly rainfall by a factor between 2 - 8 per month except for April. Though groundwater containing from 3,000 to 5,000 *ppm* of dissolved salts may still be usable for livestock and for irrigation of *salt-tolerant* crops [Larsson, 1984] and could be accepted as is the case in the Manera Farm, the same cannot be said of the *salt-sensitive* flower farming at the Three Point Farm. Therefore groundwater of total dissolved salts (TDS) of 1,850*ppm* has been chosen as the upper limit acceptable for both horticulture and dairy farming, this is based on work by Straver, (1994) on nutrient solutions for vegetable growth. *TDS* and *EC* show a very good quantitative correlation. There-

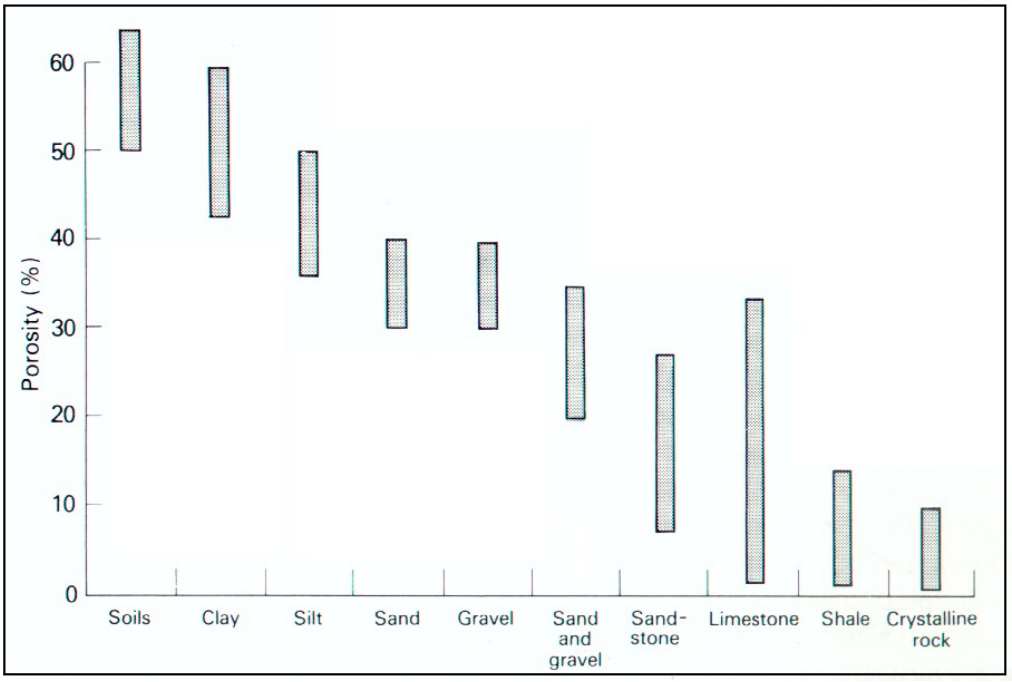

Figure 6.1: Typical ranges in measured porosity for various materials compiled from various sources by *Ward, (1990)*

fore, *EC* values can be estimated by multiplying TDS with a factor of 1.3 - 1.8 [Hounslow, 1995]. A factor of 1.6 was used, which yielded an approximate *EC* value of $3,000\mu S \cdot cm^{-1}$. This is based on M.Sc work in ITC by Morgan, (1998) on groundwater chemistry and quality assessment of the Lake Naivasha area. Therefore, electrical conductivity *(EC)* of more than $3,000\mu S \cdot cm^{-1}$ (i.e. resistivity of $< 3.3\Omega \cdot m$) has been chosen to be too saline for domestic livestock and horticulture farming. However, Three Point Farm currently adopts a maximum acceptable *EC* of $1,000\mu S \cdot cm^{-1}$, which in reality is too low a *cutoff* [SGS Laboratory Services, 2001]. On the other hand, groundwater with a resistivity greater than 30 ohm.m is unlikely to occur naturally in the study area since waters from Lake Naivasha are considered fresher (EC of $330\mu S \cdot cm^{-1}$) than the surrounding ground waters. The upper limit of groundwater resistivity of 30 ohm.m is used for the *fresh water* aquifer modeling.

- Since the aquifer material should be *clay-free* (but not totally true in reality), Archie's law can be used to calculate the formation resistivity for the aquifer from the above outline parameters, but with some caution. The relation is

given by;

$$\rho_f = \rho_w \cdot a \cdot \psi^{-m} \cdot S^{-2} \tag{6.1}$$

where ρ_f is the formation resistivity, ρ_w is resistivity of the pore-water (groundwater), ψ is the porosity, and S is the fraction of the pore volume that is filled with groundwater. The exponents a and m are the tortuosity and cementation factors respectively. The exponent a is also related in a way, to the resistivity of the solid particles alone as can seen in equation 6.2 below.

$$F = \frac{\rho_f}{\rho_w} = \cdot a \cdot \psi^{-m} \cdot S^{-2} \tag{6.2}$$

where F is the formation factor.

Tortuosity and cementation exponents of 1 and 1.5 respectively were chosen to be representative of the alluvium; this is based on the work by Jackson *et al.* (1978) on *unconsolidated* and *lithified* sands. The aquifer is fully saturated and therefore S is equal to 1.

The lower limit of formation resistivity for the aquifer described in the assumptions is calculated with Archie's law by using the highest porosity likely to occur (42%) and the lowest acceptable groundwater resistivity (3.3 Ohm.m). This yields a formation resistivity of 12 Ohm.m. If the formation material has a higher porosity or has more saline fluid, the electrical resistivity will be lower than 12 Ohm.m. Likewise, if appreciable clays are present in the formation, the electrical resistivity would also decrease. These conditions are undesirable, hence 12 Ohm.m can be used as the lower bound. The upper bound of electrical resistivity of the desired aquifer was computed in a similar manner using a porosity of 20% and groundwater (pore-water) resistivity of 30 Ohm.m. This yields a formation resistivity value of 335 Ohm.m and a formation factor F of 11. Therefore the approximate range of formation resistivity 12 - 335 Ohm.m is to be used as a guide to groundwater development in the study area which may not be applicable to all groundwater development situations in semi-arid environments. However, the approach can be adopted for other such applications by substituting appropriate values.

A minor limitation however exist in this approach of aquifer modeling. The boundaries (extent) of any aquifer in reality is that part across which no appreciable groundwater can flow (i.e. a hydraulic boundary). However, with aquifer modeling based on formation resistivity, it implies that the lower established limit (12 $\Omega \cdot m$) marks the bottom of the aquifer. This may not necessarily mean the bottom of the aquifer (a hydraulic boundary) but could likely be a saline/fresh water interface. In

an event of such a situation, it means the aquifer is made of saline water at the bottom with fresh water lying on top. In any case, this is not a problem, for it is the *fresh water aquifer* that is important and that is what is sort for and should be modeled.

Table 6.1: Resistivity range of aquifer and non aquifer materials

Resistivity Range (Ohm.m)	Material type	Remarks
< 12	clay and/or saline water	Aquiclude
12 -- 335	fine - medium sand, coarse sand, gravels and pebbles	Aquifer zone
> 335	boulders and lava	Aquitard

6.3 2D Models

Based on the model boundary conditions on formation resistivity presented above for the desired aquifer and the resistivity sections created in Chapter 4 from the resistivity imaging and TEM data, the spatial limits of the aquifer may be modeled in 2D. The resistivity imaging survey with the maximum depth of investigation of 65m could not map the bottom of the aquifer. On the hand, the TEM soundings did present the full cross-section of the desired aquifer with the average depth of investigation of 100m except in places of *down-thrown* blocks (see Figure 6.3).

In general, the aquifer zone occurs between depths of 20 - 80m in the area except in the northern and, NW and SE portions where Homegrown Farm and Boreholes 6, 7 and 8 of the Manera Farm are located respectively. In these areas, large volumes of materials have formation resistivities less than 12 Ohm.m. These have been interpreted to be either clay, saline water or both, see Figure 6.2. Overlaying the aquifer is a high resistivity unsaturated zone between depths of 3 - 15m just below the top soil. A thin layer of fine sandy clay exist between the high resistive unsaturated and the aquifer zones (see Figure 6.3). This makes the aquifer partially confined and explains why water rises in boreholes up to 2 - 6m above the level water was struck (see Table 1 in Appendix A). Excessive low resistivities observed in the bottommost regions indicate the presence of fine sands with clay saturated with saline water. This means a hydraulic connection possibly exists between the fresh water and the bottom saline water, implying that excessive pumping of the fresh water could lead to “up conning” of the bottom saline water. This may explain the deterioration of water quality in boreholes after several years of pumping.

In areas close the lake and the north, the high unsaturated sandy layer is thin,

between depths of 3 - 10m. A thin saturated silt and fine sandy layer exists between depths of 10 to 25m in what has been referred to as the top aquifer. Between depths of 25 to 30m is a clayey layer separating the top aquifer from the bottom aquifer (30 - 80m). The thickness of the clayey layer increases towards the lake leading to the bottom aquifer becoming small (see Figure 5 in Appendix 3). In reality, only one aquifer exists. Though it appears separated at some point, it remains hydraulically connected. With the exception of areas close to the lake, the clay layer occurs merely as discontinuous lenses in most parts of the area. Borehole evidence also show that at the first water strike, water level remains the same. However, when water is struck again, water level rises up, usually to the level of the first water level. The existence of a top and bottom aquifer in areas close to the Naivasha Lake was first pointed out by VIAK-EA Ltd, (1976) in their on groundwater studies in the Manera Farm .

6.4 3D Modeling

Since all geological materials and structures are three-dimensional (3D) in nature, a 3D model of the subsurface should in principle give a more complete picture of the situation. The Groundwater modeling System *(GMS)* developed by United States Department of Defense was used to build 3D images of the apparent resistivity data of the TEM and the true resistivity data from the 2D Resistivity Imaging. GMS is powerful tool for building 3D groundwater models with an excellent visualization of output.

6.4.1 3D Geostatistics

Raw TEM data was imported into GMS as 3D *Scatter point* data format as shown Figure 6.4. The gradient and quadratic functions options of the *inverse distance weighted interpolation* scheme were used in the interpolation of the data. Inverse distance weighted methods are based on the assumption that the interpolating surface should be influenced most by the nearby points and less by the more distant points. The interpolating surface is a weighted average of the scatter points and the weight assigned to each scatter point diminishes as the distance from the interpolation point to the scatter point increases.

The results of this process have been presented in a 3D block (see Figure 6.4) and 3D vertical and horizontal fence diagrams with z magnification of 3.0. The 2D Resistivity Imaging data format makes it difficult to import into GMS for such inter-

polation operations and therefore the same could be carried for the true resistivity, true depth results of the resistivity imaging.

Of the two, the interpolation of the data with the quadratic option provided a better illustration of the subsurface aquifer. However, the gradient option interpolation also sheds more light on the lateral variation in apparent resistivity in the area. The highest apparent resistivities occurs at the south-eastern corner where the Karati river flows NW and the lowest occur to the north western corner of the area.

Close to the rift wall, the area lying north (Three Point Farm) and south (Manera Farm) of the Karati river, the aquifer occurs as one continuous material between depths of 20 - 80m. The picture of a top and bottom aquifers separated by a clayey material towards Lake Naivasha in a NE-SW direction is also clearly visible (see Figure 6.4). This implies that the two aquifers are hydraulically connected laterally.

6.4.2 3D Stratigraphy Modeling

In order to build a 3D stratigraphic model of the area, both the resistivity imaging and TEM model results were converted into GMS borehole data format. Two or three (depending on the traverse length) representative locations along each 2D resistivity model section were converted into litho-logs vertically across the section. The model results of the TEM inversion includes the true geographical coordinates of sounding locations in the presentation of its output and therefore was easier to be converted into borehole data format by transforming the apparent resistivity log into lithological logs based on the inversions. The results of the 3D stratigraphy modeling of data have been presented in 3D block and 3D fence diagrams (see Figure 6.5).

6.5 Apparent Iso-resistivity images

Apparent resistivity contour images for 20, 40, 60 and 80m depth levels were made in *Oasis Montaj* to examine the spatial variation in apparent resistivity at the respective depths due to subsurface anisotropy. To better contour data, every other sounding results along the various profiles were used. The contour images were made from “inverse distance” gridding of the data. The output of the contoured images were imported into the *ILWIS* (GIS) program where the farm boundaries, the main Nakuru-Nairobi highway and railway, the Karati river and the boreholes locations were overlaid to enhance interpretation.

The *“apparent” iso-resistivity contour images* for the selected depths fairly repre-

sented the subsurface lithological variation under the existing groundwater conditions. The contour images for the four different "depths" with the depth separation of 20m provided a better comprehension of the lateral extent of the aquifer zone (see Figure 6.6). The highly resistive zones occur in the areas surrounding the eastern part of the Karati river and changes from high to low with distance away from the river (see also Figure 6.4). Beyond an approximate distance of 1000m (1km) from the river, the apparent resistivity falls below 12 Ohm.m due to deteriorating water quality and the material becoming finer. The lateral extent of the fresh water aquifer zone is clearly presented in the contour images.

The contour image for the depth of 20m (Figure 6.6), shows a larger extent of the unsaturated high resistive zone buffering the *Karati river* to the east with the patches of clayey materials to the west and the north. At depths of 40 and 60m, the *fresh water* saturated (moderately to high resistive) zone is well defined around the fault controlled portion of the Karati river. The 80m depth apparent resistive contour image marked the transition of the high resistive aquifer zone to the low resistive clays and/or saline water except for a small spot located immediately north of the Karati river on the Three Point Farm.

The analytical signal image from the magnetic data (Chapter 2) and satellite images show that the Karati river is controlled by the NW running fault up to where it makes the 90 degree turn towards Lake Naivasha in the SW. The surrounding areas of the river is block faulted and fractured leading to horst and graben topography in the area (refer to the Figure 5.4). The 2D resistivity imaging model from traverse Line2 also indicated the presence of block faulted volcanics within a distance of 200m to the river. Evidence from the closest borehole to river on the Three Point Farm (and it is also the deepest, 130m, in the area) showed the presence of sightly to moderately weathered tuff throughout. The immediate surroundings of the volcanics have relatively high formation resistivities and the yields are also very good. This is not due to the presence of a buried river channel as has been believed but rather just a contact zone, made up of a mixture of fractured volcanics and coarse lake deposits (see Figure 6.6) with good recharge. This zone extends from some 200m from the Karati river to approximately 800m away. The grains sizes become finer with greater distances from the river. This current picture, puts the ephemeral *Karati river* in an important position with regard to aquifer recharge and groundwater quality. This implies that during rainy seasons when Karati river carries enough water, there would be a good recharge into the aquifer and no recharge during the dry seasons when the river dries up. The northern side where Three Point Farm is located should receive

better recharge than the south where boreholes 10, 11, and 12 of the manera Farm are located due to the flow direction of the river.

Compartmentalization of the area based on the groundwater chemistry (hydrosome) from boreholes in the farms was carried by Aquasearch Ltd. (2001), a consulting company. The results is as shown in Figure 6.7. It accords fairly well with the interpretation from the *"apparent" iso-resistivity contour images* (see Figure 6.6). This indicates that good quality, high yielding boreholes should be located within the buffer zone 1km around the the Karati river to the east of the study area. Beyond a kilometer away from the river or even less in some cases, boreholes have been abandoned due to high EC. Borehole *A* and three other surrounding ones on the Three Point Farm have been abandoned because of high EC. Similarly, borehole numbers 5, 6, 7 and 8 on the Manera Farms have relatively high EC's with numbers 7 and 8 already abandoned (see Figure 2.5).

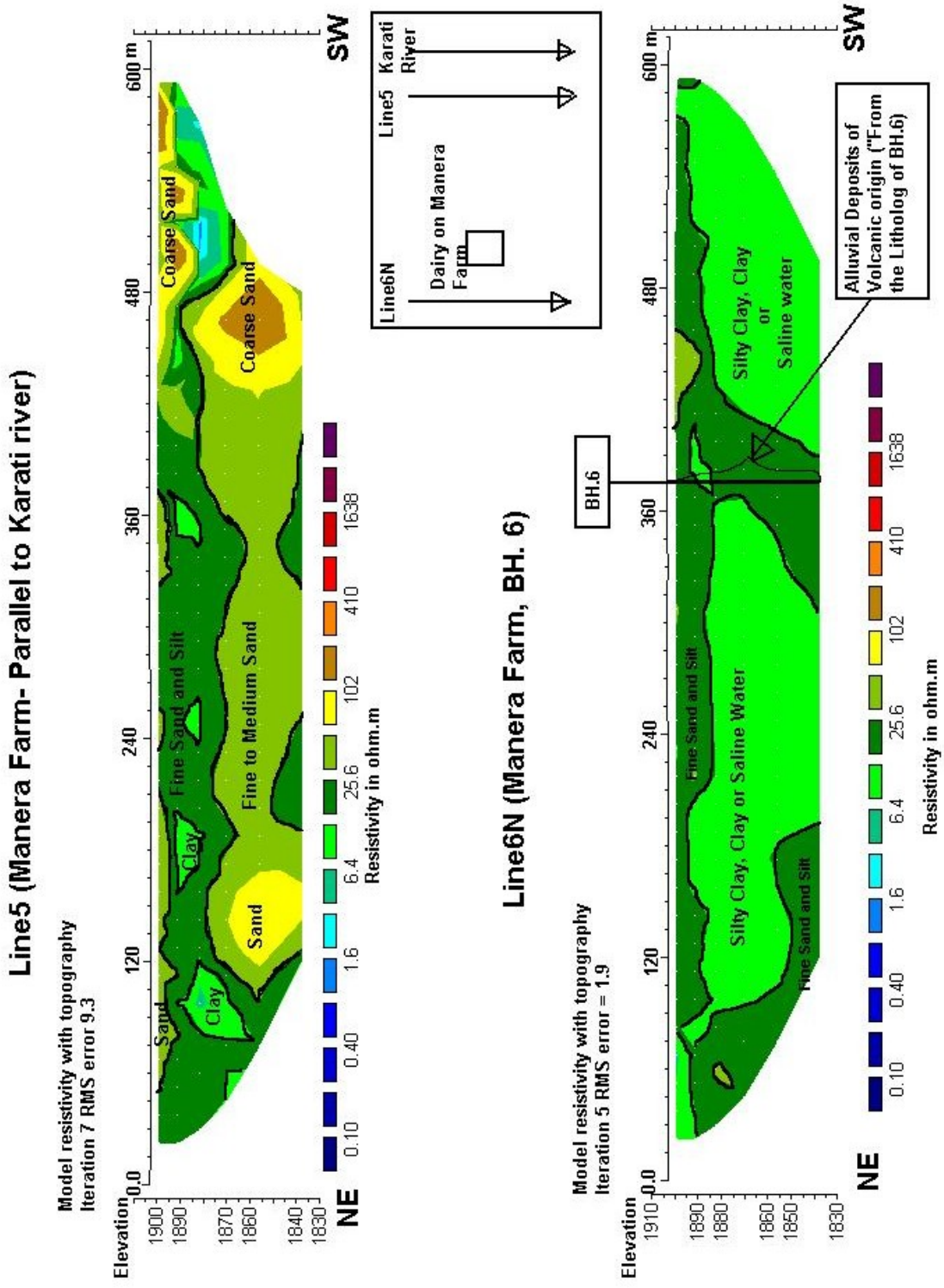

Figure 6.2: A 2D model of the subsurface aquifer zone from resistivity imaging Lines 5 and 6

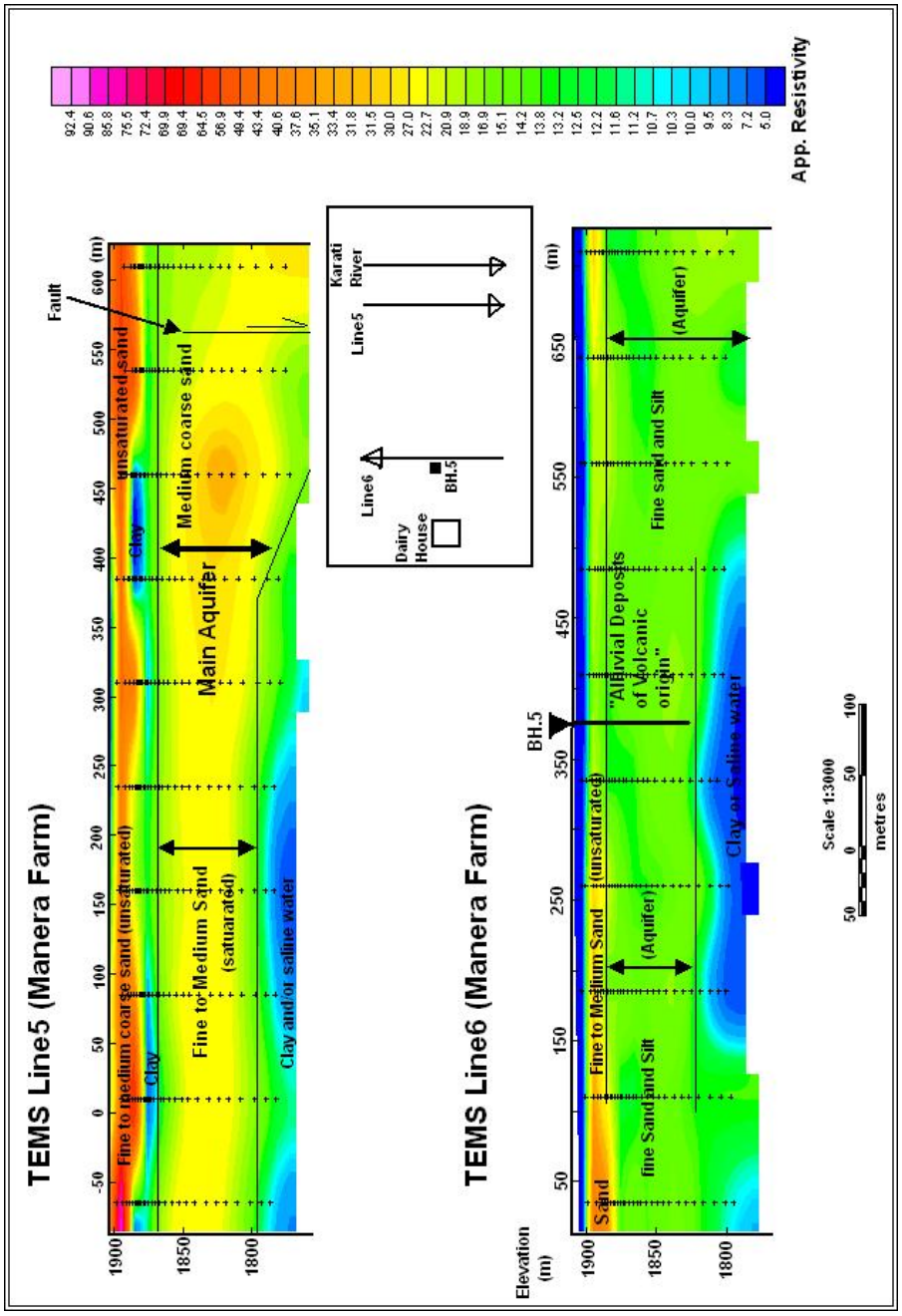

Figure 6.3: 2D model of the desired aquifer from TEM pseudo-sections along traverse Lines 5 and 6

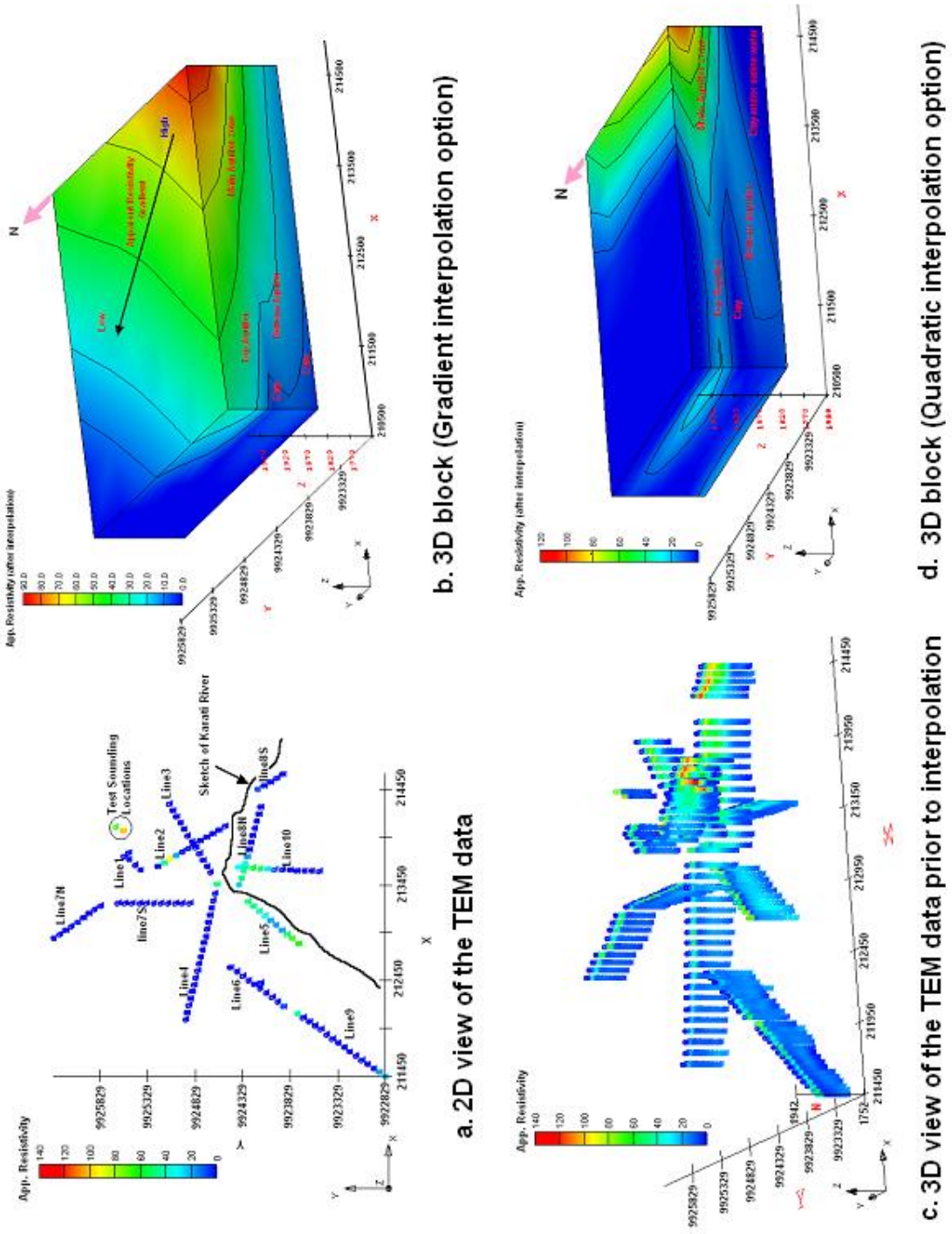

Figure 6.4: 3D blocks of the TEM data with the inverse distance method

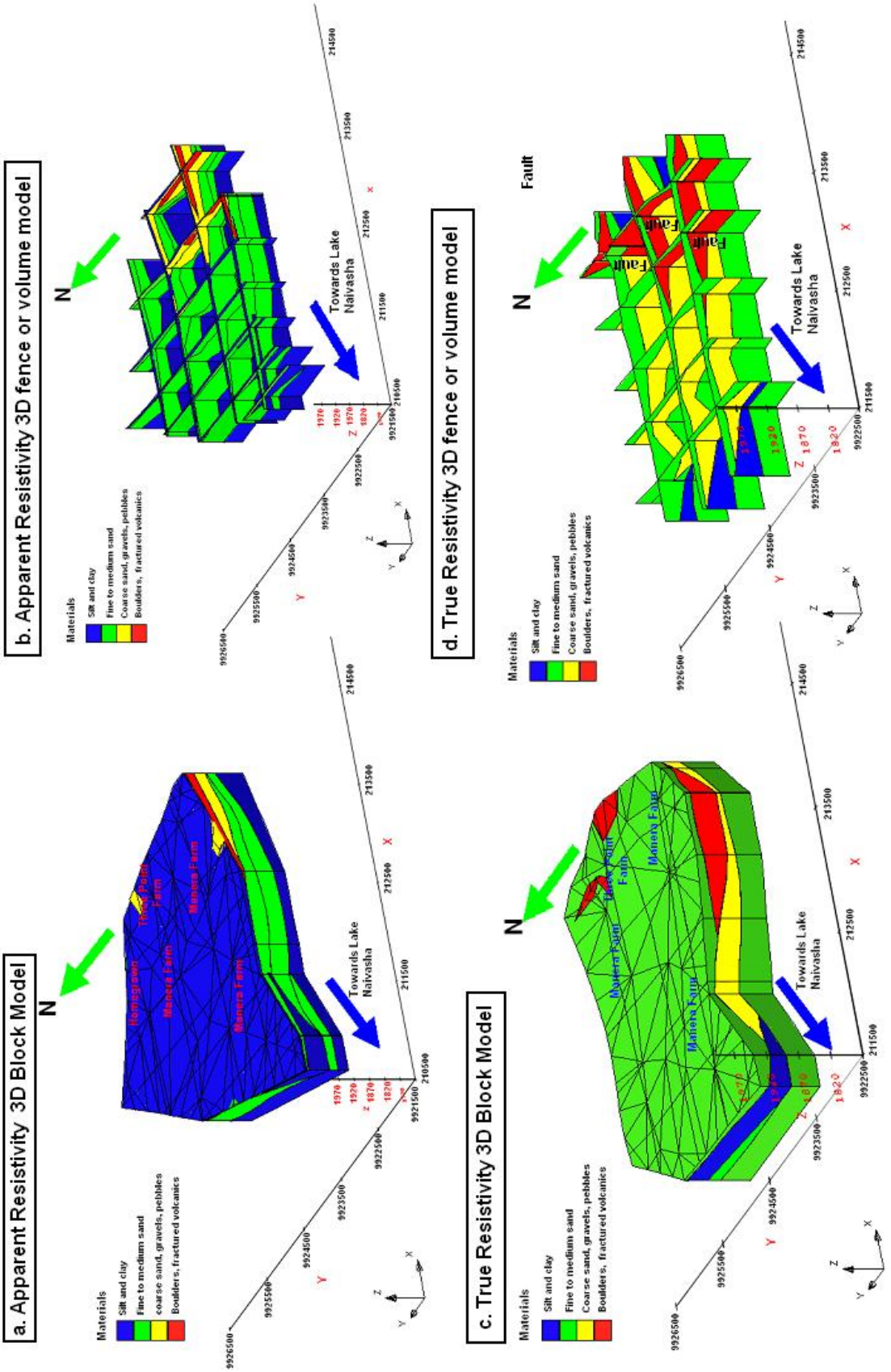

Figure 6.5: 3D stratigraphic model of the TEM data and 2D resistivity imaging

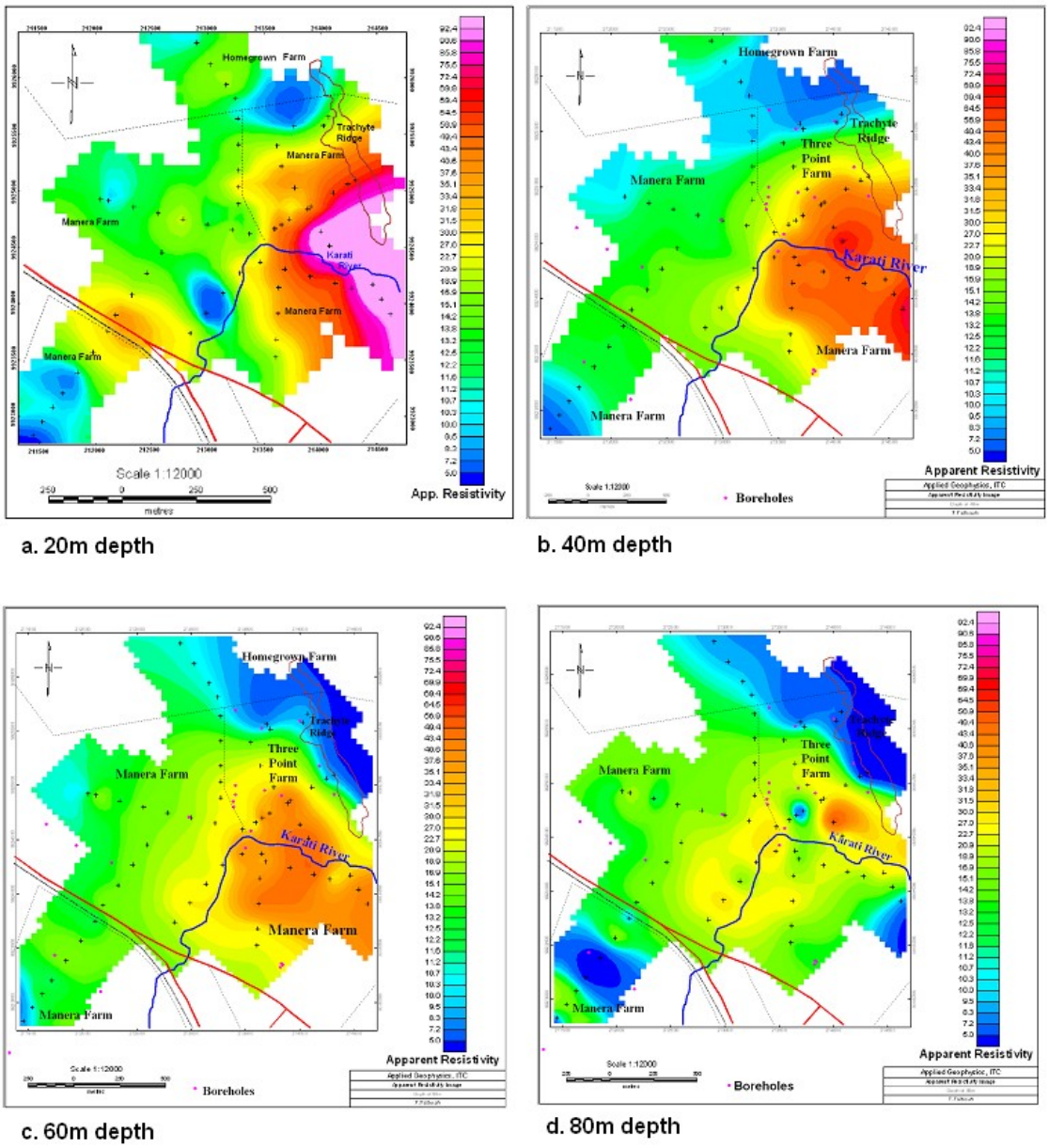

Figure 6.6: Apparent resistivity contour images for depths of 20, 40, 60 and 80m

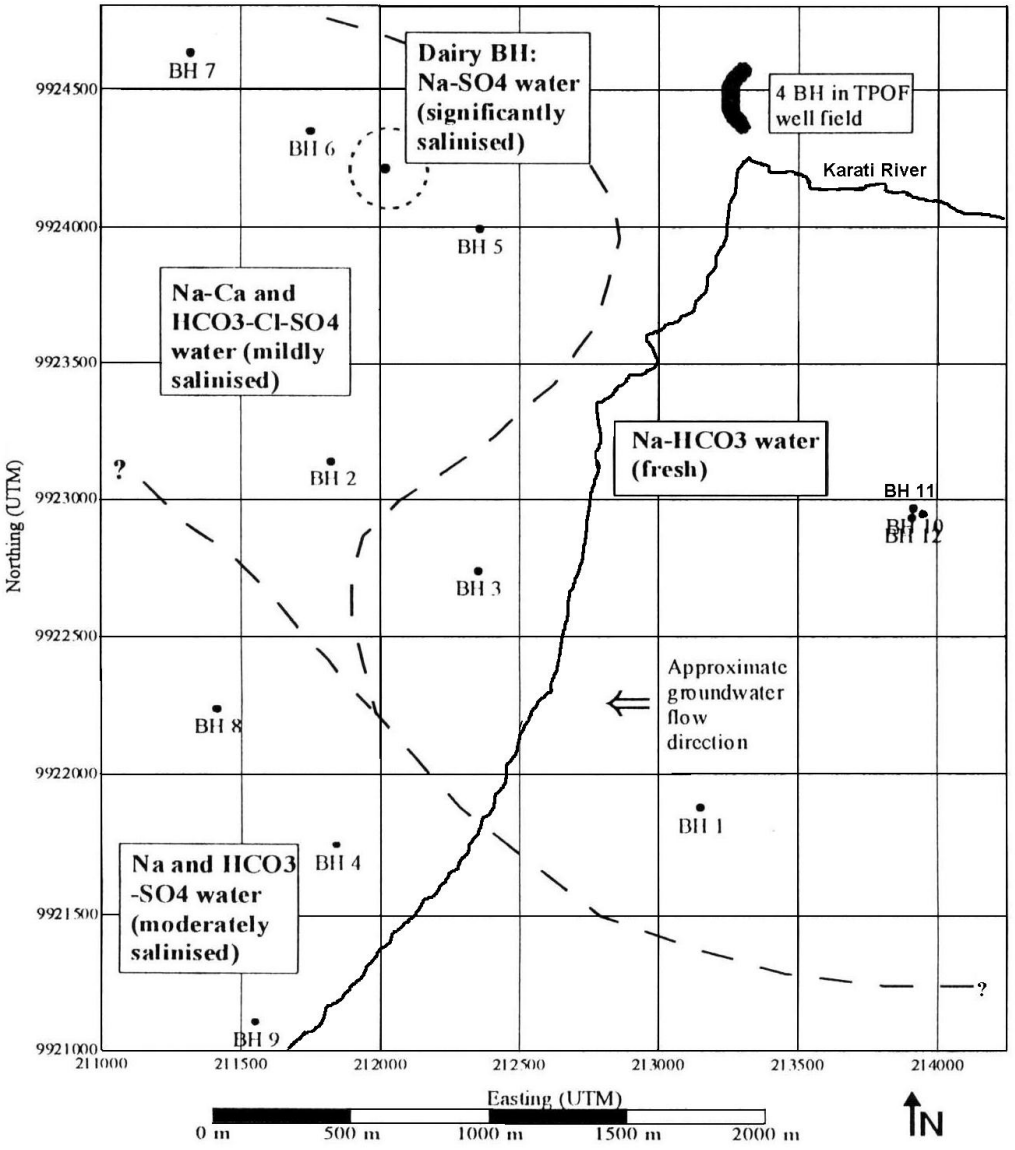

Figure 6.7: A Hydrosome map of the Manera Farm, *source:* Aquasearch, (2001)

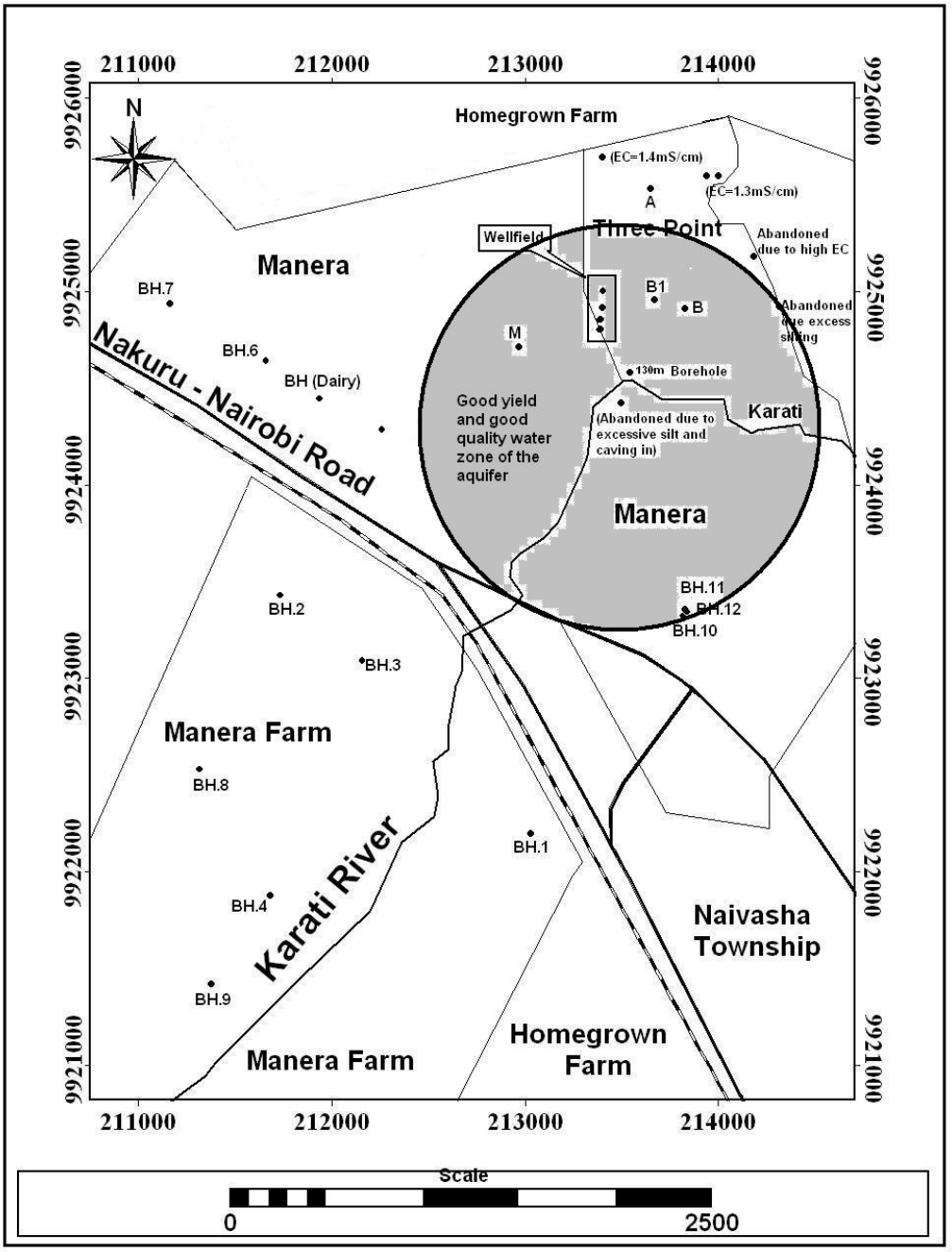

Figure 6.8: Zone of good quality and high yield portion of the aquifer

Chapter 7

Conclusions and Recommendations

Farmers in the north of Lake Naivasha in Kenya use mainly groundwater from the lakes beds for irrigated agriculture. The existence of *buried river channels* are believed to be the cause of the high yielding boreholes. However, with several years of groundwater usage from boreholes, water levels have fallen and the groundwater quality in most of the boreholes have deteriorated with EC doubling in some cases. Some have been abandoned as a result. Others were abandoned at the time of drilling mainly due to either the presence of excessive silt and clay resulting in the caving in of walls or the encounter of hard rock (volcanics).

To model groundwater system in this area, a systematic and dedicated effort was made to collect 2D Resistivity Imaging and Transient electromagnetic (TEM) data on three farms; Three Point, Manera and Homegrown. In all, 13 Resistivity Imaging Survey profiles of different lengths (total length of 8,430m) and 137 TEM soundings were made. Also, existing geophysical data (airborne magnetic and DC resistivity (Schlumberger)) were also collected for re-processing and interpretation. Borehole data and groundwater quality information were obtained from the offices of the farms and past M.Sc. theses in ITC.

The 2D Resistivity imaging data were processed with the RES2DINV program whereas the TEM data was processed in TEM-RES package and presented in Oasis Montaj. The 2D Resistivity imaging allowed a distinction to be made between very high resistive volcanics, the moderately high resistivity freshwater saturated zone and the very low resistive clays, and/or saline water. It was possible to locate the zones of low-quality groundwater with the fresh water aquifer zones. The TEM

soundings results allowed a distinction to be made between the fresh water saturated zone, the high resistive unsaturated material at the top and the low resistivity clay and/or saline water saturated zone at the bottom. A discontinuous thin clay layer that caps the aquifer zone in most parts of the area was well defined. The relatively accurate delineation of the deteriorating low quality groundwater zones as well as the groundwater table were possible due to the precision employed in the data collection, processing and presentation of the TEM soundings. The geological interpretation of the surveys correlated very well with the borehole data. Vertical faults have resulted in minor down-throwing of blocks in areas close to the rift wall on the east.

The *formation resistivity* physical property, groundwater quality and lithology were used to model of the aquifer. A representative aquifer model to meet the desires of the farmers had a formation resistivity range of 12 - 335 Ohm.m. The aquifer exists generally between depths of 20 to 80m in the Three Point Farm area where coarser materials exists. However, in the Manera Farm, the aquifer splits up into two but remains hydraulically connected; a *top* (between 20 - 40m) and *bottom* (between 50 - 80m) aquifers towards the Lake. The main aquifer materials include fine sands, medium coarse sands, gravels, pebbles and fractured volcanics. Laterally, the main aquifer zone occurs within a radius of approximately 1km from the main Karati river *(90^o)* "bend" on the Three Point Farm (see Figure 2.5). The *ephemeral* Karati river has also been identified as the main source of recharge into the aquifer. However, recharge to the immediate north would be high compared to the southern portions due the flow direction of the river. The very low resistivities at depths greater than 80m have been identified as a mixture of clayey materials and saline water. This warns of the danger of "up conning" of deep saline water that exists particularly in areas far way from the Karati river and also in areas near Lake Naivasha. Groundwater quality also deteriorates with larger distances away from the river to the N and NW.

2D and 3D models of the aquifer have been presented. Also Apparent resistivity contour images made for depths of 20, 40, 60 and 80m were made. The findings of the study agree fairly well with all the available ground information and also provide answers to the groundwater problems currently existing in the study area.

Based on this work the following recommendations have been made;

- 3 - 4 observation wells should be drilled within a kilometer radius from the Karati river bend (2 on the north and 1 in the south). It is recommended that the wells should be drilled with modern equipment preferably geophysically logged with Long Normal (LN) and Short Normal (SN) resistivity, SP, natural

gradient, caliper and gamma - gamma radiation (neutron).

- A proper pumping test should be carried out and mini-filters should be installed to observe variation of groundwater quality.
- These wells must be preserved solely for observation purposes (i.e. they should not be used for production purposes.
- If possible, there should be installation of monitoring electrodes (“salt watches”) to monitor changes in groundwater conductivity.

References

[AEMR, 1996] AEMR (1996). *TEM-FAST ProSystem Manual*. Applied Electromagnetic Research, Holland.

[AEMR, 1999] AEMR (1999). *TEM-RESEARCHER*. Applied Electro-Magnetic Research, the Netherlands.

[Allen et al., 1989] Allen, D., Darling, W., and Burgess, W. (1989). Geothermics and hydrogeology of the southern part of the Kenya rift valley with emphasis on the Magadi-Nakuru area. Research Report SD/89/1, British Geological survey, UK.

[Aquasearch-Ltd., 2001] Aquasearch-Ltd. (2001). Water resources assessment study, Manera farm, Naivasha. Final draft report, Delamere Estates Limited, Naivasha, Kenya.

[Ase et al., 1986] Ase, L., Sernbo, K., and Syren, P. (1986). Studies of Lake Naivasha, Kenya, and its drainage area. Stockholms Universitet Naturgeografiska Institutionen, Forskningsraport 63, ISSN 0346-7406.

[Barritt, 1993] Barritt, S. (1993). The African Magnetic Mapping Project. *ITC Journal*, 2:122–131.

[Bonini and Hickok, 1969] Bonini, W. and Hickok, E. (1969). Seismic refraction method in ground-water exploration. *Am. Inst. Min., Metallurg., Petr. Eng. Trans.*, 211:485–488.

[Carmichael and Henry, 1977] Carmichael, R. and Henry, G. J. (1977). Gravity exploration for groundwater and bedrock topography in glaciated areas. *Geophysics*, 42:850–859.

[Clarke et al., 1990] Clarke, M., Woodhall, D., Allen, D., and Darling, G. (1990). Geological, volcanological and hydrological controls of the occurrence of geothermal activity in the area surrounding Lake Naivasha. Technical report, Government of Kenya, Ministry of Energy/British Geological Survey.

[Darling et al., 1990] Darling, W., Allen, D., and Armannsson, H. (1990). Indirect detection of outflow from a Rift Valley Lake. *Journal Hydrology*, 113:297–305.

[DeGroot-Hedlin and Constable, 1990] DeGroot-Hedlin, C. and Constable, S. (1990). Occam's inversion to generate smooth, two dimensional models form magnetotelluric data. *Geophysics*, 55:1613–1624.

[Dey and Morrison, 1979] Dey, A. and Morrison, H. (1979). Resistivity modelling for arbitrary shaped two dimensional structures. *Geophys. Prospect.*, 27:106–136.

[EarthWatch, 2002] EarthWatch (2002). Lakes of the Rift Valley. $http://www.earthwatch.org/expeditions.html$.

[EMRL, 1999] EMRL (1999). *Groundwater Modeling System*. The Department of Defense, United States.

[ESA, 1992] ESA (1992). Olkaria environmental assessment: Water quality issues, north-east Olkaria geothermal power station near Naivasha, Kenya. Working paper by environmental services australia, Kenya Power Company Limited.

[Fitterman, 1987] Fitterman, D. (1987). Examples of transient sounding for groundwater exploration in sedimentary aquifers. *GROUND WATER*, 25(6):685–692.

[Fitterman and Stewart, 1986] Fitterman, D. and Stewart, M. (1986). Transient electromagnetic sounding for groundwater. *Geophysics*, 51(4):995–1005.

[Gressando, 1999] Gressando, Y. (1999). Application of geophysical techniques for goundwater investigation in lake naivasha area, kenya. M.Sc. thesis, International Institute for Aerospace Survey and Earth Sciences, The Netherlands.

[Griffiths and Baker, 1993] Griffiths, D. and Baker, R. (1993). Two-dimensional resistivity imaging and modelling in areas of complex geology. *Journal of Applied Geophysics*, 29:211–226.

[Griffiths and Turnbull, 1985] Griffiths, D. and Turnbull, J. (1985). A multi-electrode array for resistivity surveying. *First Break*, 3(7):16–20.

[Group-Seven-Inc., 1972] Group-Seven-Inc. (1972). Electrical resistivity survey in the rift valley. Final Report.

[GSK-Ltd, 1989] GSK-Ltd (1989). Hydrological investigation north-east of lake Naivasha, Nakuru district. Final report, National Animal Husbandary Research Centre, Naivasha.

[Hernandez, 1999] Hernandez, R. R. (1999). Groundwater modelling of the Naivasha basin, Kenya. M.sc. thesis, International Institute for Aerospace Survey and Earth Sciences (ITC), Enschede, The Netherlands.

[Hounslow, 1995] Hounslow, A. (1995). Water quality data: Analysis and interpretation. Oklahoma State University Stillwater, Olklahoma, Lewis Publishers.

[Jackson et al., 1978] Jackson, P., Taylor-Smith, D., and Stanford, P. (1978). Resistivity-porosity-particle shape for marine sands. *Geophysics*, 43:1250–1268.

[Keller and Frischknecht, 1966] Keller, G. and Frischknecht, F. (1966). *Electrical Methods in Geophysical Prospecting*. Pergamon Press.

[Larsson, 1984] Larsson, I. (1984). Ground water in hard rocks. International Hydrological Programme 8.6, Unesco.

[Loke, 2000] Loke, M. (2000). Electrical imaging surveys for environmental and engineering studies; a practical guide to 2d and 3d surveys. www.geoelectrical.com.

[Loke and Barker, 1996] Loke, M. and Barker, R. (1996). Rapid least-squares inversion of apparent resistivity pseudosections by a quasi-newton method. *Geophysical Prospecting*, 44:131–152.

[Loke, 1997] Loke, M. H. (1997). Res2dinv software user's manual.

[McNeill, 1989] McNeill, D. J. (1989). Advances in electromagnetic methods for groundwater studies. *Proceedings of Exploration '87, Ontario Geological Survey, Canada*, 3:678–695.

[Michel et al., 1999] Michel, R., Jean-Claude, P., Diouf, S., Beauvais, A., Dione, F., and Dione, F. (1999). Electrical imaging of lateritic weathering mantles over granitic and metamorphic basement of eastern Senegal, West uppercaseAfrica. *Journal of Applied Geophysics*, 41:335–344.

[Morgan, 1998] Morgan, N. (1998). Groundwater chemistry and quality assessment of the Lake Naivasha area, Kenya. M.sc. thesis, International Institute for Geoinformation Science and Earth Observation, The Netherlands.

[Nace, 1969] Nace, R. L. (1969). *Human use of groundwater, in Water, earth and man*. Methuen, London.

[Olayinka and Weller, 1997] Olayinka, A. and Weller, A. (1997). The inversion of geoelectrical data for hydrogeological applications in crystalline basement areas of nigeria. *Journal of Applied Geophysics*, 37:103–115.

[Oppong-Boateng, 2001] Oppong-Boateng, R. (2001). Assessment of the use of groundwater for irrigation in the southern part of lake Naivasha, Kenya. M.sc. thesis, International Institute for Aerospace Survey and Earth Sciences (ITC), Enschede, The Netherlands.

[Pastor, 2001] Pastor, M. S. (2001). Geophysical study of the groundwater system south of lake Naivasha, Kenya. M.Sc. thesis, International Institute for Aerospace Survey and Earth Sciences, The Netherlands.

[RES2DINV, 2000] RES2DINV (2000). *Geolectrical Imaging 2D & 3D User Guide*. GEOTOMO SOFTWARE, Malaysia, 3.4 edition.

[Roy and Lubczynski, 2000] Roy, J. and Lubczynski, M. (2000). The mrs technique for groundwater resources evaluation - test results from selected sites in South Africa. *Proceedings of IAH-2000, Groundwater: Past achievements and future challenges, Cape Town*.

[SGS-Chemisch-Laboratorium, 2001] SGS-Chemisch-Laboratorium (2001). Chemical analysis of irrigation water for Three Point Farm. Analysis Report.

[Sporry, 2001] Sporry, R. (2001). Lecture material on Resistivity. Earth System Analysis Department, ITC.

[Straver, 1994] Straver, N. (1994). Nutrient solutions for vegetable grown in water or substrates. 10th Edition.

[Taylor et al., 1992] Taylor, K., Widmer, M., and Chesley, M. (1992). Use of transient electromagnetics to define local hydrogeology in an arid alluvial environment. *Geophysics*, 57(2):343–352.

[Trottman, 1997] Trottman, D. (1997). Modelling groundwater storage change in response to fluctuating levels of lake Naivasha, Kenya. M.Sc. thesis, International Institute for Aerospace Survey and Earth Sciences (ITC), The Netherlands.

[UNESCO, 1998] UNESCO (1998). Unesco handbook for grounwater investigations. Technical report, ITC.

[Vander Velpen, 1988] Vander Velpen, B. (1988). Resist: a computer processing package for dc resistivity interpretation for the ibm pc and compatibles. M.sc. thesis, ITC-Delft, The Netherlands.

[VIAK-EA, 1976] VIAK-EA (1976). Naivasha water supply project: Groundwater investigation. Technical report, Ministry of Water Development, Kenya.

[Vincent et al., 1979] Vincent, C., Davies, T., and Beresford, A. (1979). Recent changes in the level of Lake Naivasha, Kenya, as an indicator of equatorial westerlies over East Africa. *Climate Change*, 2:175–189.

[Ward and Robinson, 1990] Ward, R. and Robinson, M. (1990). *Principles of Hydrology*. McGraw-Hill Book Company Europe, third edition.

[Zohdy et al., 1974] Zohdy, A., Eaton, G., and Mabey, D. (1974). Application of surface geophysics to groundwater investigations. *Techniques of Water-Resources Investigation of the United States Geological Survey, Book 2, D1*.

Appendix A

.1 Borehole Data and Farm Information

Table 1: Summary of borehole data in the study area

Borehole data on some boreholes with desired details provided							
Key:							
No.	Borehole number (C-prefix), given by the Water Apportionment Board						
Year:	Year drilled						
Location:	Geographic descriptor eg. Farms						
Elevation:	Approximate location (interpolated from contours)						
TD:	Total depth of borehole as drilled						
Struck:	Struct water level: multiple aquifer strikes reported where indicated in records						
Rest:	Rest or static water level: static water levels reported for separate aquifers where indicated						
$EC_{25:}$	Electrical conductivity at 25^{o}C where reported at the time the borehole was drilled						
No.	**Year**	**Location**	**Elevation m amsl**	**TD m**	**Struck m bgl**	**Rest m bgl**	**EC_{25} mS/cm**	**Remarks**
C-2246	1954	KARI	1899	40	17	14	640	EC in 1989 was 2400µS/cm
C-3216	1962	Manera	1890	42.7	6.1	4.9		BH.9; all Lake Beds
C-3217	1962	Manera	1890	42.7	6.1	4.9		Abandoned; all Lake beds
C-3289	1964	Manera	1898	79			591	BH.1 ?
C-3365	1965	Manera	1898	82.3	15.2	11	543	BH.3
C-3366	1965	Manera	1897	76.8	13.7	9.9	653	BH.2; all Lake Beds
C-3472	1968	KARI	1898	76	14	11	940	NAHRC 1; all Lake Beds
C-3675	1970	Manera	1896	61	9.1	4.9	1125	BH.4; all Lake Beds
C-3676	1968	Manera	1899	91.4	18.3	13.7	761	BH.5; all Lake Beds
C-3677	1968	Manera	1900	91.4	18.3	15.2	920	BH.6; all Lake Beds
C-3678	1970	Manera	1902	72.5	21.3	16.8	1025	BH.7; Lake Beds and Lava
C-6907	1985	Manera	1905	64	36	24	600	BH.10; Lake Beds
Un-known	1968	Manera	1899				5550	Dairy House BH
Un-known	1999	Three Point	1910	62	28	24.56	600	Pivot B

Table 2: Summary of Chemical Analysis of borehole water from Three Point Farm

Borehole Name:		A	C	B(roses)	B	B1	M	G1
Analised by:		SGS*	SGS*	SGS*	SGS*	SGS*	SGS*	SGS*
Sample Date:		Unknown	2/3/1999	14/06/2001	Unknown	23/12/1998	Unknown	2/4/2000
Analysis Date:		24/11/1998	8/3/1999	20/06/2001	24/11/1998	7/1/1999	24/11/1998	7/4/2000
Parameter:	Units							
pH		7.9	7.9	7.6	7.7	7.8	6.9	5.6
EC	mS/cm	900	800	500	600	700	500	1000
NH^{+}_{4}	ppm	<1.8	<1.8	<3.6	<1.8	<1.8	<1.8	<1.8
K^{+}	ppm	31	35	16	27	23	23	59
Na^{+}	ppm	140	150	71	58	78	41	76
Ca^{2+}	ppm	20	20	32	68	56	36	64
Mg^{2+}	ppm	<2.4	<2.4	<4.9	<2.4	<2.4	4.9	7.3
Si	ppm	45	39	39	51	48	51	17
NO^{-}_{3}	ppm	<43	43	<6.2	<43	<43	<43	440
Cl^{-}	ppm	18	14	18	14	14	11	36
SO_{2}^{-4}	ppm	29	<19	<48	<19	<19	<19	38
HCO^{-}_{3}	ppm	440	450	305	350	380	270	<6.1
$H_{2}PO^{-}_{4}$	ppm	<9.70	<4.85	<9.7	<9.7	<9.70	<9.70	<4.85
Fe	ppb	<28	1400	<22	<28	<28	<28	73
Mn	ppb	5.5	44	<11	27	100	360	<5.5
Zn	ppb	<13	<13	<13	<13	<13	26	<6.5
B	ppb	46	26	<54	26	<22	24	39
Cu	ppb	19	13	<13	19	13	19	25
Mo	ppb	<48	<48	<9.6	<48	<48	<48	<9.6

SGS* = SGS Laboratory Services, B.V., Sector Tuinbouw, Holland

Table 3: Litho-log of the the 130m borehole close to Karati River, on the Three Point Farm

From (m)	To (m)	Description of Formation Penetrated
GL	8	Brownish clayey material with fine sandy products
8	18	Light brownish fine volcanic sands with clayey materials
18	20	Brownish fine to coarse sands
20	26	Brownish fine sands with clayey materials
26	36	Fine to coarse brownish sands
36	50	Greyish fine to coarse sands
50	62	Fine to coarse rounded sands
62	70	Light brownish clayey materials mixed with fine sands
70	78	Light greyish fine to coarse volcanic sands
78	84	Dark compacted clayey materials
84	96	Fine grey sands
96	112	Greyish fine to coarse rounded sands
112	124	Whitish fine to coarse sands mixed with clayey materials
124	130	Greyish moderately hard rock

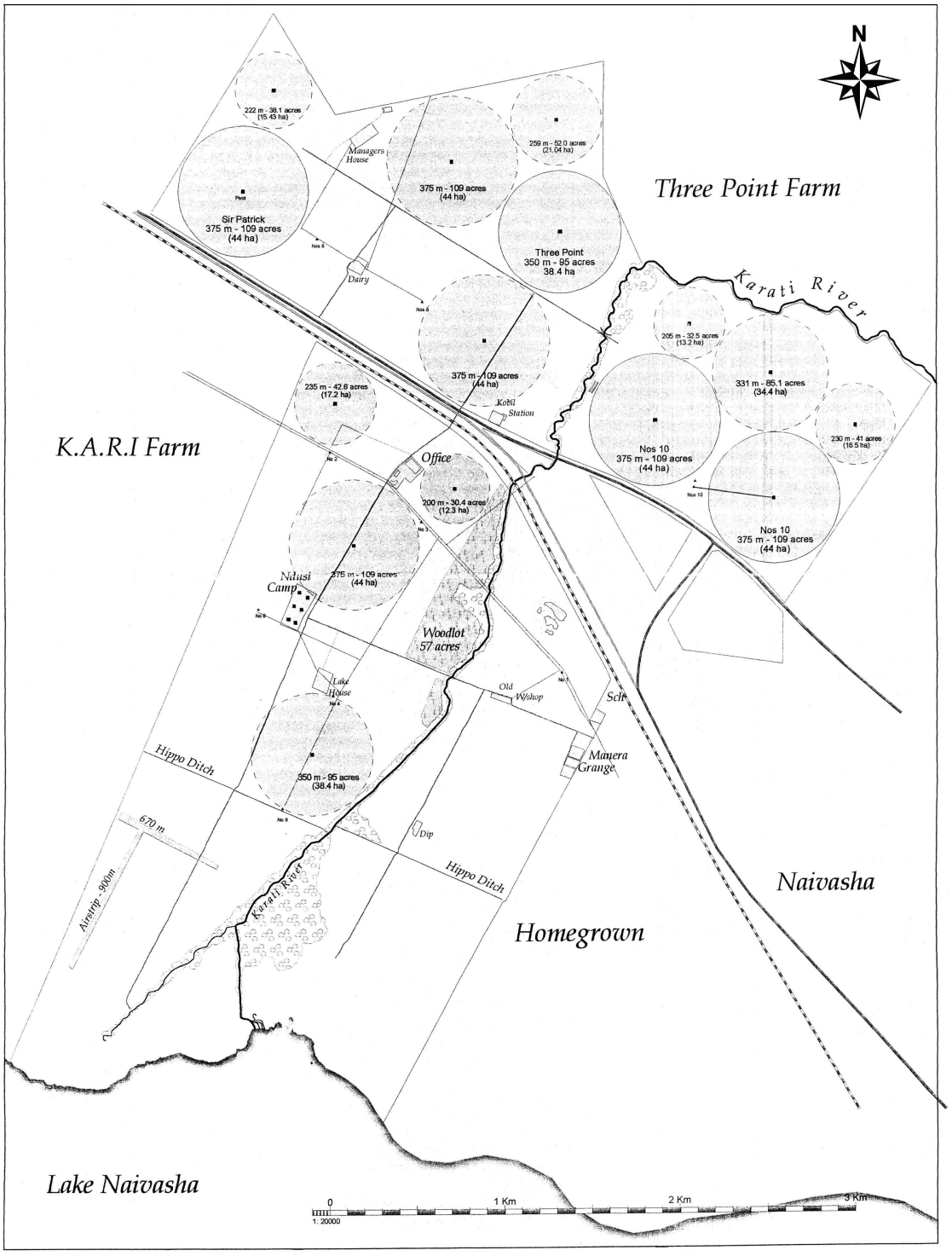

Figure 1: Manera Farm

Appendix B

.1 Some TEM test sounding results

Table 4: TEM Test sounding 1 near a power line

TEM-FAST SYSTEM Date: Fri Sept 14 04:50:17 2001
Place: office panda w of powerline
#Set 6 Sens. 1 Stacks 1
T-LOOP (m) 75.000 R-LOOP (m) 75.000 TURN= 1
Comments: test6
Location:x= +213951.000 y= +9955230.000

Channel	Time	E/I[V/A]	Err[V/A]
1	4.06	2.291e+001	0.000e+000
2	5.07	1.060e+001	0.000e+000
3	6.07	5.699e+000	0.000e+000
4	7.08	3.436e+000	0.000e+000
5	8.52	2.171e+000	0.000e+000
6	10.53	1.529e+000	0.000e+000
7	12.55	1.220e+000	0.000e+000
8	14.56	9.092e-001	0.000e+000
9	17.44	7.370e-001	0.000e+000
10	21.46	5.832e-001	0.000e+000
11	25.49	4.729e-001	0.000e+000
12	29.50	3.965e-001	0.000e+000
13	35.28	3.122e-001	0.000e+000
14	43.30	2.384e-001	0.000e+000
15	51.40	1.917e-001	0.000e+000
16	59.41	1.554e-001	0.000e+000
17	70.95	1.181e-001	0.000e+000
18	87.07	8.447e-002	0.000e+000
19	103.16	6.231e-002	0.000e+000
20	119.22	4.752e-002	0.000e+000
21	142.33	3.352e-002	0.000e+000
22	174.54	2.299e-002	0.000e+000
23	206.71	1.667e-002	0.000e+000
24	238.83	1.200e-002	0.000e+000
25	285.04	7.593e-003	0.000e+000
26	350.00	4.848e-003	0.000e+000
27	413.83	4.830e-003	0.000e+000
28	478.06	2.671e-003	0.000e+000
29	570.47	1.435e-003	0.000e+000
30	699.41	6.996e-004	0.000e+000
31	828.06	9.231e-004	0.000e+000
32	956.53	7.118e-004	0.000e+000

Table 5: TEM Test sounding 2 near a power line

TEM-FAST SYSTEM Date: Fri Sept 14 04:53:07 2001
Place: office panda w of powerline
#Set 7 Sens. 1 Stacks 2
T-LOOP (m) 75.000 R-LOOP (m) 75.000 TURN= 1
Comments: test7
Location:x= +213951.000 y= +9955230.000

Channel	Time	E/I[V/A]	Err[V/A]
1	4.06	2.267e+001	1.006e-001
2	5.07	1.058e+001	4.722e-002
3	6.07	5.659e+000	1.414e-002
4	7.08	3.379e+000	8.841e-003
5	8.52	2.161e+000	3.052e-003
6	10.53	1.516e+000	5.120e-003
7	12.55	1.217e+000	4.693e-003
8	14.56	9.050e-001	2.101e-003
9	17.44	7.295e-001	3.233e-003
10	21.46	5.789e-001	2.678e-003
11	25.49	4.730e-001	1.481e-003
12	29.50	3.942e-001	1.475e-003
13	35.28	3.108e-001	6.749e-004
14	43.30	2.374e-001	3.533e-004
15	51.40	1.899e-001	3.537e-004
16	59.41	1.553e-001	3.954e-005
17	70.95	1.176e-001	2.318e-004
18	87.07	8.437e-002	6.098e-005
19	103.16	6.260e-002	5.099e-004
20	119.22	4.814e-002	4.833e-004
21	142.33	3.351e-002	8.623e-005
22	174.54	2.181e-002	6.353e-004
23	206.71	1.566e-002	4.201e-004
24	238.83	1.131e-002	8.832e-005
25	285.04	7.699e-003	2.581e-004
26	350.00	5.284e-003	1.310e-004
27	413.83	3.835e-003	3.492e-004
28	478.06	2.658e-003	4.844e-004
29	570.47	1.902e-003	2.355e-005
30	699.41	1.011e-003	5.329e-004
31	828.06	1.126e-003	8.046e-005
32	956.53	5.068e-004	3.001e-004

Table 6: TEM Test sounding 3 near a power line

```
TEM-FAST SYSTEM        Date:  Fri Sept 14 04:54:31 2001
Place:      office panda w of powerline
#Set   8           Sens.       1    Stacks        3
T-LOOP (m)   75.000      R-LOOP (m)  75.000     TURN=   1
Comments:    test8
Location:x=  +213951.000       y=   +9955230.000
Channel     Time  E/I[V/A]    Err[V/A]
 1      4.06      2.237e+001  2.373e-002
 2      5.07      1.051e+001  1.502e-002
 3      6.07      5.560e+000  1.071e-002
 4      7.08      3.380e+000  1.110e-002
 5      8.52      2.130e+000  1.716e-003
 6     10.53      1.502e+000  6.435e-004
 7     12.55      1.201e+000  2.340e-003
 8     14.56      8.951e-001  1.901e-003
 9     17.44      7.233e-001  1.486e-003
10     21.46      5.745e-001  1.006e-003
11     25.49      4.677e-001  8.792e-004
12     29.50      3.901e-001  2.761e-004
13     35.28      3.073e-001  3.601e-004
14     43.30      2.352e-001  7.728e-004
15     51.40      1.884e-001  3.133e-004
16     59.41      1.533e-001  2.866e-004
17     70.95      1.160e-001  3.395e-004
18     87.07      8.282e-002  4.997e-004
19    103.16      6.121e-002  2.679e-004
20    119.22      4.691e-002  3.752e-004
21    142.33      3.305e-002  4.966e-004
22    174.54      2.174e-002  5.853e-004
23    206.71      1.513e-002  5.561e-004
24    238.83      1.145e-002  4.393e-004
25    285.04      8.431e-003  3.554e-004
26    350.00      5.982e-003  1.280e-004
27    413.83      4.040e-003  8.924e-005
28    478.06      2.899e-003  2.762e-004
29    570.47      1.828e-003  5.071e-004
30    699.41      1.273e-003  3.642e-004
31    828.06      1.394e-003  1.689e-004
32    956.53      7.367e-004  1.978e-004
```

Table 7: TEM Test sounding 4 near a power line

```
TEM-FAST SYSTEM        Date:  Fri Sept 14 04:56:18 2001
Place:      office panda w of powerline
#Set   9           Sens.       1    Stacks        4
T-LOOP (m)   75.000      R-LOOP (m)  75.000     TURN=   1
Comments:    test9
Location:x=  +213951.000       y=   +9955230.000
Channel     Time  E/I[V/A]    Err[V/A]
 1      4.06      2.270e+001  2.583e-001
 2      5.07      1.054e+001  7.372e-002
 3      6.07      5.591e+000  2.636e-002
 4      7.08      3.353e+000  1.135e-002
 5      8.52      2.137e+000  5.711e-003
 6     10.53      1.501e+000  4.194e-003
 7     12.55      1.202e+000  3.742e-003
 8     14.56      8.967e-001  1.599e-003
 9     17.44      7.218e-001  1.366e-003
10     21.46      5.750e-001  1.686e-003
11     25.49      4.663e-001  1.001e-003
12     29.50      3.898e-001  6.698e-004
13     35.28      3.076e-001  8.655e-004
14     43.30      2.349e-001  4.243e-004
15     51.40      1.889e-001  6.593e-004
16     59.41      1.536e-001  6.149e-004
17     70.95      1.164e-001  3.765e-004
18     87.07      8.326e-002  2.879e-004
19    103.16      6.141e-002  2.755e-004
20    119.22      4.703e-002  1.669e-004
21    142.33      3.305e-002  1.798e-004
22    174.54      2.187e-002  2.834e-004
23    206.71      1.551e-002  2.322e-004
24    238.83      1.162e-002  2.376e-004
25    285.04      8.011e-003  2.646e-004
26    350.00      5.127e-003  4.998e-004
27    413.83      3.538e-003  2.804e-004
28    478.06      2.657e-003  2.213e-004
29    570.47      1.645e-003  1.652e-004
30    699.41      1.108e-003  7.036e-005
31    828.06      7.717e-004  1.028e-004
32    956.53      5.964e-004  4.260e-004
```

Table 8: TEM Test sounding 5 near a power line

```
TEM-FAST SYSTEM        Date:  Fri Sept 14 04:57:37 2001
Place:      office panda w of powerline
#Set   10          Sens.       2    Stacks        1
T-LOOP (m)   75.000      R-LOOP (m)  75.000     TURN=   1
Comments:    test10
Location:x=  +213951.000       y=   +9955230.000
Channel Time      E/I[V/A]    Err[V/A]
 1      4.06      2.067e+001  0.000e+000
 2      5.07      9.781e+000  0.000e+000
 3      6.07      5.176e+000  0.000e+000
 4      7.08      3.159e+000  0.000e+000
 5      8.52      2.022e+000  0.000e+000
 6     10.53      1.435e+000  0.000e+000
 7     12.55      1.152e+000  0.000e+000
 8     14.56      8.585e-001  0.000e+000
 9     17.44      6.929e-001  0.000e+000
10     21.46      5.529e-001  0.000e+000
11     25.49      4.493e-001  0.000e+000
12     29.50      3.756e-001  0.000e+000
13     35.28      2.959e-001  0.000e+000
14     43.30      2.265e-001  0.000e+000
15     51.40      1.821e-001  0.000e+000
16     59.41      1.482e-001  0.000e+000
17     70.95      1.123e-001  0.000e+000
18     87.07      8.028e-002  0.000e+000
19    103.16      5.944e-002  0.000e+000
20    119.22      4.559e-002  0.000e+000
21    142.33      3.189e-002  0.000e+000
22    174.54      2.121e-002  0.000e+000
23    206.71      1.525e-002  0.000e+000
24    238.83      1.126e-002  0.000e+000
25    285.04      7.568e-003  0.000e+000
26    350.00      4.929e-003  0.000e+000
27    413.83      3.546e-003  0.000e+000
28    478.06      2.608e-003  0.000e+000
```

Appendix C

.1 More Resistivity Imaging and TEM models

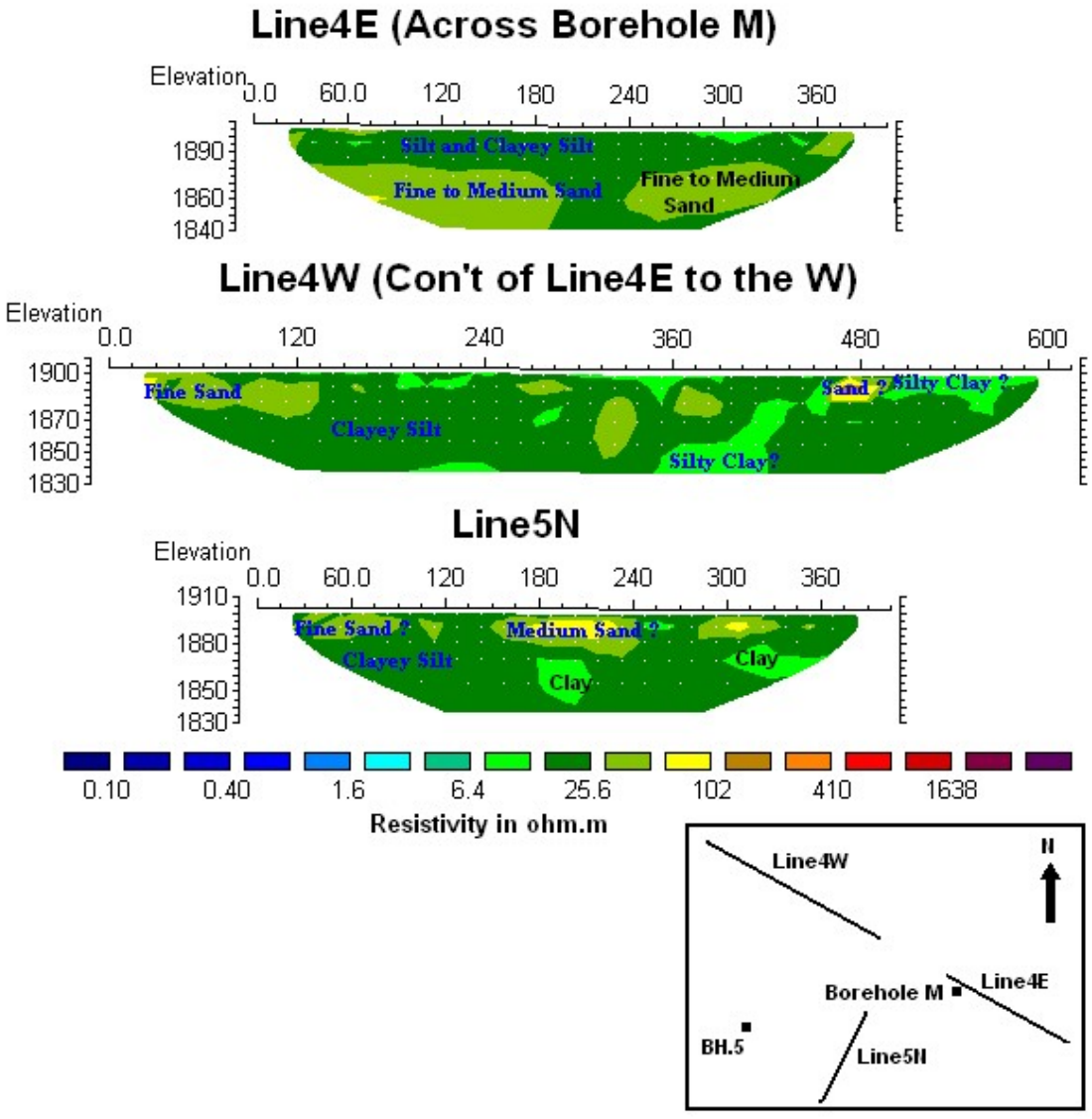

Figure 2: Geological interpretation of the 2D Resistivity Imaging model sections of Lines 4E, 4W and 5N

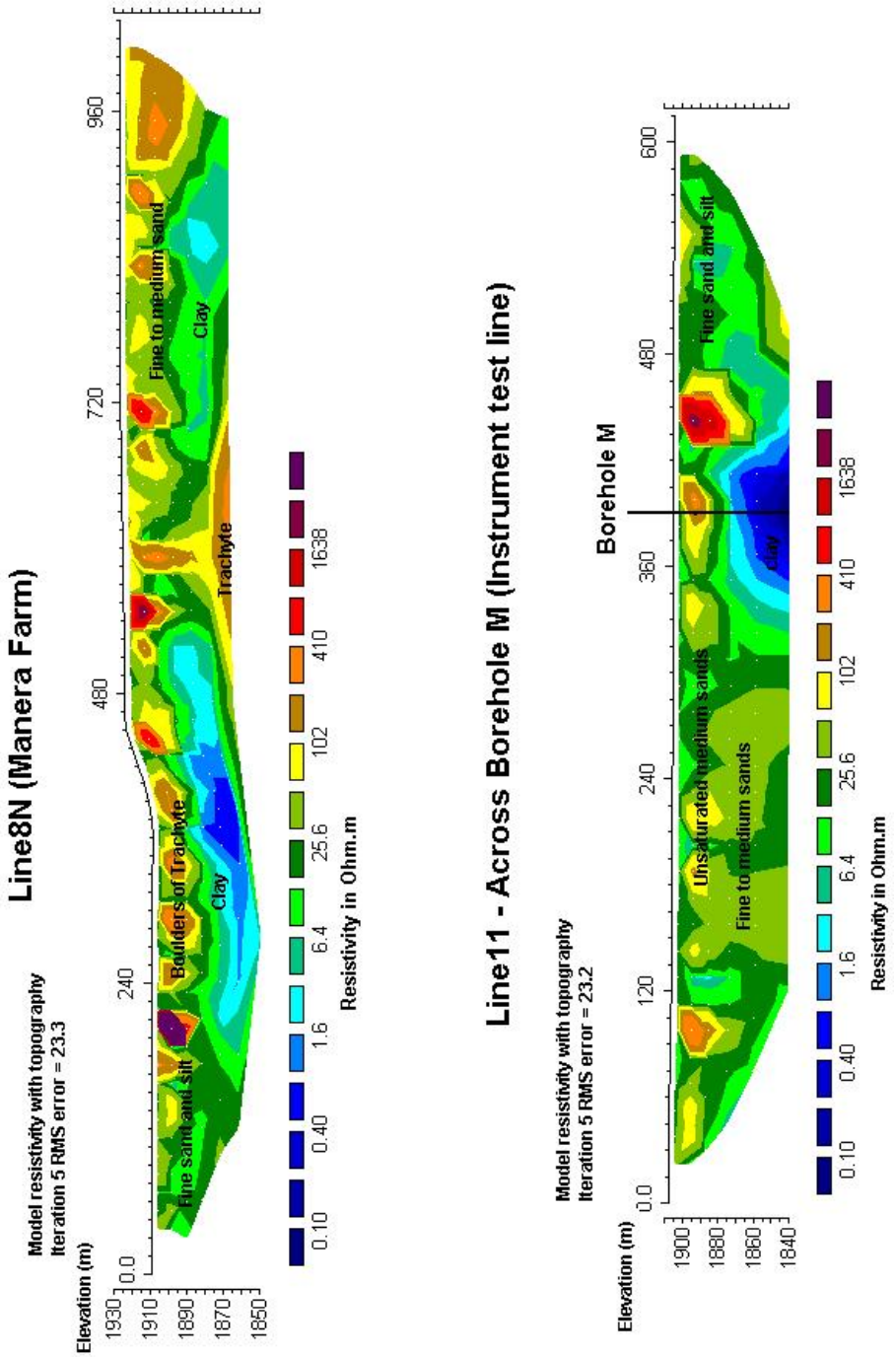

Figure 3: Geological interpretation of the 2D Resistivity Imaging model sections of Lines 8N and 11

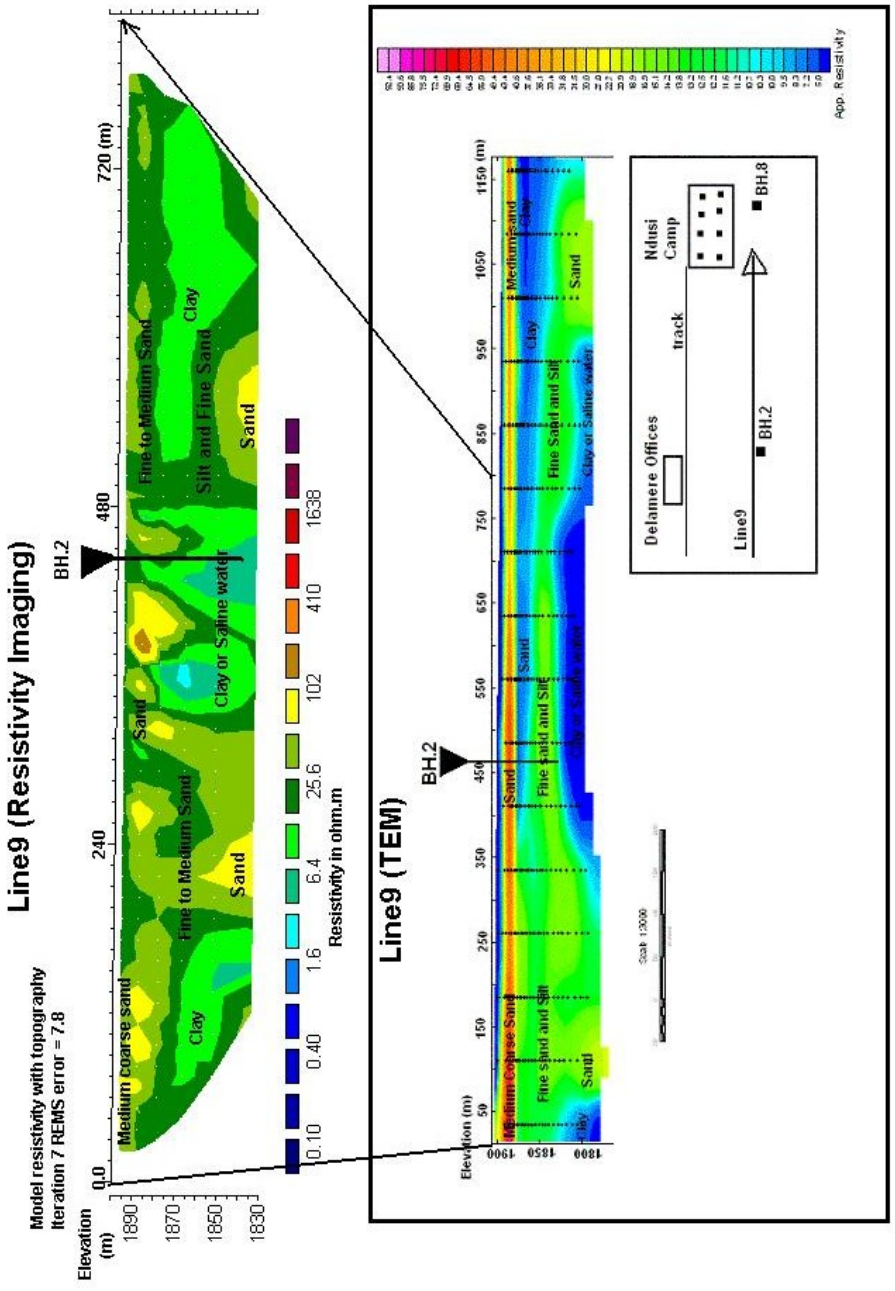

Figure 4: Geological interpretation of the model sections of Line9 for resistivity imaging and TEM

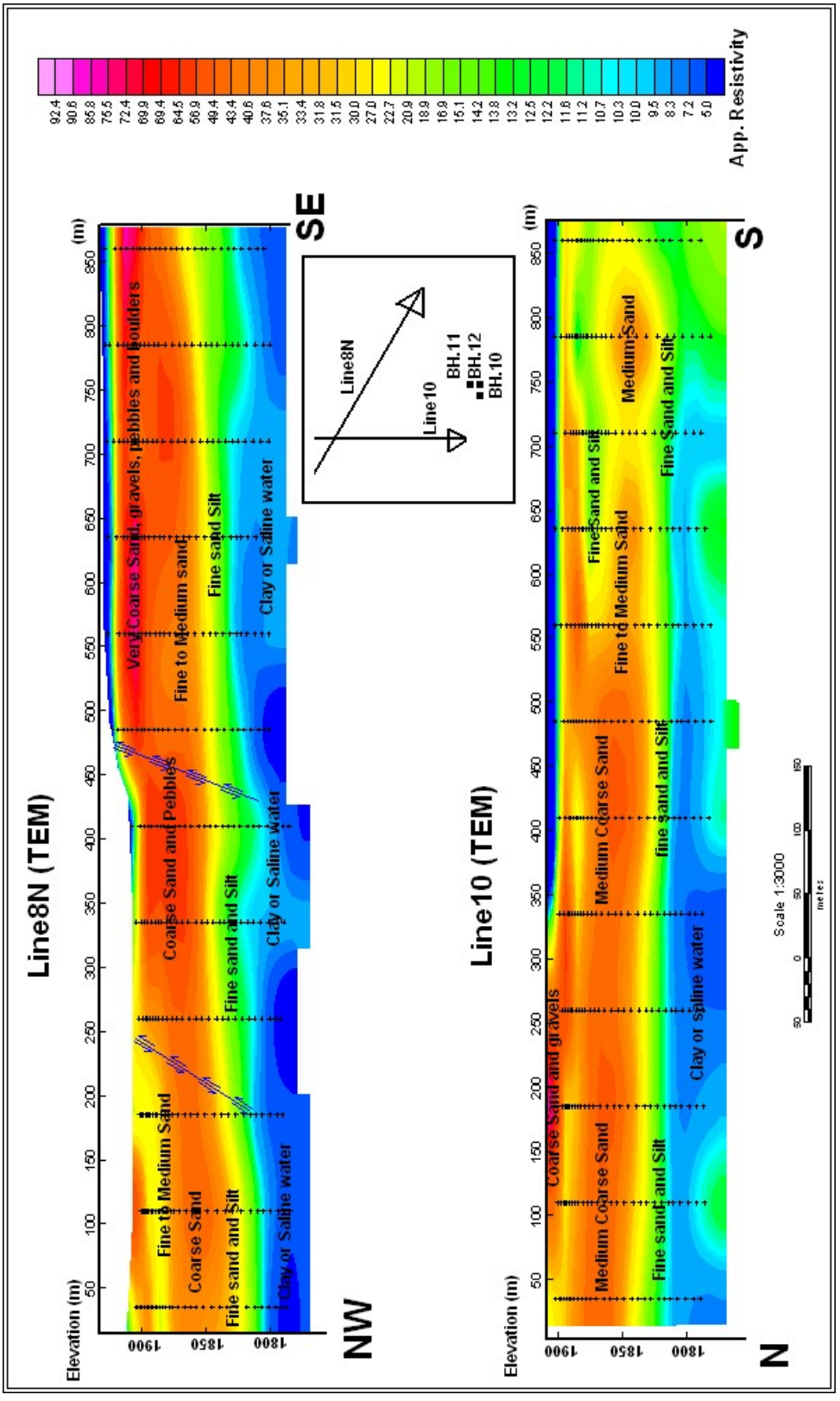

Figure 5: Geological interpretation of the TEM survey profiles 8N and 10

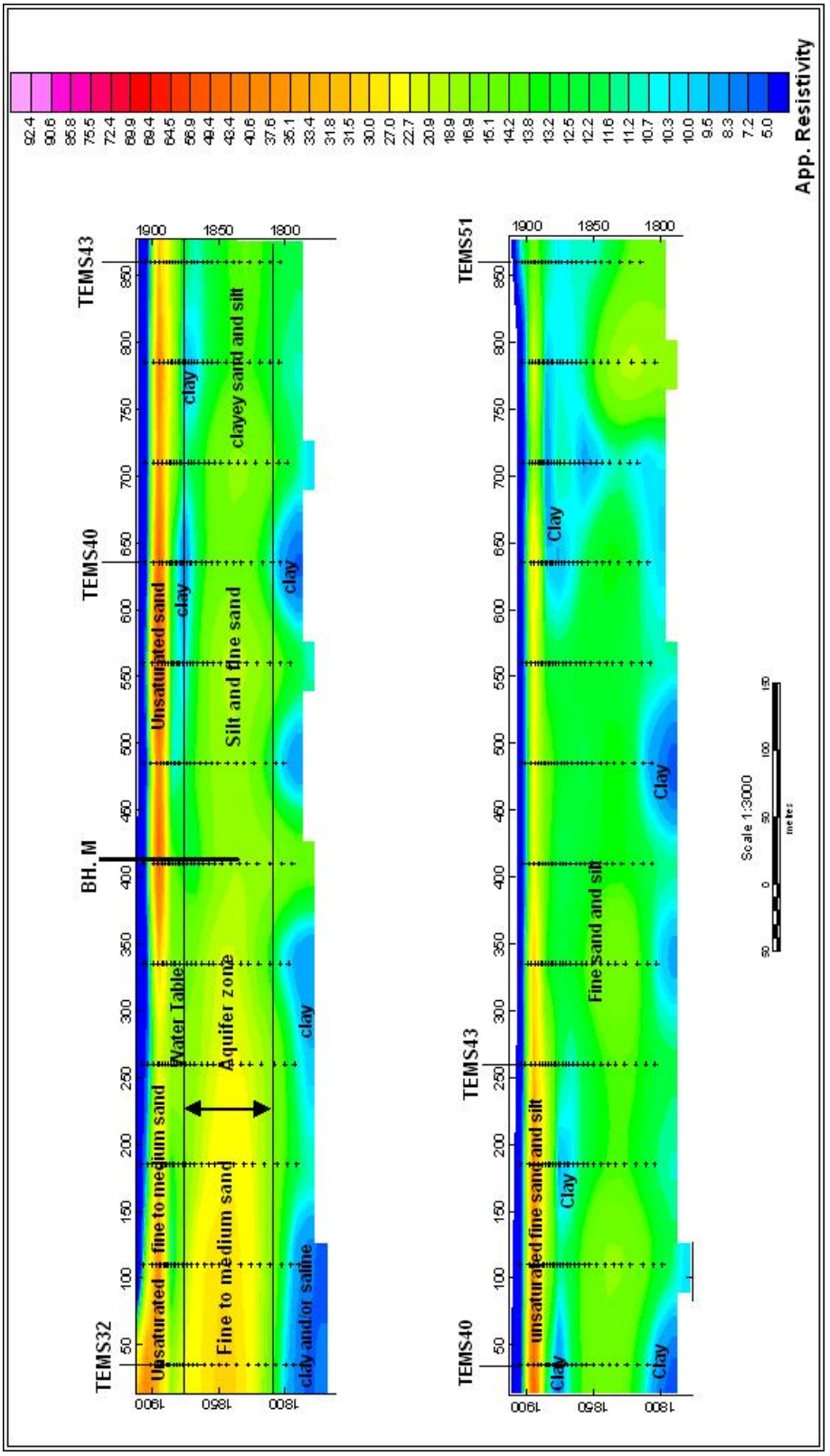

Figure 6: 2D aquifer model of traverse Line4 of TEM

Appendix D

.1 More DC Sounding Results

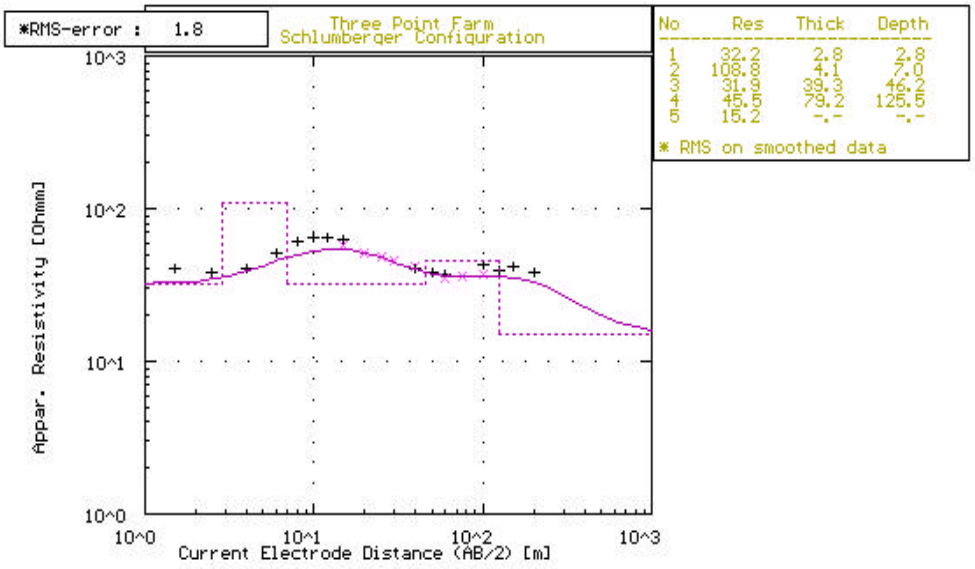

a. VES17 – Pivot B on the Three Point Farm. Co-ordinates (213854, 9924903) at bearing of S 152 E.

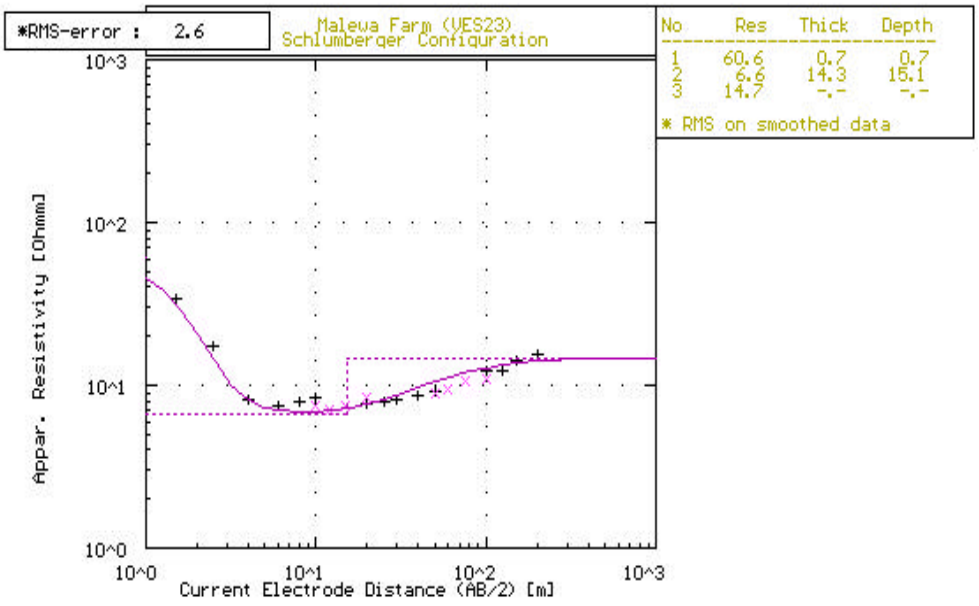

b. VES23 – Manera Farm along the road. Co-ordinates (211331, 9921888) at a bearing of S 220 W.

Figure 7: DC Schlumberger soundings *source:* Gressando, (1999)

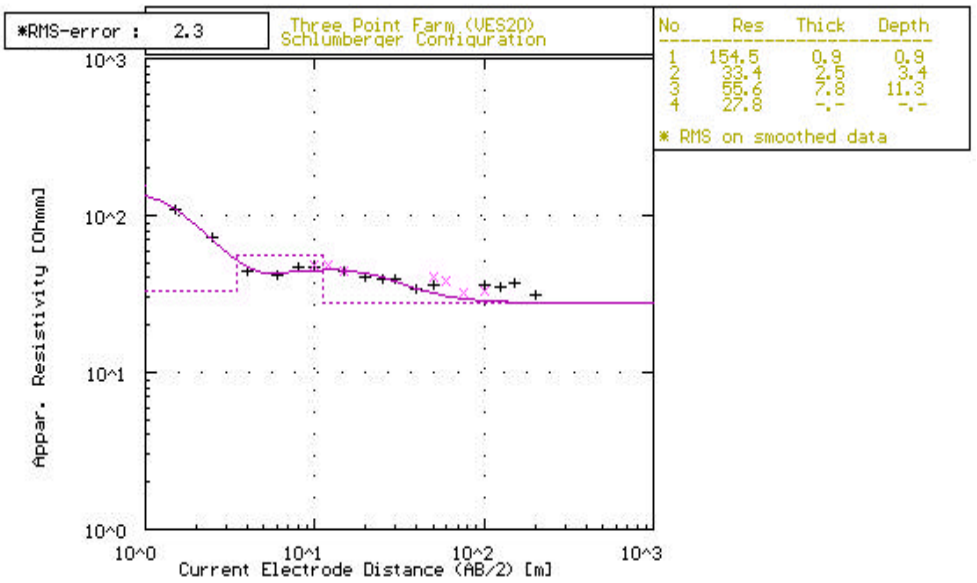

a. VES20 – western part of VES17. Co-ordinates (213590, 9925296) at a bearing of S 160 E.

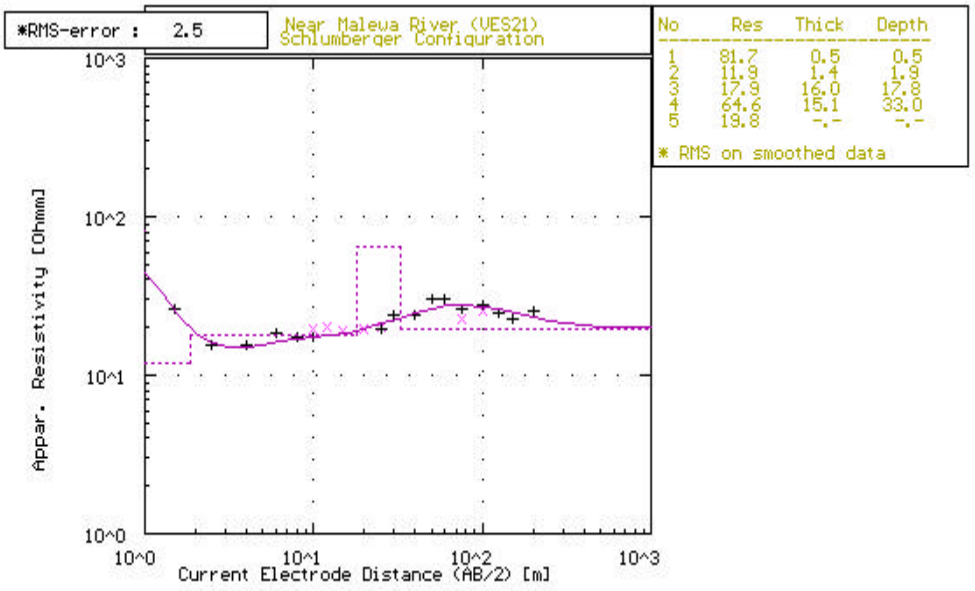

b. VES21 – 75m east of the Malewa River. Co-ordinates (212248, 9927325) at a bearing of S216 W.

Figure 8: DC Schlumberger soundings *source:* Gressando, (1999)

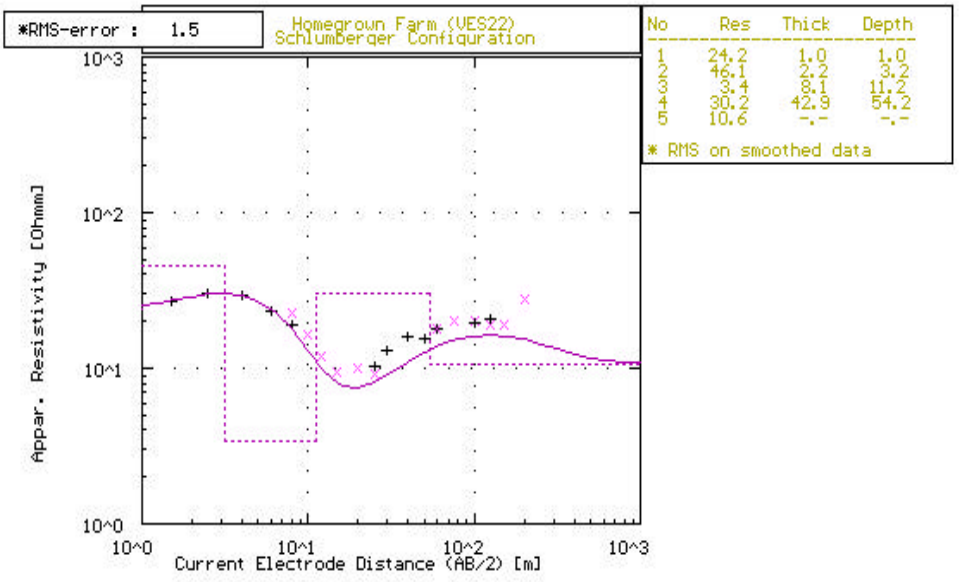

a. VES22 – Homegrown Farm (near the Malewa River)

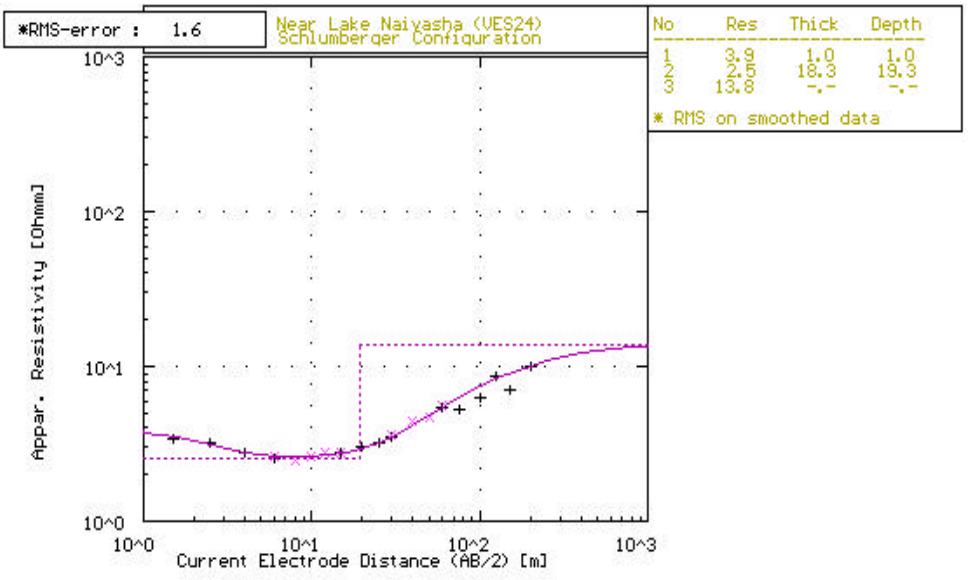

b. VES24 – Manera Farm near the Karati River

Figure 9: DC Schlumberger soundings *source:* Gressando, (1999)